Catechins against Sodium Iodate-induced Retinal Degeneration

YANG, Yaping

A Thesis Submitted in Partial Fulfilment

of the Requirements for the Degree of

Doctor of Philosophy

in

Ophthalmology and Visual Sciences

The Chinese University of Hong Kong

September 2013

Thesis/Assessment Committee

Professor Chee Yung Tham (Chair)

Professor Chi Pui Pang (Thesis Supervisor)

Professor Sun On Chan (Committee Member)

Professor Fuk Loi Li Benjamin (Committee Member)

Professor Kwok Fai So (External Examiner)

Abstract

Background: Catechins, the major biologically active constituents of green tea extract (GTE), are anti-oxidative compounds from natural resources. The pharmacokinetics of catechins and their oxidation capability in the rat eye after oral administration have been studied. (-)-Epigallocatechin gallate (EGCG) is the most abundant of the catechins in GTE, accounting for 50-75% of the total amount of the catechins. Other catechins, like (-)-epicatechin (EC), (-)-epigallocatechin (EGC), and (+)-gallocatechin (GC), are present in smaller quantities, less than 15%. Catechins possess strong anti-oxidant properties, especially EGCG. They also act as free radical scavengers that neutralize free radical mutagens and prevent formation of reactive oxygen species. It has been proposed that catechins consumption, through green tea, could benefit the eye. But how catechins affect mammalian eyes with oxidative stresses remain to be investigated.

It is known that systemic administration of oxidant sodium iodate selectively impairs the retinal pigment epithelium atrophy by oxidative stress, subsequently, resulting in photoreceptor degeneration, as seen in the pathogenesis of many retinal diseases. This can lead to severe visual loss and eventually blindness. Sodium iodate-induced retinal degeneration in rats can be employed as an animal model to explore the biological effects of chemical molecules which therapeutic potential. In

this thesis, the work on the biological effects of GTE and catechins in healthy rats and sodium iodate treated rats are described.

Objectives: To test the ocular uptake and distribution of cathechins in GTE (Theaphenon®E) in plasma, vitreous, and retina. EGCG, catechin combinations and GTE preparation Theaphenon®E, will be fed to adult Sprague-Dawley rats in an attempt to explore the biological effects of exogenous catechins against oxidative stress-induced retinal degeneration induced by sodium iodate.

Methods: In healthy adult Sprague-Dawley rats, the rats were randomly assigned to 9 groups: viz. 0, 0.5, 1, 2, 4, 6, 10, 15, 20 hours. 550 mg/kg Theaphenon®E was suspended in 500µl water for intragastric feeding to each rat. After the experiment the eyes were enucleated, the retina and vitreous dissected immediately. Plasma was obtained from peripheral whole blood. Negative control was performed according to each time point. The catechins contents in each eye compartment were analyzed by High Performance Liquid Chromatography with electrochemical detection (HPLC-ECD) after β-D-glucuronidase and sulfatase digestion.

Retinal degeneration was induced to adult Sprague-Dawley rats by single-dose intravenous injection of 40 mg/kg sodium iodate. The retinal degeneration profile was assessed by a new in vivo procedure on confocal scanning laser ophthalmoscopy (CSLO) and spectral domain optical coherence tomography (SD-OCT) for longitudinal studies of living rat retinas. After the in vivo experiments the rats were sacrificed for histological examinations of retinas. The sodium iodate treated rats were also administered intra-gastrically with 550 mg/kg Theaphenon®E, 387.8 mg/kg EGCG, 438.0 mg/kg catechins combination (EGCG, GC, EGC, and EC), and 50.3 mg/kg catechins combination (GC, EGC, and EC), respectively. Controls were injected intravenously with normal saline or 40 mg/kg sodium iodate only. After in

vivo examination of the retinas by CSLO and SD- OCT, the rats were sacrificed for histological analysis. Biochemical analyses included determination of superoxide dismutase (SOD), glutathione peroxidase (GPx), caspase 3 mRNA, and an oxidative stress marker, 8-Iso-PGF$_{2\alpha}$, concentration in the retina.

Results: In healthy rats catechins were differentially distributed in eye tissues. EGCG presents at high levels in the plasma, retina and vitreous at 6686.8±4437.1 nM, 784.4±195.9 nmol/kg, and 2224.4±805.4 nM respectively. In the retina, EGCG was the dominant constitute and maintained to 20 hours. The order of dominance of catechins levels in plasma was EGC>EC>C>GC, in galloyl catechins was EGCG>ECG>GCG>CG. Catechins were absorbed at short time, with 30 minutes after administration.

In the sodium iodate treated rats confocal scanning laser ophthalmoscopy revealed hyper-reflective blots in the retina 7 days after intravenous injection of sodium iodate (25, 40, 50, 75 mg/kg). Occurrence of lesions coincided with the time when degenerative changes were observed in the outer retinal layers which appeared in OCT images and histological sections. Further analyses of retinas with restricted distribution of blots showed a concomitant localization of degenerative profiles in histological preparations, suggesting that the blots shown in CSLO corresponded to the deteriorating photopigments and outer nuclear layer (ONL). Quantitative analyses showed that the changes in blot number are dose dependent, again concomitant with results showing dose dependent lesions in photopigment layer and ONL in histological sections of the retina. Furthermore, we found that 40 mg/kg is a feasible dose that generates consistent damage to the retina without causing obvious systematic damage to other organs, and can serve as the selected dosage for testing the anti-oxidation effect of the EGCG, catechin combinations, and GTE

(Theaphenon®E).

CSLO and OCT measurements revealed decreases in hyper-reflective blots in the retina specimens after treatment with EGCG, catechins combination (EGCG, GC, EGC, and EC), and Theaphenon®E. Concomitant protective effects of these catechins were observed in histological preparations with reduction of disrupted ONL in retina. Expressions of SOD, GPx, Caspase 3 and 8-Iso-PGF$_{2\alpha}$ level in the retina were reduced, indicating strong anti-oxidant effects of the EGCG, catechins combination (EGCG, GC, EGC, and EC), and Theaphenon®E. However, catechins combination without EGCG (GC, EGC, and EC) on the mRNA level was slightly attenuated, but the difference was not statistically significant.

Conclusions: We found catechins distribution in different compartments of the eye. Our findings also showed that degenerative changes observed in *in vivo* retinal imaging using CSLO and OCT can reflect cellular damages in outer retinal layers in the adult rat treated by sodium iodate. These techniques allow quantitative measures of degenerative changes in a large area of retina in longitudinal assessments. Moreover, EGCG, catechins combination (EGCG, GC, EGC, and EC) and Theaphenon®E attenuated sodium iodate-induced retinal degeneration in rats. Catechins combination without EGCG (GC, EGC, and EC) gave insignificant protective effect. Our results support the notion that catechins alleviate oxidative stress in the retina, with EGCG providing the important effect.

摘要

背景知识：儿茶素，是绿茶提取物中的主要生物活性元素， 是自然生物中的抗氧化剂。老鼠口服儿茶素后其药代动力学和抗氧化能力进来被学者研究。(-)-epigallocatechin gallat (EGCG) 是儿茶素中含量最多的，大概占儿茶素总量的 50-75%。其它的儿茶素，像(-)-epicatechin (EC), (-)-epigallocatechin (EGC), 和 (+)-gallocatechin (GC) 含量都是很少的，只占了不到 15%。儿茶素拥有很强的抗氧化性，尤其是 EGCG, 它还可以清除自由基，中和自由基的诱变剂，阻止氧化还原物质的生成。 有一些研究提出使用儿茶素对眼睛有好处。但是当眼睛受到氧抑制的损坏时儿茶素是否会有保护作用呢，这有待于我们进一步研究。

静脉注射碘酸钠可以通过氧抑制选择性损坏视网膜色素上皮细胞，接着导致视网膜光感受层变性，这一病变可以体现在很多视网膜疾病中，最终导致失明。碘酸钠在老鼠体内诱导视网膜变性已经作为一个成熟的动物模型去研究检测一些药物的作用。在这个课题中，绿茶提取物和儿茶素的生物活性作用在正常的和被碘酸钠诱导视网膜变性的大鼠都被研究。

目的：研究绿茶提取物 Theaphenon®E 在老鼠血浆，玻璃体，视网膜中的吸收和分布。随即我们将 EGCG, 儿茶素混合物 (EGCG, EC, EGC, GC), 儿茶素混合物 (GC, EGC, EC), 绿茶提取物 Theaphenon®E 喂给同时注射了碘酸钠的大鼠，研究这些药物对抗碘酸钠引起视网膜变性的能力。

方法：大鼠被随机分配成 9 组，分别是 0, 0.5, 1, 2, 4, 6, 10, 15, 20 小时， 550 mg/kg Theaphenon®E 在 500 微升的中的悬浮溶液喂给正常的大鼠，对照组在相应的时间点给予水。这些老鼠的眼睛被摘下来， 视网膜，玻璃体立即被分离。 血浆来自外周血。儿茶素在这些组织中被高压液相层析-电化学侦测计检测。应用共

焦激光扫描检眼镜和光学相干断层成像术纵向评估了碘酸钠诱导活体小白鼠视网膜变性。

大鼠静脉一次性注射 40 mg/kg 的碘酸钠的同时口饲 550mg/kg 绿茶提取物 Theaphenon® E，387.8 mg/kg EGCG，387.8 mg/kg 的儿茶素混合物 (EGCG，GC，EGC，和 EC)，50.3 mg/kg (GC, EGC, and EC)。这些不同组的老鼠在完成共焦激光扫描检眼镜和光学相干断层成像之后，眼球取出做进一步的生物化学和组织学分析。

结果：我们检测儿茶素分布在健康的大鼠眼组织中到。EGCG 以很高的含量出现在血浆，视网膜，玻璃体中 (6686.8±4437.1 nM, 784.4±195.9 nmol/kg, 和 2224.4±805.4 nM)。EGCG 的含量在视网膜可以维持在 20 小时以上， 儿茶素的吸收很快，在喂完后 30 分钟，即可在血液及视网膜中检测到。

在 25mg/kg-75mg/kg 剂量的碘酸钠静脉注射后第 7 天，从共焦激光扫描检眼镜照片中可以看到视网膜中出现了高反射的点，这个发现与之后 14 天的光学相干断层成像看到视网膜外核层的高反射以及组织学切片的结果相一致。而且我们发现 40 mg/kg 剂量的碘酸钠是最佳的剂量可以诱导视网膜变性但是对其它重要脏器没有影响。共焦激光扫描检眼镜的结果显示在用高剂量的 EGCG, 儿茶素混合物 (EGCG，GC，EGC，和 EC), 和绿茶提取物 Theaphenon®E 降低了视网膜中的高反射点，光学相干断层成像术和组织切片也支持这一观点，超氧（化）物歧化酶，谷胱甘肽过氧化物酶，caspase 3 和 8-Iso-PGF$_{2\alpha}$ 的表达下降更证明了儿茶素及其提取物的抗氧化性。

结论：我们研究发现儿茶素分布在眼组织。利用共焦激光扫描检眼镜和光学相干断层成像可以观察碘酸钠诱导的活体大鼠的视网膜变化。并且我们发现儿茶

素 EGCG，儿茶素混合物 (EGCG，GC，EGC，和 EC) 以及绿茶提取物 Theaphenon®E 可以减少碘酸钠诱导的视网膜变性。 但是儿茶素混合物中没有 EGCG，对视网膜没有保护作用。

Acknowledgements

First, I am very grateful to my PhD thesis supervisor Professor Chi-Pui PANG, for his valuable guidance and continuous support on my PhD program and also for his training on my writing and presentation skills. He brought me into the fascinating research field. What I learned from him is not only the academic knowledge, but also the way to become a person who is honorable, faithful and helpful.

I also would like to express my sincere gratitude to Professor Hector S.O. Chan for his endless support and valuable advices. I am very grateful to Professor Ben F.L. Li and Dr. Chu Kai On for their guidance and insightful discussion when I met the difficulties.

I would also want to express my sincere thanks to Dr. Michael T. K. Ng who initial start this work with me. I am very appreciated Dr. Yolanda. Y. W. Yip, Dr. Ye Cong and Dr. Yongjie Qin for their contribution in taking the in vivo images, without their help, this work cannot be completed. I am indebted to Ms. Winnie W. Y. Lee and Ms. Pancy. O. S. Tam for their technical assistances in cutting sections and histological staining.

Finally, I must express my great gratitude to my family, thanks for their support during the study period. Without their moral support I would never come this far.

Table of Contents

Chapter 1: Introduction

List of Figures

List of Tables

Abbreviations

Abbreviations	Full name
ACE	angiotensin- converting enzyme
AMD	age-related macular degeneration
AUC	area under curve
Cl/F	oral clearance
BHT	butylated hydroxytoluene
BSTFA	N, O-bis-(trimethylsilyl) trifluoroacetamide
C	(+)-catechin
CAT	catalase
CG	(-)-catechin gallate
CSLO	confocal scanning laser ophthalmoscopy
CNV	choroidal neovascularization
Cox-2	cycloxygenase -2
Cmax	Maximum concentration
DIPE	diisopropyl Ether
DNA	deoxyribonucleic acid
ECM	extracellular matrix
EC	(-)-epicatechin
ECG	(-)-epicatechin gallate
EGC	(-)-epigallocatechin
EGCG	(-)-epigallocatechin gallate
ERKs	extracellular-signal-regulated kinases
EGFR	epidermal growth factor receptor
FR	free radicals
GA	geographic atrophy
GC	(+)-gallocatechin
GCG	(-)-gallocatechin gallate
GCL	ganglion cell layer
GO	graves' ophthalmopathy
GPX	glutathione peroxidase
GSH	glutathione
GSSG	glutathione disulfide
GTE	green tea extract
GC-MS	gas chromatography–mass spectrometry
HCEpiC	human corneal epithelial cells
HPLC-ECD	high Performance Liquid Chromatography with electrochemical detection
HUVECs	human umbilical vein endothelial cells

H₂O₂	hydrogen peroxides
IGF	Insulin-like growth factor
INL	inner nuclear layer
IS/OS	inner/outer segments
IOP	Intraocular pressure
IPL	inner plexiform layer
i.p.	intraperitoneal
i.v.	intravenous
JNKs	c-Jun N-terminal kinases
MAPK	Mitogen activated protein kinases
MEK1	mitogen-activated protein kinase kinase 1
MMPs	Matrix metalloproteinase
NADPH	nicotinamide adenine dinucleotide phosphate
NF-kB	nuclear factor kB
NO	nitric oxide
OCT	optical coherence tomography
OD	optic disc
ONL	outer nuclear layer
PBS	Phosphate Buffered Saline
PCR	polymerase chain reaction
PDGFAB	platelet Derived Growth Factor AB
PDR	proliferative diabetic retinopathy
PFBB	pentafluorobenzyl bromide
PVR	proliferative vitreoretinopathy
ROP	retinopathy of prematurity
ROS	reactive oxygen species
RP	retinitis pigmentosa
RPE	retinal pigment epithelium
SD	mean standard
SOD	superoxide dismutase
TPA	tissue plasminogen activator
TLC	thin layer chromatography
Tmax	maximum peak time
UV	ultraviolet
uPA	urokinase plasminogen activator
Vz	Volume of distribution
VEGF	vascular endothelial growth factor
8-OHdG	8-hydroxy-2'-deoxyguanoin

Publications

(1) Kai On Chu, **Ya Ping Yang**, Chi Chiu Wang, Chi Pui Pang. Biological effects of green tea catechins in ocular tissue cells. Tea in Health and Disease Prevention, 1st Edition. United States of America. 2012.p 1309-1322.

(2) Kai On Chu, Kwok Ping Chan, **Ya Ping Yang**, Yong Jie Qin, Wai Ying Li, Chi Pui Pang. Investigation of pharmacokinetics, prooxidant, and antioxidant effects of green tea extract with high level of (-)-epigallocatechin gallate (EGCG) on various ocular compartments in normal physiological and oxidative induced retina degeneration model. (Submission to *Journal of Medicinal Chemistry*).

(3) **Ya Ping Yang**, Tsz Kiz Ng, Cong Ye, Yolanda W. Y. Yip, Kasin Law, Sun On Chan, Chi Pui Pang. A novel method of assessing degenerative changes in outer retinal layers in adults rats using in vivo confocal scanning laser ophthalmoscopy and optical coherence tomography (Submission to *Investigative Ophthalmology and Visual Science*).

(4) **Ya Ping Yang**, Yong Jie Qin, Yolanda W. Y. Yip, Kwok Ping Chan, Kai On Chu, Sun on Chan, Chi Pui Pang. Catechins attenuate sodium iodate induced retinal degeneration. (Submission to *Journal of Medicinal Chemistry*).

Conference presentations

(1) **Ya Ping Yang**, Tsz Kin Ng, Cong Ye, Kasin Law, Yolanda W. Y. Yip, Sun On Chan, Chi Pui Pang. In vivo imaging for longitudinal assessment of sodium iodate-induced rat retinal lesions. The 8th international symposium of Ophthalmology. Hong Kong. Dec 14-16, 2012. Vitreo-Retina, section: VR-FP01.

(2) **Ya Ping Yang**, Yong Jie Qin, Yolanda W. Y. Yip, Kwok Ping Chan, Kai On Chu, Sun On Chan, Chi Pui Pang. Catechins attenuate sodium iodate induced retinal degeneration. ARVO 2013 Annual Meeting, the Association for Research in Vision and Ophthalmology. May 5-9, Seattle, Washington. Oxidative/ER Stress and Autophagy in RPE and Retina, 1799.

Chapter 1: Introduction

1.1 Oxidative stress definition and characterization

Oxidative stress is the disrupture of the balance between the free radicals (FR)/reactive oxygen species (ROS) and endogenous antioxidant defense system. (Chandra et al., 2000). Oxidant and antioxidant defense system are the key factors for maintain the cellular metabolism, cell signal transduction and regulation inside the body in normal situation. Therefore, each cell in tissues keeps the balance between the oxidant and antioxidant status (Poli et al., 2004). The hypoxia/hyperoxia and reperfusion generate reactive oxygen species include free radical surges and peroxides cause oxidative stress, which lead to biological disturbances and finally cause tissue cell damage and dysfunction.

The ROS include reactive chemical species (Sohal and Weindruch, 1996), can be divided into two subgroups: free radicals ROS such as superoxide radicals, peroxyl, alkoxyl, hydroxyl, and nitric oxide; non- radical ROS such as hydrogen peroxide, singlet oxygen, and hypochlorous acid. Both radicals and non-radical are common in the presence of oxygen atom. ROS exist in the environment, can be generated by pollutant, tobacco smoke, iron salts, and radiation, and also can be produced in side cells, it is shown that ROS can be generated through several mechanisms. Commonly, most of the ROS are continuous take places in mitochondria (Valko et al., 2006, Inoue et al., 2003). Moreover, cytochrome 450 enzymes are also known to induce ROS (Parke and Sapota, 1996). ROS produce single or double-stranded DNA breaks and cross- links; prolong DNA damage; induction of signal transduction pathways;

induction of transcription, replication errors, and genomic instability (Ogasawara and Zhang, 2009).

1.2 Cellular and molecular mechanism of oxidative stress

Reactive oxygen species are known to damage cellular functions, however, they also can serve as subcellular messengers in gene regulation and cell signal transduction pathways. Oxidative stress status involved in cell growth, transformation, differentiation, induced apoptosis by altering DNA binding; activation of transcriptional factors or alter biochemical pathways lead to affect gene expression.

The ROS involve changes in the redox state of protein sulfhydryl groups and enzyme conformation; DNA binding stability and protein complex formation. So, the ROS can modulate the cytokines, growth factors, hormone secretion, ion transport, neuron-modulation transcription and apoptosis.

1.3 Oxidative stress affects gene expression and signal transduction

The cellular actions of the external signaling molecules like growth factors and cytokines transmit signals from receptor sites in the plasma membrane to the nucleus for gene expression through protein kinase activity in cytoplasm. Mitogen activated protein kinases (MAPK) include four subtypes: extracellular-signal-regulated kinases (ERKs); c-Jun N-terminal kinases (JNKs); p38 and MAP kinase. In ERKs and JNKs pathways, growth factor receptors activation by tyrosine autophosphorylation and reactants of SH-Grb2 protein complex and consequently leads to SH2- Grb2-Sos complex formation. However, oxidants like H_2O_2 can activate this complex formation. Oxidizing status such as hypoxia/reperfusion or hydrogen peroxides

(H_2O_2) can activate Raf-1 phosphorylation to stimulate mitogen-activated protein kinase kinase 1 (MEK1) to regulate downstream such as apoptosis, mitogenesis and differentiation.

In addition, the nuclear factor kB (NF-kB) Rel family of transcription factors regulates cell surface receptors, cytokines, acute phase proteins and also antioxidative defense involving superoxide dismutase-2 transcription and Y-glutamylcysteine synthetase. However, ROS activate the NF-kB through degrade the Iκ-Bα, which is an inhibitory protein. This is followed by the translocation of NF-kB to nuclear and bind to DNA to initiate gene transcription. Antioxidants such as catechins can decrease NF-kB activity by impeding Iκ-Bαdegradation so that to prevent NF-kB translocate to the nuclear (Allen and Tresini, 2000).

Hydrogen peroxides also can stimulate protein phosphorylation such like protein kinase p38-MAPK through inhibiting protein dephosphorylation by tyrosine phosphatase. Therefore, stimulate transcription factors to induce inflammation. It also stimulates transcription of pro-apoptotic such as caspase 3.

1.4 Oxidative stress plays roles in ocular disorders

The retina is a highly metabolic system; the photoreceptors are particularly susceptible to oxidative damage not only because of photo–chemical reactions (Wang et al., 1994) but also because of their high polyunsaturated fatty acid (Bazan, 1989, Fliesler and Anderson, 1983) content and rich supply of oxygen from the choroidal circulation (Alder and Cringle, 1985).

Oxidative stress has been suggested to play an important role in the pathogenesis of many common ocular diseases, especially retinal diseases, such as age-related macular degeneration (AMD), glaucoma, diabetic retinopathy, Graves'

ophthalmopathy, retinopathy of prematurity, cataract **(Figure 1.1)**.

1.4.1 Age-related macular degeneration

Age-related macular degeneration (AMD) is a leading cause of irreversible visual impairment in the developed countries, affecting 50 million elderlies worldwide (Klein et al., 2004, Congdon et al., 2004). It is a progressive neurodegenerative disease affecting the macula, resulting in a significant loss of central vision in advanced stages. AMD can be classified into dry and wet forms, represented by their respective clinical hallmarks of geographic atrophy (GA) and choroidal neovascularization (CNV) (Jager et al., 2008). In atrophic form, the pathological characteristics are atrophy of the choriocapillaries, disruptions of the associated retinal pigment epithelium (RPE) and derangements of the underlying photoreceptors (Coleman et al., 2008). Histological evidence shows that RPE dysfunction as a primary and major causative role in the pathogenesis of AMD (Zarbin, 2004). One of the proposed mechanisms of RPE dysfunction in AMD assumption accumulation of oxidative damages to the RPE cells, and subsequently RPE mitochondrial dysfunction, accumulation of deposit in the sub epithelial space, and inflammation triggered at the RPE choroid interface. The RPE is an oxygen- rich environment and the RPE mitochondrial is prone to oxidative damage (Jarrett et al., 2008, Liang and Godley, 2003).

AMD is a complex disease, influenced by multiple genes and environmental factors. Epidemiological studies have identified several risk factors, including age, cigarette smoking, sunlight exposure, high-fat diet, low anti-oxidant intake, and genetic variants such as polymorphism of complement factor H. All these risk factors are associated with oxidative stress. Chronic oxidative stress is regard as an
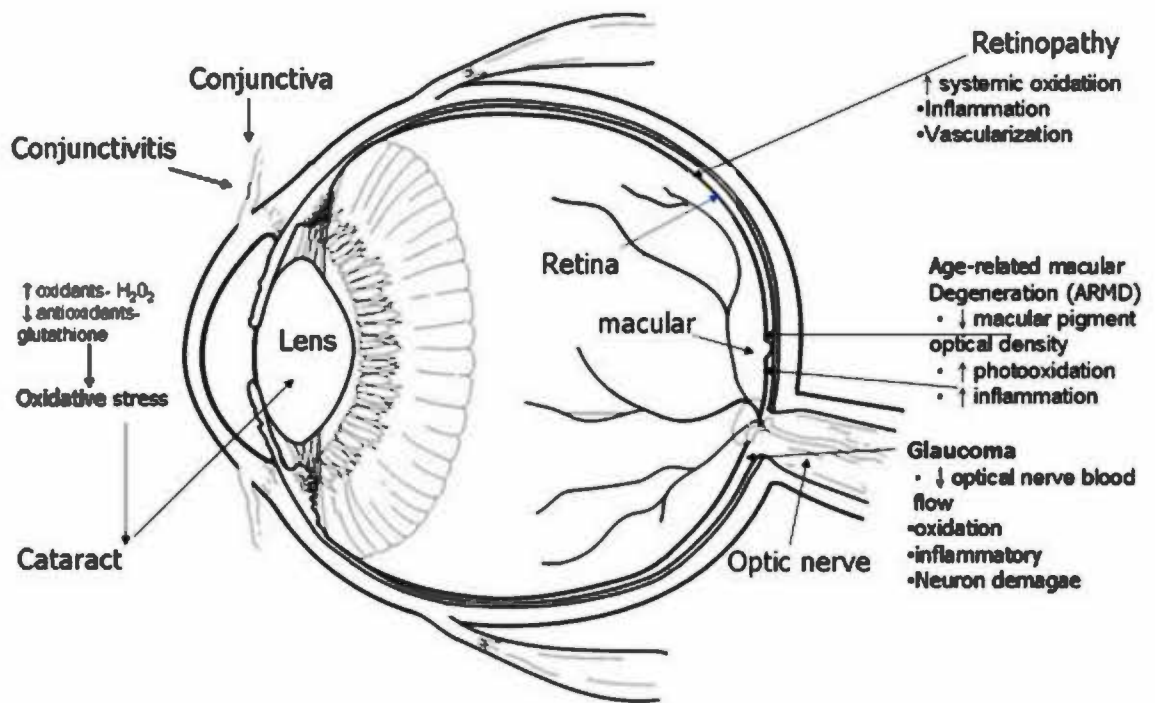
Figure 1.1 Role of oxidative stress in ocular disorders. Figure shows various agents which could cause oxidative stress, lead to different ocular diseases in different ocular compartments. (Picture from Chu KO, Yang YP, Wang CC, Pang CP. Biological effects of green tea catechins in ocular tissue cells. Tea in Health and Disease Prevention, 1st Edition. United States of America. 2012.p 1313.)

important contributing environmental factor to the development of AMD, which causes retinal tissue damage, including damage of the photoreceptor cells, retinal pigment epithelium, and choroidal capillaries, resulting in macular degeneration. The retina is an environment that metabolically active tissues generation of reactive oxygen species (ROS) in the body and result in oxidative damage, retina is one of the highest oxygen- consuming tissues in the human body. It also receives high levels of radiation, e.g. ultraviolet (UV) exposure. Phagocytosis in retinal pigment epithelium cells gives rise to high levels of reactive intermediates. These elevated levels of oxidative stress conditions increase with age, causing the susceptible polyunsaturated fatty acid (DHA) on the photoreceptor membrane to be per-oxidized. Oxidative stress induces vascularization in the choroid, decreases macular pigment in the retina, and forms sub retinal pigment epithelium deposits (Espinosa-Heidmann et al., 2006). Excess body weight activates the renin-angiotensin system which induces superoxide production, lipid oxidation, glutathione level reduction in erythrocytes, and decreases lutein and zeaxanthin levels in the retina. These increase endogenous oxidation injury to the retina, resulting in retinopathy.

1.4.2 Retinitis pigmentosa

There are several retinal diseases in which the primary and predominant site of retinal dysfunction is localized in the RPE or/and photoreceptors. Retinitis pigmentosa (RP) is a group of inherited retinal disease caused by complicated molecular etiology, characterized by a progressive loss of visual function due to the RPE and photoreceptors degeneration. Oxidative stress can be a risk factor for the onset and progression of RP. There are a great number of animal models developed and studied for studying the pathophysiology and new treatment of this disease.

Systemic administration of sodium iodate has been reported it selectively damage the RPE, and subsequently lead to degeneration of photoreceptors.

1.4.3 Glaucoma

Glaucoma is a leading cause of irreversible blindness in developed country; it is a group of diseases characterized by progressive optic neuropathies, loss of visual field. Glaucoma is often come along with elevated intraocular pressure as a result of obstruction of aqueous humor outflow due to abnormalities within the drainage system of the anterior chamber angle or damaged access of aqueous humor to the drainage system. Oxidative injury to glaucoma appears to play a role in the pathogenesis of glaucomatous neuro-degeneration. It may cause direct cytotoxic effects cause retinal ganglion cell death through nitrogen oxide metabolism modifications, vascular alterations, and generation of reactive oxidative intermediates (Chrysostomou et al., 2013). Oxidative proteins may exert immune-stimulatory signals; alter neuro-supportive and immune-regulatory functions of glial cells. Oxidant involve in initiation of the apoptotic cascade in glaucomatous retinopathy (Aslan et al., 2013).

1.4.4 Diabetic retinopathy

Diabetic retinopathy is a microcirculatory disease of the retina. From experimental studies, increasing evidence showed that chronic inflammation and oxidative stress are involved. Diabetes mellitus increase oxidative stress level to induce capillary cell apoptosis and retinal microvasculature damage. Elevated levels of glutamate, oxidants, the overexpression and the up-regulation of renin-angiotensin system play an essential role in the retinal neuro-degeneration induced by diabetes mellitus

(Hernandez and Simo, 2012). Oxidative stress lead glyceraldehyde-3-phosphate dehydrogenase activity impairment and activation of major undesirable biochemical pathways (Duarte et al., 2012).

1.4.5 Graves' ophthalmopathy

Graves' ophthalmopathy (GO) is a most common caused by hyperthyroidism characterized by protrusion of the eyeball, affecting 25-50% patients with Graves' Disease. Around 3%-5% GO patients have potential sight-threatening risk. Accumulating evidence has shown that oxidative stress is an important factor for the disease (Ademoglu et al., 2006, Tsai et al., 2011). Over-production of thyroid hormones accelerates the basic metabolic rate and cellular oxidative metabolism in mitochondria leading to ROS over-generation. Increased extracellular levels of ROS have been noted in the blood, urine, and fibroadipose. This oxidative environment stimulates retro-ocular fibroblast proliferation leading to eye protrusion. Urinary 8-hydroxy-2′-deoxyguanosine (8-OhdG) is a biomarker for oxidative DNA damage. In GO patients, there was significant correlation between thyroid stimulating hormone receptor antibody levels and 8-OhdG (Zarkovic, 2012). The mechanism was supported by the increase level of 8-hydroxy-2'-deoxyguanoin (8-OHdG) in urine of active GO patients and higher levels of 8-OHdG, malondiadehyde, superoxide anions and hydrogen peroxide in orbital fibroblasts GO patients (Tsai et al., 2010).

1.4.6 Retinopathy of prematurity

Retinopathy of prematurity (ROP) is an ocular disease of the retina cause of visual impairment and blindness in premature babies, characterized by the onset of vascular

abnormalities in the developing retina. ROS and oxidative stress has been suggested to contribute to the retinal vaso-oblitreation in ROP. Nitric oxide can react with ROS by the nitro-oxidative stress process affecting the cell function, generate nitrites, and protein tyrosine nitration products, all cytotoxic to retina-vascular endothelium, causing vaso-obliteration, can enhance increasing retinal micro-vascular degeneration (Checchin et al., 2006). The retina is highly susceptible to lipid peroxidation as it has high level of polyunsaturated fatty acids. Lipid peroxidation together with nitrative stress lead inadequate oxygen environment is pivotal to the pathogenesis of ROP. Oxidative stress is possible to induce peroxidation and nitration which is cytotoxic to retinal microvasculature (Rivera et al., 2011).

1.4.7 Cataract

Cataract occurs when the normally clear lens in the eye becomes opacity. It is the leading cause of reversible reduced vision worldwide. Cataract is consistently subjected to light-induced photo-oxidation. Crystallin is a major constituent of the lens (Mathew et al., 2012). α-crystallin is essential in preventing the light-scattering and maintenance of lens transparency, thereby prevention of cataract. Oxidation may cause cross-linking of sulfhydryl groups in lens proteins, such as crystalline, resulting in aggregation of proteins, cell damage, and optical opacity. In cataract lenses have been found to contain low levels of the natural anti-oxidant glutathione, and high levels of H_2O_2, indicating that oxidation reactions are believed to be potent etiological factors in the development of cataract.

1.5 The antioxidant system

In general, antioxidants are reducing agents, are the compounds of exogenous or endogenous in nature exist both intracellular and extracellular which either prevent the generation of oxidants or react with free radicals and reactive oxygen species, thereby block the propagation of chain reaction produced by these oxidants, delay or preventing oxidative stress (Rangan and Bulkley, 1993).

Antioxidants can be synthesized both *in vivo* and absorbed through diet. They can be divided into several groups: enzymatic and nonenzymatic; endogenous antioxidants such as uric acid, produced form metabolism of purines; natural antioxidants obtained from the diet such as ascorbic acid, α-tocopherol, β-carotene.

1.5.1 Anti-oxidative enzymes

The antioxidants defense enzymes include superoxide dismutase (SOD), glutathione peroxidase (GPX), and catalase (CAT). These enzymes seated in different component of the cell, and account for scavenging of ROS.

SOD is a major antioxidant defense enzyme in the tissue; it plays a key role in reducing and eliminating superoxide. SOD has three subtypes in tissues: copper-zinc superoxide dismutase (Cu/ZnSOD; encoded by the *SOD1* gene); manganese superoxide dismutase (MnSOD; encoded by the *SOD2* gene), and extracellular superoxide dismutase (ECSOD; encoded by the *SOD3* gene). These three isoforms of SOD have different functions in form of protein structure, chromosome localization, and gene regulation (Miao and St Clair, 2009). SOD also can catalyze the superoxide radicals into oxygen and hydrogen peroxides.

Glutathione peroxidase (GP_X) located in the cytosol and the mitochondria, to take away the hydroperoxides into H_2O_2, protect membrane lipids, proteins, and DNA against oxidation (Margis et al., 2008).

Catalase (CAT) is a ferriheme-containing enzyme inside the cell; the major function of the CAT is catalyzing the H_2O_2 into H_2O and O_2. But, compare to GPx, CAT has less affinity with H_2O_2 (Droge, 2002).

The nonenzymatic antioxidant contains glutathione, vitamin C, vitamin E, carotenoids, and flavonoids. Glutathione (GSH) is water-soluble and can be formed from glutamate, cysteine, and glycine by daily consumption of food. GSH can be synthesized nearly in all types of cells but there are easy to degrade into amino acid (Valencia et al., 2001, Wu et al., 2004, Gomes et al., 2012). GSH can remove ROS and FR so that can against forming of oxidative stress status. Once GSH is oxidized, GSH will convert to the glutathione disulfide (GSSG) by the catalysis of the glutathione peroxidase. However, GSSG also can convert back to GSH by the reductase enzyme nicotinamide adenine dinucleotide phosphate (NADPH). So, when the tissues suffered from oxidative stress, the level of the GSH and the oxidized GSH formed GSSG ratio is a good and reliable biochemical marker to present the oxidative level in the tissues.

1.5.2 Endogenous antioxidants

Uric acid and melatonin are two important endogenous antioxidants. Uric acid and melatonin possess strong anti-oxidative properties, and sustain higher level in fluid circulation and in tissues.

Oxidation of xanthine and hypoxanthine can generate uric acid. Uric acid is an important oxidation scavenger because it effective in removing hydroxyl, peroxyl and singlet oxygen in human body. It has been reported that uric acid also have the capability to react with ions like Fe^{2+} or Fe^{3+} (Filipe et al., 2001).

Melatonin, is also an important endogenous antioxidant in human body, is a

neuro-hormone, melatonin is almost exclusively produced by the photoreceptor cells (Liu et al., 2004). The amount of melatonin produced by the retina is small compared to that in the pineal gland, and retinal melatonin is thought to act as a local neuromodulator within the eye. It can scavenge $^1O_2$ and ^-OH. It has been shown that melatonin modulation of intraocular pressure (IOP), and it has been suggested that melatonin or melatonin analogs may be useful in the treatment of glaucoma (Belforte et al., 2010). Melatonin protects cultured RPE cells from oxidative stress and ischemia-induced cell death and delays photoreceptor degeneration in *rds* mutant mice (Osborne et al., 1998, Liang et al., 2004, Liang et al., 2001). It has been reported that daily administration of melatonin (3 mg) may protect the retina and delay the progression of age-related macular degeneration (AMD) (Rosen et al., 2009).

1.5.3 Antioxidants obtain from diet

Vitamin C (Ascorbic acid) is a water-soluble nutrient known to have antioxidant properties. It has also been shown to be a cofactor in the regeneration of Vitamin E in the retina (Stoyanovsky et al., 1995). Ascorbic acid can be deacidizing by NADPH and glutathione reductase. On the other hand, it can be a pro-oxidant in the presence of transition metals. Cho et al. reported it has a mild protective effect in the prevention of early AMD.

Vitamin E is a lipid-soluble antioxidant and has four common subtypes: α-tocopherol, β-tocopherol, δ-tocopherol, and γ-tocopherol. α-Tocopherol has been reported as the most effective antioxidant protects against lipid peroxidation among this group (Handelman et al., 1985) but can act as a pro-oxidant if there is transition metals presence. Vitamin E as a supplement was included in the Age-Related Eye

Disease Study trial.

Over 600 known carotenoids, only dozen can be found in the human body. Lutein and zeaxanthin are the only two that exist in the human retina. These retinal carotenoids have been shown to absorb blue light and serve to scavenge free radicals (Parker, 1989). β- carotene can quench singlet oxygen, the ability of quenching is higher than vitamin C and vitamin E.

Over the last century, flavonoids have been identified as the most common group of plant polyphenols that give colour and flavour to fruits and vegetables. Flavonoids can be classified into several subclasses, which include flavones, flavonols, flavanones, flavanols, isoflavones and catechins. Flavonoids are able to reduce the highly oxidizing free radicals (e.g. superoxide, peroxyl, alkoxyl and hydroxyl), resulting in more stable, less reactive radicals (Pietta, 2000, Nijveldt et al., 2001).

With this knowledge, before applying the catechins, we have to understand the physiological and chemical properties of catechins.

1.6 History and green tea ingredients

Green tea has been consumed as a beverage for thousands of years. It is mainly produced from freshly harvested leaves of *Camellia sinensis*, a small plant grown mainly in China and Southeast Asia, consumed predominantly in China, Japan, India, and some countries in North Africa and the Middle East. It is originated in southwest China 5000 years ago as a medicine. The brewed extract of green tea leaves contains carbohydrates, cellulose fibers, polyphenols, caffeine, amino acids, and vitamins.

Green tea is rich in polyphenolic which make up about 35% of the dry weight of green tea extract (GTE), polyphenols are the most biologically active substances present, capable of slowing or preventing the oxidation of other molecules.

Polyphenols are reducing agents, can help diminish the oxidative damage by acting directly on reactive oxygen species or stimulating endogenous defence systems. The phenols can accept an electron to form relatively stable phenoxyl radicals, therefore, disrupt chain oxidation reactions in cellular compounds.

Green tea contains large amounts of various flavonoids, which are characterized by the benzopyrane skeleton, with the pyrane ring bearing at least one aromatic ring. One of the major classes of flavonoids is catechins, which include (-)-epigallocatechin gallate (EGCG), (-)-epicatechin (EC), (-)-epigallocatechin (EGC), (-)-epicatechin gallate (ECG), EGCG is the most abundant of the catechins, accounts for 50-75% of the total amount of the catechins, other catechins, like (+)-catechin (C), (+)-gallocatechin (GC), (-)-catechin gallate (CG), and (-)-gallocatechin gallate (GCG) are only present in small quantities **(Figure 1.2)**. Catechins are synthesized via the malonic acid and shikmic acid metabolic pathways. The galloyl esters of catechins are synthesized by esterification with gallic acid. Both catechins and their esters possess strong anti-oxidant properties, especially EGCG. Green tea contains catechin- based flavonoids with EGCG being the most abundant and possessing the most potent antioxidative activity. Catechins are present in higher quantities in green tea as compared to black and oolong tea, due to the different methods of leave processing.

1.7 Biological effects of catechins

Catechins has been claimed to possess biological effects potentially beneficial to human health. Most of these functions are attributed to the multi-functional and multi-targeting properties of green tea catechins, such as metal chelation, anti-oxidation, anti-oxidation, cell signaling modifications, anti-angiogenesis,
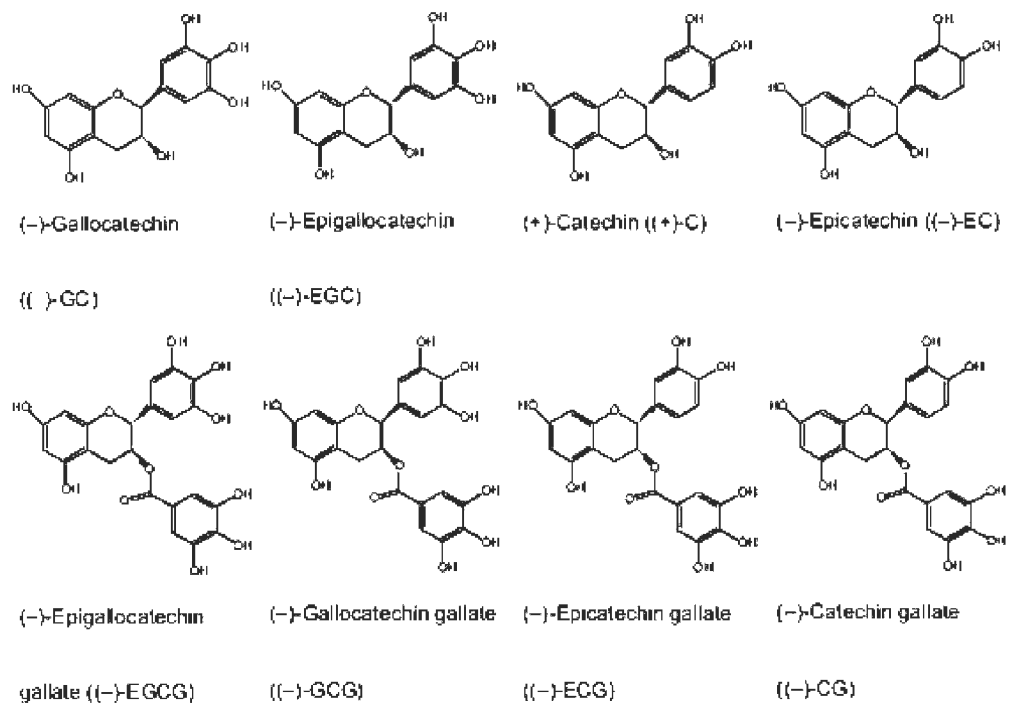
Figure 1.2 Chemical structures of Catechins.

(Picture modified from www.sciencedirect.com)

anti-microbial, anti-arteriosclerosis, anti-carcinogenesis, and anti-mutagenesis properties (Ahmad and Mukhtar, 1999). Catechins also has been studied extensively for their beneficial effects might be useful in the treatment and prevention of several chronic disease such as cancer, heart diseases, diabetes, obesity and neurodegenerative diseases (Higdon and Frei, 2003, Khan et al., 2006, Kuriyama et al., 2006).

Therefore, a better understand of mechanisms of catechins will provide a rationale way to the clinical development of tea polyphenol alone or combination strategies. The efficiency of polyphenols as antioxidant compounds mainly depends on their chemical structure. Reported studies have shown the capability of green tea catechins in anti-oxidation, cell signaling modification, and anti-microbial capabilities relevant to the treatment of ocular diseases.

1.7.1 Anti-Oxidant nature of catechins

Polyphenols in green tea extract, especially EGCG, have been found to act as free radical scavengers that neutralize free radical mutagens, prevent of formation of ROS. The polyphenolic structure of EGCG consists of 4 rings, A, B, C, D (**Figure 1.3**). A and C rings constitute benzopyran ring. The B ring of EGCG has vicinal trihydroxy group, the D ring galloyl moiety in EGCG is the form of an ester at C3. Many studies have demonstrated the strong antioxidant nature of EGCG is attribute to their polyphenolic structure, the presence of the meta-5,7-dihydroxyl groups on the A ring plays important role in their anti-oxidative action, the ortho-dihydroxyl and the ortho-trihydroxyl group in the B ring is essential for its scavenging properties (**Figure 1.4**). The B ring consisting of vicinal dihyoxy or trihydroxy groups is the
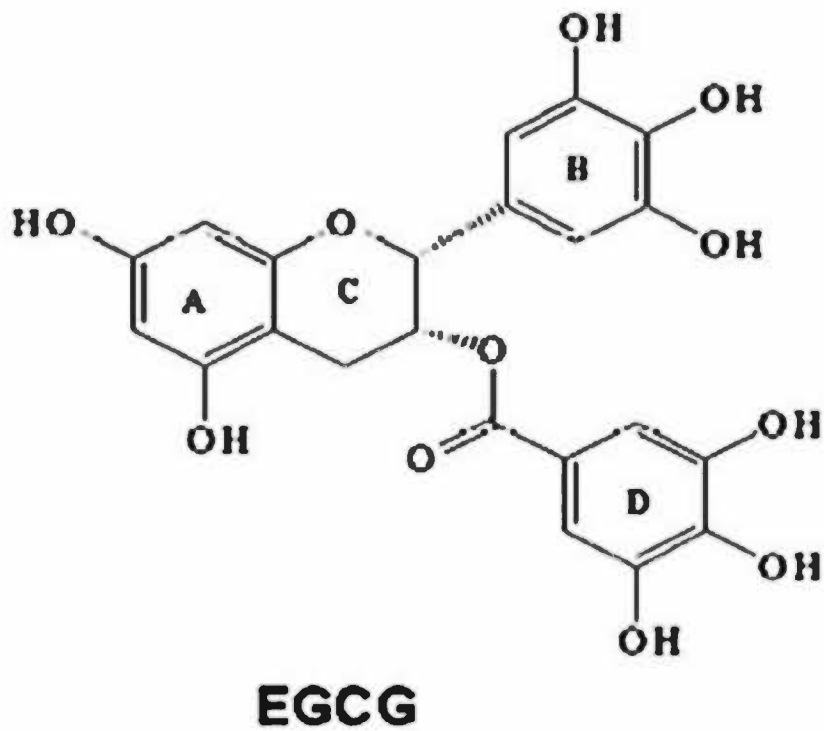
Figure 1.3 Chemical structure of EGCG.

(Picture from Kanwar J, Taskeen M, Mohammad I, Huo C, Chan TH, Dou QP. Recent advances on tea polyphenols. Front Biosci (Elite Ed). 2012 Jan 1;4:111-31.)
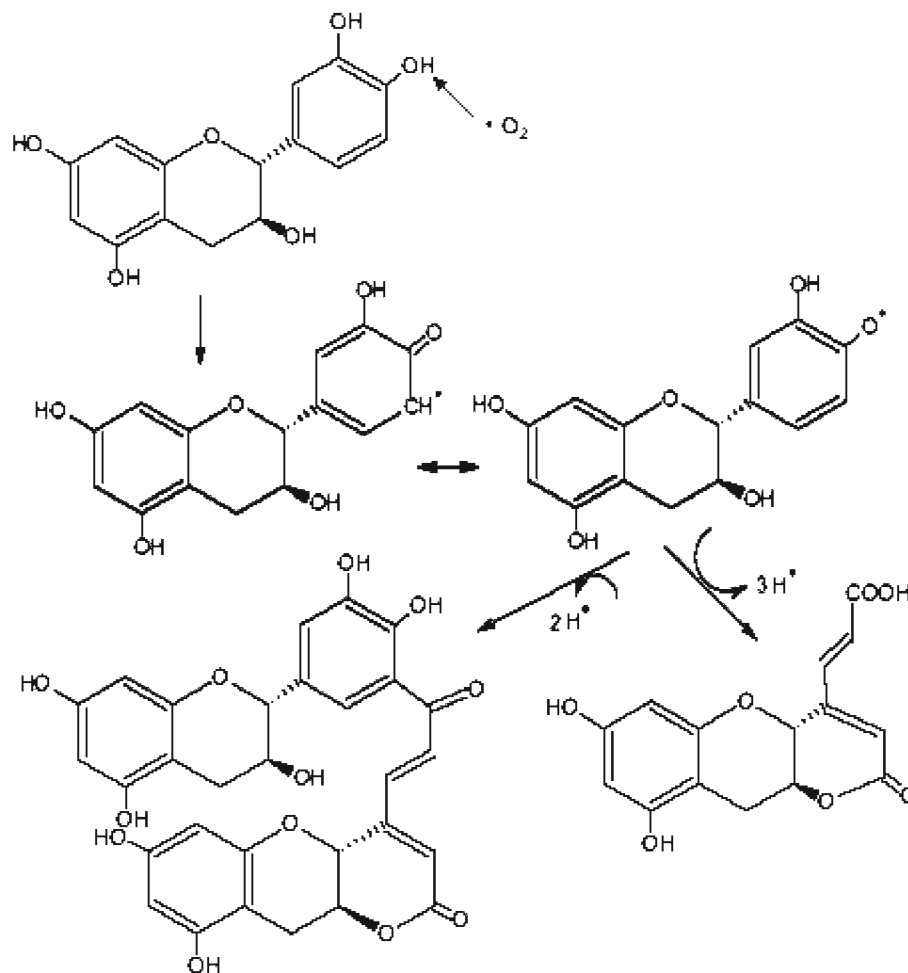
Figure 1.4 Schematic oxidation of catechin. Figure demonstrates how catechin neutralizes reactive oxygen species and propagates polymerization to a stabilized final product. (Picture from Chu KO, Yang YP, Wang CC, Pang CP. Biological effects of green tea catechins in ocular tissue cells. Tea in Health and Disease Prevention, 1st Edition. United States of America. 2012.p 1311.)

preferred site for antioxidation. In the polyphenols with the pyrogallol type B ring and/or galloyl group, electron-withdrawing substituents and/or intramoleular hydrogen bonding constituted structural against the antoixdation. The binding site for reactive carbonyl species is the A ring of the catechins, however, the preferred sites for the antioxidant activity is on the B ring. Scavenging properties can be further synergistically enhanced by the presence of other anti-oxidants with different solubility such as L-ascorbic acid and tocopherols. Moreover, EGCG can chelate catalytic metal ions and quench singlet oxygen (Kuo et al., 1998), preventing DNA damage from ROS. Catechins can scavenge ROS (Frankel et al., 1993) through inhibition of xanthin oxidase and nicotinamide adenine dinucleotide phosphate (NADPH) oxidase activities, activation of catalase and glutathione peroxidase activities. The ability of scavenge free radicals works well at acidic medium. EGCG is less stable in neutral and alkaline medium due to the hydroxyl groups on the phenyl ring are attacked by the basic medium results to the formation of a more active phenoxide anion.

1.7.2 Anti-angiogenesis effect

Vascular endothelial growth factor (VEGF) is a major angiogenic factor. It stimulates new blood vessels development from micro-vascular bed through increase vascular permeability, induce extracellular matrix degradation, and stimulate endothelial cell migrations and proliferation. The production of VEGF is redox status dependent (Frankel et al., 1993). Catechins have been reported possess the capability of scavenging ROS (Rosenkranz et al., 2002); inhibiting xanthin oxidase, and nicotinamide adenine dinucleotide phosphate (NADPH) oxidase activities; increasing catalase and glutathione peroxidase activity.

EGCG also can prevent Platelet Derived Growth Factor AB (PDGFAB) which induced by VEGF inhibit phosphorylation of p38 MAPK signaling (Masuda et al., 2002).

1.7.3 Cell signaling modification and mechanism of action

Catechins can interact with some important molecules or transcription factors which regulate cell signal transduction pathways play a key role in modifying different cellular functions. Catechins can affect various tyrosine kinase receptors and downstream or upstream their gene expression level, therefore, affecting cell proliferation, angiogenesis, and apoptosis.

1.7.3.1 Mitogen activated protein kinases (MAPK) and activator protein-1 (AP-1) inhibition

MAPKs can activates transcription factors like ERK and c-Jun which affect AP-1 gene expression leading to cell proliferation, migration, and apoptosis. Cells pre-treated with. EGCG can inhibit H_2O_2 induced phosphorylation of ERK 1/2, JNK, and p38 in oxidative stress model (Katiyar et al., 2001). The inhibition causes cells in G2 status. Topical application of catechins can inhibit UVB irradiation induced by ERK1/2, JNK, and p38 phosphorylation in fibroblasts (Bae et al., 2008). Thus it prevents dermal cells from apoptosis possibly through changing the balance of BAX/Bcl2 (Chung et al., 2003). Through inhibition of AP-1 transciption activity, catechins, especially EGCG, can inhibit tissue plasminogen activator (TPA) or epidermal growth factor (EGF) induced cellular transformation in epidermal cell (Kim et al., 2004). Therefore, catechins can modify cellular transformation, survival, differentiation, proliferation under stress.

1.7.3.2 Nuclear factor – kappa B inhibition (NF-κB)

NF-κB is a transcription factor involving inflammatory and innate immune responses. It is a sequence specific transcription factor sensitive to oxidative stress. NF-κB is found in the cytoplasm interacting with Iκ-Bα as an inactive form. Phosphorylation of Iκ-Bα causes its degradation and subsequently releasing NF-κB. NF-κB then translocates to the nucleus and induces the expression of more than 200 genes. Many of these genes suppress apoptosis and induce proliferation; it can bind to the promoter regions of genes relating to inflammation such as MEKK, IL-6, and TNF-α. EGCG inhibits NF-κB binding and phosphorylation to down regulate the inflammatory response through reducing the production of TNF-α, IL-6, and IL-8 (Shin et al., 2007). EGCG also suppress monocytes chemotactic protein-1 expression in endothelial cells (Hong et al., 2007). Through blocking Iκ-Bαphosphorylation, topical application of EGCG also suppress UVB damage of epidermal cells (Gupta et al., 2004).

1.7.3.3 Epidermal growth factor receptor (EGFR) inhibition

EGFR regulates cell proliferation and differentiation. EGCG inhibits phosphorylation of EGFR and EGF binding to EGFR. Thus, EGCG suppress its subsequent downstream signaling pathways (Chan et al., 2008). It prevents uncontrolled cell growth and metastasis (Hou et al., 2005).

1.7.3.4 Insulin-like growth factor (IGF)-1 inhibition

IGF is a complex system of peptide hormones, cell surface receptors, circulating binding protein. The isoforms -1, -2, can regulate cell proliferation, differentiation, and apoptosis. EGCG can inhibit IGF-1R and increase IGFBP-3 protein expression

decreasing the levels of mRNAs of MMPs-7 and -9 to suppress cell proliferation and differentiation (Shimizu et al., 2005).

1.7.3.5 Proteasome activities inhibition

Proteasome destroys intracellular proteins including cyclins, cyclin-dependent kinase inhibitors, p53, Bcl-2, and Iκ-Bαwhich involve cell cycle, apoptosis, and transcriptional regulation. Through inhibition of chymotryptin, catechin gallates such as EGCG and ECG accumulate p27 and Iκ-Bα to induce growth arrest in the G (1) phase of the cell cycle (Nam et al., 2001).

1.7.3.6 Matrix metalloproteinase (MMPs) inhibition

MMPs are zinc-dependent endopeptidase. They can degrade extracellular matrix (ECM). They involve various physiological and pathological conditions including inflammation, vascular, and autoimmune disorders, and carcinogenesis. They can alter cell-cell and cell-ECM interaction. They can facilitate cells go through tight basement membrane. Therefore, MMPs can promote angiogenesis stimulate growth, regulate innate immunity, and exhibit anti-apoptotic properties. EGCG can inhibit MMP-2 activity to prevent cells from invasion, migration, and G (1) to S phase cell cycles in vascular smooth muscles (Kim and Moon, 2005, Ho et al., 2007).

1.7.3.7 Urokinase plasminogen activator (uPA) inhibition

UPA can remove blood clots and stimulate angiogenesis. It can also help degrade and regulate basement membrane and extracellular matrix (Dass et al., 2008). EGCG can block urokinase catalytic triad to inhibit uPA activity. EGCG can also suppress VEGF, uPA, and angiopoietin 1 and 2 expression.

1.7.3.8 Induction of apoptosis and cell cycle arrest

Apoptosis involves in a series of biochemical events, resulting to a variety of morphological changes. It has been reported that EGCG inhibit the expression of anti-apoptotic proteins Bcl but increasing the expression of pro-apoptotic proteins Bax (Qin et al., 2007). EGCG can trigger the intrinsic apoptosis pathway by regulating the mitochondrial functions, activating the caspase-3 and caspase-9 (Roy et al., 2005).

EGCG can induce expression of p21 and p27 and inhibit CDK2 and CDK4 activity to negatively regulate cell cycle progression resulting in G0/G1 phase cell cycle arrest (Liang et al., 1999). Unlike other antioxidants, catechins not only can scavenge free radicals to against apoptosis, necrosis and uncontrolled cell cycling, but also can participate in the molecular regulatory process to attenuates oxidative stress induced apoptosis. EGCG can block the extracellular signaling by growth factors include EGF, PDGF, FGF binding to receptors and inhibit tyrosine kinase induced uncontrolled cell cycling; inhibits cyclin dependent kinases 2 and 4; down regulates nitric oxide (NO) synthase and NF-κB. So, EGCG can serve as inhibitor to inhibit tumor initiation and promotion.

1.7.4 Toxicity

Testing the safety and tolerability of a drug are very important issues before approval for clinical use. Green tea has a long history of use as a beverage is generally regarded as safe. Numerous human bioavailability and intervention studies using around 20~800 mg green tea preparations have report no severe side effects (Chow et al., 2006, Bettuzzi et al., 2006, Lee et al., 2002). Pro-oxidative effect of EGCG may underlie the observed toxicity. Laboratory studies of green tea

preparations in rodents revealed toxic effects at high doses (>1000 mg/kg) (Isbrucker et al., 2006). No significant damage was reported with 2% Polyphenon 70 S[TM] (Mitsui Norin Co., Ltd.) treated on mice for six months, a green tea extract which contains more than 70% catechins. In other studies, the LD50 of green tea polyphenols (Sunphenon with 60% polyphenols) was 3.1 g/kg for female and 5.0 g/kg for male mice. 75 mg/kg green tea extract was daily administrated on male mice for 88 days did not give any toxicity effect.

1.7.5 Effects of catechins on ocular tissue/cells

Oxidative stress has been contributed to many pathogenesis of the common eye diseases, anti-oxidants have been widely used to protect against oxidative damage, including lutein, vitamin C, zeaxanthin, and vitamin E. But, their prophylactic and protective effects are not so effective. A great number study have shown the capability of GTE and catechins in antioxidation effect, cell cycle arrest and induction of apoptosis, anti-microbial activities and affect transcription factors which are relevant to treat retinal degeneration and inflammation in the eye. It is possible because they have several biological effects on ocular tissue cells and plenty studies have proved this. The natural product EGCG is an abundant and major active component in GTE, account for more than 50-75% of the total amount of catechins in GTE preparations. It is responsible for most of the potential health benefits of green tea. Up to now, a literature search on PUBMED shows that more than 10,000 reports have been published refers to the area on the effects of the chemistry, bioactivity, production, and health benefits of green tea. Over 4,000 publications on EGCG (Nagle et al., 2006).

1.7.5.1 The reported effect of EGCG in retinal pigment epithelial (RPE) cells

RPE plays an important role in maintenance the proper function of the neural retinal. It is a polarized, pigmented, cuboidal epithelial cell layer situated between the photoreceptors and choroidal vasculature in the outer retina. It delivers glucose consumed by the neural retina, performs various functions crucial for retinal homeostasis, including delivery amino acids and docosahexaenoic acid for metabolic mechanisms essential for phototransduction; maintenance of the blood retinal barrier; secretion of growth factors.

Oxidative stress damages the RPE and subsequently cause photoreceptor degeneration plays a significant role in the pathogenesis of AMD and retinitis pigmentosa. Exposure to solar ultraviolet can cause damage to RPE cells because it may generate ROS. Studies have shown that EGCG, even at 1 μM, inhibits ultraviolet irradiated intracellular H_2O_2 in RPE cells in a concentration-dependent manner, and 10μM produced a marked effect (Chan et al., 2008).

RPE cells can initiate cell proliferation, migration and secrete extracellular matrix (ECM) as seen in some retinal diseases such as proliferative vitreoretinopathy (PVR), proliferative diabetic retinopathy (PDR). It has reported that EGCG is effective in inhibiting RPE cell proliferation and migration (Peng et al., 2010). Chan et al. found that EGCG can inhibit RPE cell migration through by preventing platelet-derived growth factor (PDGF)-BB and RPE cell adhesion to fibronectin in a dose-dependent manner. The inhibition of EGCG does not directly binding to the PDGF-BB but involves inhibition of phosphorylation of PDGFR-βreceptors, downstream molecules like PI3K/Akt and Mitogen-activated protein kinase (MAPK) phosphorylation. EGCG also inhibited fibronectin-induced cytoskeletal reorganization of RPE cells essential for migration processes (Peng et al., 2010). Moreover, another study also

investigated the inhibitory effect of EGCG on proliferation in PVR of human retinal pigment epithelial cells by using the ARPE19 cell line and human RPE cells, EGCG inhibited cell proliferation showed induced the least cell death when compare to the resveratrol and the curcumin (Alex et al., 2010). EGCG, at 100 μM, inhibited cell proliferation without inducing significant toxicity to the cell as proved by flow cytometric, and apoptosis assay (Alex et al., 2010). This provided the evidence that polyphenols may aid treatment of PVR and PDR.

1.7.5.2 The protective effect of EGCG on retinal degeneration

Several group studies have indicated that intravitreal injection of oxidants such as sodium nitroprusside, which effectively generate nitric oxide into the eye of the rat, caused specific photoreceptor degeneration, while other layers of the retina were unaffected (Zhang and Osborne, 2006). Combination of 15 μM EGCG and 100 μM sodium nitroprusside , the detrimental effects to the photoreceptor induced by the SNP was significantly blunted as shown by using histological, electroretinogical **(Figure 1.5)** and biochemical methodologies; expressions of photoreceptor-specific markers, such as RET-P1, rhodosin kinase; the apoptosis marker caspase-3.

Moreover, Zhang et al. induced ischemia and reperfusion in rats' eyes (Zhang et al., 2007). Ischemia was delivered by increasing the intraocular pressure higher than the systemic blood pressure, sustained for 45 minutes. EGCG was delivered using two approaches; 25 mg/kg EGCG intraperitoneally injected before ischemia and 5 μl of 200μM EGCG intravitreally injected, giving the final vitreous concentration is 10 μM after ischemia; in another experiment, 25 mg/kg EGCG intraperitoneally injected two days before and after ischemia. The ischemic damage was reduced in retinal ganglion cells (RGCs) as proved by photoreceptor-specific proteins, retinal glial
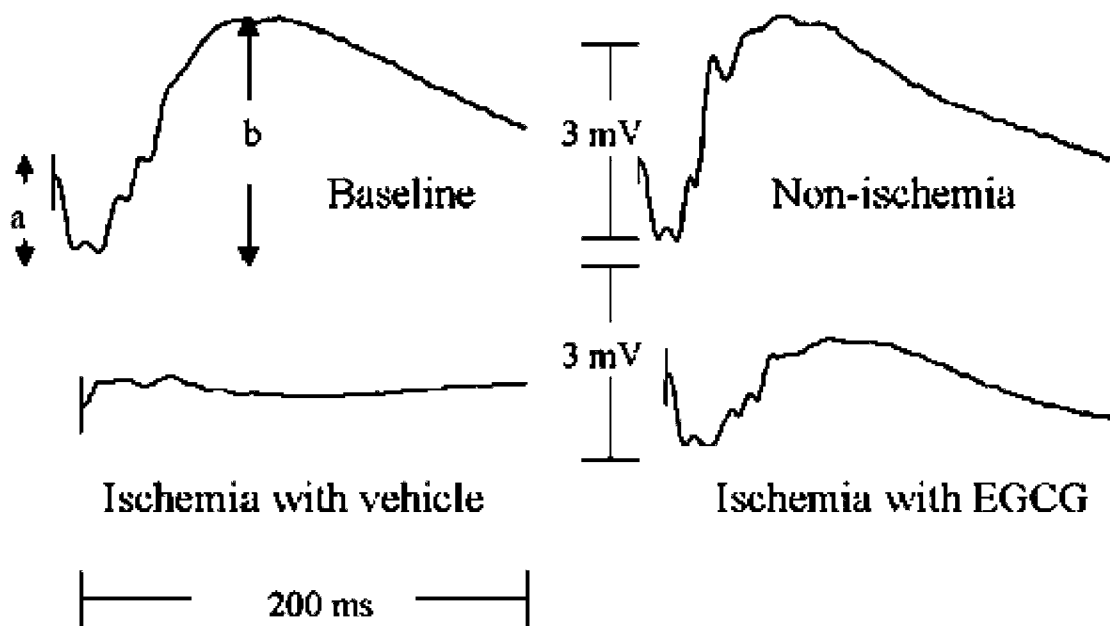
Figure 1.5 Electroretinograms (ERG) of rat eyes after ocular ischemic/reperfusion insult with EGCG treated. The a- and b-wave amplitudes of the ERGs were drastically reduced after ischemia/reperfusion, however, these were alleviated significantly when treated with EGCG. Individual characteristic ERGs recordings showed that a control eye taken before ischemia (baseline) and after ischemia almost identical. The wave was much affected by ischemia but less affected in rats treated with EGCG. (Picture from Zhang B, Safa R, Rusciano D, Osborne NN. Epigallocatechin gallate, an active ingredient from green tea, attenuates damaging influences to the retina caused by ischemia/reperfusion. Brain Res. 2007 Jul 23;1159:40-53.)

fibrillary acidic protein (GFAP), mRNA levels were attenuated by EGCG seven days after ischemia significantly (Zhang et al., 2007). The thickness of the inner plexiform and inner nuclear layer became thinner caused by ischemia were also blunted by the EGCG administrated.

In in vitro studies, 10 μM EGCG significantly blocked RGC-5 cell death caused by 400 μM H_2O_2-induced oxidative stress. EGCG blunts the influence of H_2O_2 and inhibits intracellular H_2O_2 generation, against apoptosis and the generation of ROS (Zhang and Osborne, 2006).

1.7.5.3 EGCG against human lens epithelial cells (HLE) from oxidative stress

Oxidative stress has been reported as a major factor to induce human lens epithelial cells apoptosis and also considered as an important mediator in the pathogenesis of cataracts. Yao et al. used HLEB-3, a human lens epithelial cell line, was exposed to different concentrations of H_2O_2 and EGCG, subsequently assessed cell death by cell viability assay; apoptosis effect was using flow cytometric analysis with Annexin V and propidium iodide (PI) (Yao et al., 2008). The ability of EGCG to protect HLE cells against apoptosis, which was caused by accumulation of intracellular ROS and the loss of mitochondrial membrane potentials induced by H_2O_2, was determined by dichlorofluorescein (DCF) fluorescence and 5,5',6,6'-tetrachloro-1,1',3,3'-tetrathylben-zimidazol carbocyanine iodide (JC-1).

EGCG blocked the loss of mitochondrial membrane potential and the release of cytochrome C from mitochondria into the cytosol, EGCG inhibited H_2O_2-induced caspase-9 and caspase-3 expression, and the decreased of the BCL-2/Bax ratio. EGCG also can activate the mitogen-activated protein kinase (MAPK), p38 Mitogen-activated protein kinase, and extracellular-signal-regulated kinases (ERKs)

activities (Zhao et al., 2011).

1.7.5.4 Reported anti-angiogenesis effect of catechins

Cao et al. in 1998 has been reported that EGCG suppresses endothelial cell growth in in a dose-dependent manner. This coincided with the studies EGCG against VEGF-induced endothelial cell proliferation and migration by a scratch-wound model in human umbilical vein endothelial cells (HUVECs) (Cao et al., 2010) **(Figure 1.6)** and suppressed endothelial cell growth and formation in chick chorioallantoic membrane. In one study, it has already reported EC, EGC, ECG and EGC also can inhibit angiotensin- converting enzyme (ACE) activity that increased nitrogen oxide (NO) production in a dose-dependent manner by using HUVEC model **(Figure 1.7)** (Persson et al., 2006).

1.7.5.5 Reported anti-inflammation and anti-microbial action of EGCG in corneal epithelium

The corneal epithelium act as physical barrier to infection and insult, and involve in the ocular immune response by generating cytokines. Ocular surface inflammation included the appearance of pathogens, allergic, and dry eye. While inflammation cytokines and hyperosmolarity of the tears plays a key role in the dry eye disease.

In the in vitro study, human corneal epithelial cells (HCEpiC) were challenged with interleukin-1b (IL-1b) for 18 hours or hyperosmolarity (440 mOsm) for 24 hours to induce corneal inflammation (Cavet et al., 2011). Application of EGCG at doses from 0.3-30 μM caused a dose-effect suppression phosphorylation of MAPKs p38, c-Jun- N-terminal kinase (JNK), and transcription factors sun as nuclear factor kappa B (NF-kB) and activator protein-1 (AP-1) which regards as an important

A

Toxicity assay

EGCG

Viability ratio vs Time (days)

- ◆ Control
- ● EGCG 10 μM
- ▲ EGCG 50 μM
- ✕ EGCG 100 μM

B

HUVEC migration assay

EGCG

Cells / mm² area vs Time (hours)

- ● VEGF
- ● VEGF + EGCG 10 μM
- ▲ VEGF + EGCG 20 μM
- ✚ VEGF + EGCG 50 μM
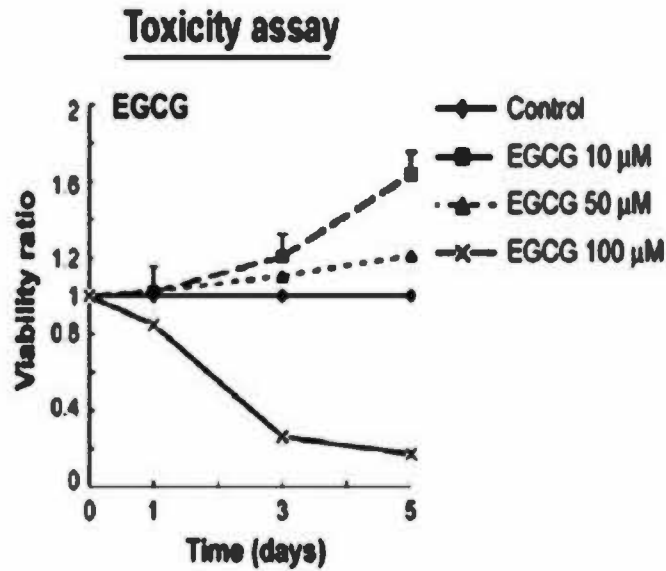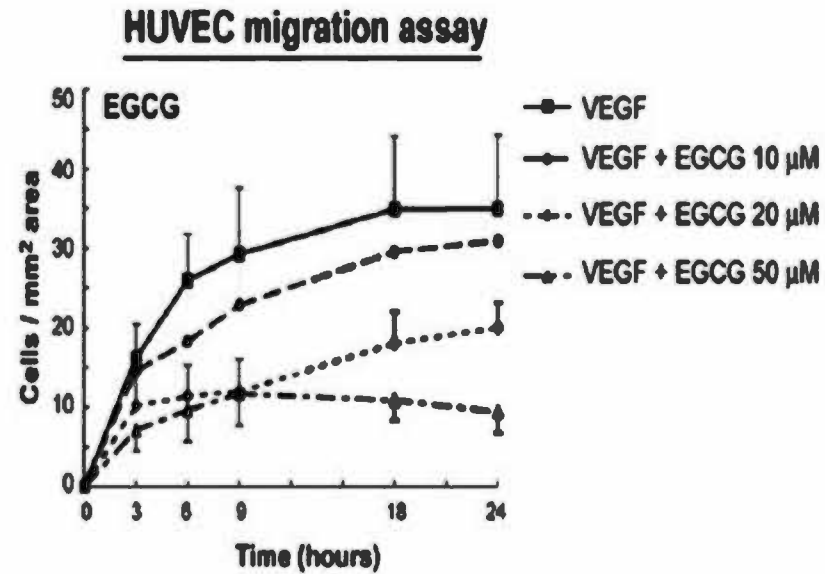
Figure 1.6 Viability and Migration Tests on ARPE19 Cells with. ARPE19 cell viability after treatment with various Concentrations of EGCG (0-100μM) (A). Investigate HUVEC proliferation and migration after treatment with EGCG (0-50 μM) by using scratch-wound model (B). (Picture from Cao L, Liu H, Lam DS, Yam GH, Pang CP. In vitro screening for angiostatic potential of herbal chemicals. Invest Ophthalmol Vis Sci. 2010 Dec;51(12):6658-64.)
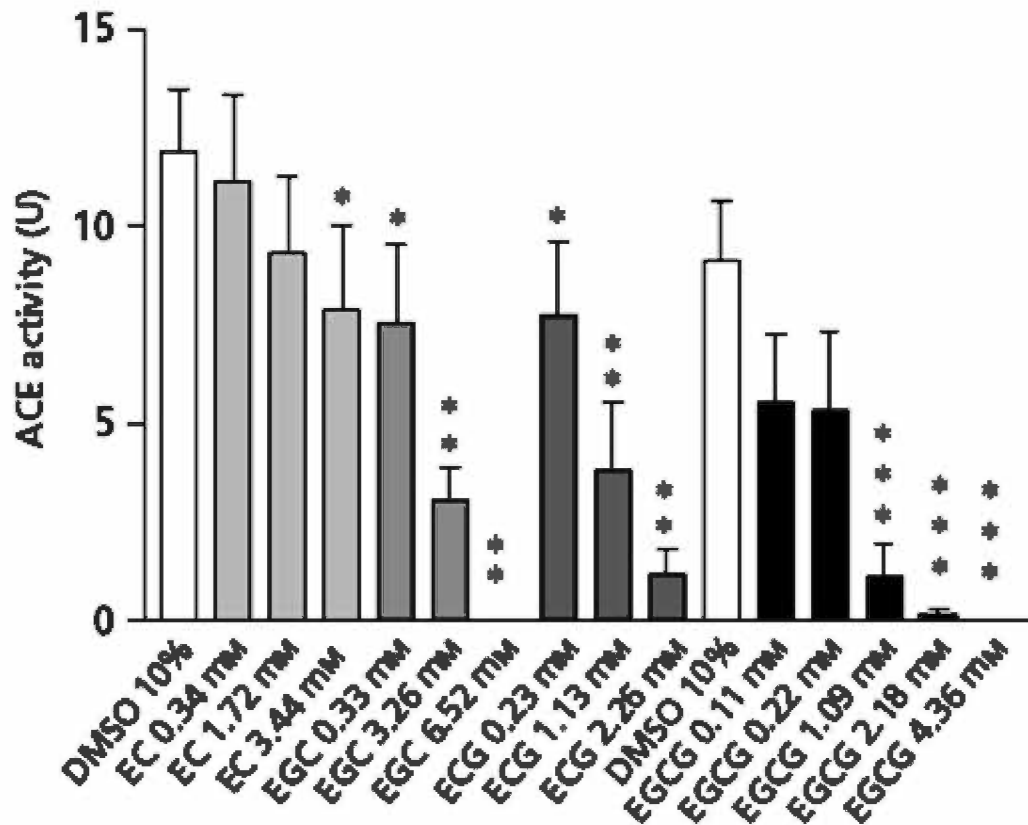
Figure 1.7 Angiotesin-converting enzyme activity in HUVEC. After 10 minutes incubation with: EC n=6; EGC, n=6; ECG, n=6; or EGCG, n=8. *P<0.05, **P<0.01 and ***P<0.001. (Picture from Persson IA, Josefsson M, Persson K, Andersson RG. Tea flavanols inhibit angiotensin-converting enzyme activity and increase nitric oxide production in human endothelial cells. J Pharm Pharmacol. 2006 Aug;58(8):1139-44.)

mediator in the inflammatory response. It also inhibited glucose oxidase-induced ROS levels in dose-dependent manner. So, EGCG may act as anti-inflammation and anti-oxidant potential drug for therapeutic HCEpiC in ocular inflammation such as dry eye.

Bacterial conjunctivitis and keratitis are common ocular infections. Bacterial strains such as Staphylococcus aureus, Pseudomonas aerugenosa, Streptococcus are among the most common bacteria isolated from ocular infections. Bacterial invasion involves cells move to the affected area, and proteolysis for inner tissue spreading. Some kinds of bacteria produce gelatinase that acts as a protease, causing hydrolysis of the peptides in structural proteins and hence leading to breakdown of the host's tissue cells and allowing the bacteria to spread. EGCG inhibits the metalloproteases and gelatinase activities (Garbisa et al., 2001). EGCG inhibit bacterial gelatinase with an IC50 at about 0.2 mM and limit gelatinase-positive bacteria invasion at about 2 mM (Blanco et al., 2003). EGCG inhibit the biofilm formation in an ocular staphylococcal isolation at sub-microliter (250-500 μM) level, suggesting that EGCG inhibit pathogen adhesion to the ocular surface these might attribute to the inhibitory of bacterial growth or slime production (Blanco et al., 2005).

1.8 The mechanisms of sodium iodate as retinotoxin

Systemic administration of sodium iodate ($NaIO_3$) has been widely reported it selectively impair the retinal pigment epithelial (RPE) by oxidative stress, resulting in patchy loss of RPE and subsequent degeneration of photoreceptors (Kiuchi et al., 2002). Why sodium iodate has selective effect on RPE cells may due to several mechanisms. First, $NaIO_3$ inhibits enzyme activities of RPE cells. such as triose phosphate dehydrogenase (Ashburn et al., 1980), succcinodehydrogenase, lactate

dehydrogenase (Birrer, 1970). Sodium iodate damages the anionic sites on the basal membrane, lead cell organelles swelling, loss of apical microvilli, and then finally cause RPE cells necrosis. So, the junction between RPE and Bruch's membrane is became loose (Yoon and Marmor, 1993). Second, the sodium iodate destroys the blood-retina-barrier by affecting the zonula occludens (Konda et al., 1994). Finally, the inner/outer segment of photoreceptor become disorganized, and photoreceptor cells degenerated, and the choriocapillaris are atrophies (Anstadt et al., 1982). Third, a chemical reaction between the sodium iodate and melanin, melanin, absorbs scattered light, which otherwise disturb visual acuity, and in cooperation with various anti-oxidative enzymes protects against reactive oxygen species produced by phagocytosis of photoreceptors (Miceli et al., 1994). Sodium iodate can increase the ability of melanin to affect the glycine to glyoxylate. Melanin is the source of the zinc and plays a key role in the retina metabolism (Schraermeyer and Heimann, 1999). So, sodium iodate is a potentially cell toxic compound (Baich and Ziegler, 1992). However, this chemical reaction was suggested as a partial explanation to the specificity of iodate toxicity to the RPE and photoreceptor.

1.8.1 Reported activities of sodium iodate-induced retinal degeneration

Systemic administration of different dosages of sodium iodate has been used in various of rodents (I have summarized as seen in **Table 1.1**) to evaluate the effect on visual function (Enzmann et al., 2006, Franco et al., 2009), retinal morphology (Kiuchi et al., 2002) and other functional features (Machalinska et al., 2010). Sodium iodate-induced retinal degeneration in rats was employed as an animal model to explore the capability of stem cells in differentiation into RPE and photoreceptors

Table 1.1 Reported activities of sodium iodate-induced retinal degeneration

No.	Author	Journal	Year	Model(s)	Assessments	Dosage of sodium iodate	Activities to report
1	Ohtaka *et al*	Curr Eye Res	2006	SD rats 5 weeks old	Histology, ERG, Immunohistochemistry	40 mg/kg, caudal vein injection	Intra-vitreal injection of HGF significant protection against photoreceptor and RPE degeneration induced by systemic administration of NaIO3.
2	Gong *et al*	Clin Experiment Ophthalmol	2008	Wistar rats 3 week old	Histology	40 mg/kg, caudal vein injection	Bone marrow MSCs transplanted into the sub-retinal space of sodium iodate-injected rats have the ability to differentiate into RPE, photoreceptor and glial lineage cells.
3	Machalin′ska *et al*	Neurochem Res	2010	C57BL mice	Histology,ERG, TUNEL assay	40 vs. 20 mg/kg, orbital venous plexus inection	Peripheral area of the retina reveals better resistance to NaIO3 injury than its central part.
4	Luisa et al	Invest Ophthalmol Vis Sci	2010	C57BL mice	Histology, Immunohistochemistry	15, 25, 35 mg/kg , i.v. injection	RPE necrosis was observed with a low concentration of NaIO3.
5	Enzmann *et al*	Expe Eye Res	2006	C57BL mice	Histology, behavioral testing	35, 50, 75 mg/kg, i.v. injection	NaIO3 can produce permanent deficits in retinal morphology and visual function.
6	Kiuchi *et al*	Curr Eye Res	2002	C57BL mice	Histology, TUNEL assay Immunohistochemistry	100 mg/kg, i.p.injection	Retinal toxicity evoked by NaIO3 was characterized by RPE cell necrosis followed by photoreceptor cell apoptosis
7	Yoon *et al*	Ophthalmic Res	1993	Rabbit	Electron microscopy	i.v. 20 mg/kg	Large patches of RPE separated, adhered to peeled retina
8	Nilsson *et al*	Acta Ophthalmol	1977	Sheep	Histology	i.v. 30 mg/kg	RPE swollen and ruptured, c-wave was abolished immediately
9	Kiryu *et al*	Vision Res	1992	Cat	Histology, ERG	i.v. 30 mg/kg	Change in the c-wave amplitude

after transplantation into the subretinal space (Enzmann et al., 2003, Gong et al., 2008), and investigate the protective effect of hepatocyte growth factor against retinal degeneration (Ohtaka et al., 2006). Sodium iodate-induced retinal degeneration is also reported in rabbits (Grignolo et al., 1966, Suyama, 1967, Flage, 1983, Yoon and Marmor, 1993) and sheep (Nilsson et al., 1977a). The sodium iodate causes retina degeneration in sheep through disrupture of basal membrane, swelling of intracellular organelles. In rabbit, within 7 hr after injection, changes are observable in the ultrastructure of the retinal pigment epithelium; 10 hr after injection, all the cells of the pigment epithelium are severely damaged, and irregularities of the outer segments of the receptors can be detected; after 15 hr injection of iodate, regeneration of rhodopsin is severely impaired. After several days, the pigment epithelium and outer segments of the receptors show gross degeneration (Clifton and Makous, 1973). In cat, the amplitude of the c-wave decreased in ERG (Kiryu et al., 1992), subsequently followed by: the severe atrophy of the choriocapillaris (Korte et al., 1984), the a-and b-waves, which represent the neural retina, were decreased significantly (Hosoda et al., 1993), considered as the retinal photoreceptor degeneration (Nilsson et al., 1977b).

Although a great number of previous studied have shown the consistency of the sodium iodate causes RPE and photoreceptor degeneration, the mechanism of how $NaIO_3$ affect the RPE neural retina damage, the reasons are not fully understand some issues remain have to investigate. These include: Traditional assessments in sodium iodate induced retinal degeneration are based on electrophysiology and histological staining. Electrophysiology can be monitored longitudinally; however, cellular changes in the retina are not visible. Histological staining enables clear

assessment on retinal structures; however, animals are sacrificed and a large number is needed for longitudinal study. Therefore, development of an in vivo longitudinal assessment method is needed, especially for stem cell and drug therapeutic.

To fill these gaps in our understanding of $NaIO_3$-induced retinal degeneration, we examined the effects of four concentrations and several post injection time points on both intraperitoneal and intravenous injection retinal morphology in adult Sprague-Dawley rats. In addition, we assessed retinal layer changes in histological preparations were correlated with that in confocal scanning laser ophthalmoscopy (CSLO) and Spectral domain optical coherence tomography (OCT) images. Although the mechanism of the RPE cell death and neural degeneration in the sodium iodate model may different from that patient suffer from the outer retinal degenerative diseases in clinic, the presentation of the RPE and the photoreceptor degeneration might be similar. Therefore, sodium iodate induced retinal degeneration can be used as a reliable model for studying human retinal degenerative diseases which RPE and photoreceptor degeneration are involved in.

1.9 Confocal scanning laser ophthalmoscopy and Spectral domain optical coherence tomography

The confocal scanning-laser ophthalmoscopy (CSLO) provides predominantly surface information but has a very restricted depth resolution. CSLO is a noninvasive imaging technique that allows examination of specific tissues and retinal layers and of their vascular structures in the human and rodent retinas. CSLO imaging was performed with a commercial scanning laser ophthalmoscope (HRA2; Heidelberg Engineering GmbH, Dossenheim, Germany). The confocal diaphragm of the CSLO allows the visualization of different planar images of the posterior pole, ranging from

the surface of the retina to the RPE even the choroid. The HRA features to argon wavelengths (488 nm excitation, 795 nm detection), barrier filters at 500 nm and 810 nm. **Figure 1.8** shows a schematic diagram of a CSLO.

Spectral domain optical coherence tomography (OCT) is a non-invasive technique for in vivo cross-sectional imaging of the retina (Huang et al., 1991). The OCT has several advantages for visualizing retina layers in animal models mimic ocular diseases. It can provide histology- homologous sections so that the researchers can do the correlation of the in vivo images with the histology sections at the same retina. This is very important and useful for longitudinal investigate the retina changes and also essential for the quantification analysis of localized lesions and degeneration profile in each retina layer. The histological sections can be replaced by the in vivo images in some situations, so it decreased the number of the animals to be sacrificed. The OCT images also help to determine when is the optimal time point to sacrifice the animal to get the traditional histological sections for progressive study. So, the OCT can serve as an important tool for the in vivo investigate retina changes of eyes. The Spectral domain optical coherence tomography could be useful in retinal degeneration studies as a noninvasive tool for investigating cell death in vivo since it has been demonstrated recently that cell apoptosis and necrosis cause changes in the tissue optical reflectivity parallel layers, all intra-retinal layers are clear visible in the saline retina.

The OCT is based on light reflectivity, light shade means weak reflectivity, and dark shade represents strong reflectivity. Retinal layers with much membrane and less optical dense are presented as a darker shade, for example plexiform and nerve-fiber layers appeared as dark in OCT images, retinal layers with more optically dense and less membrane are present as light shade, such as the outer nuclear layer,
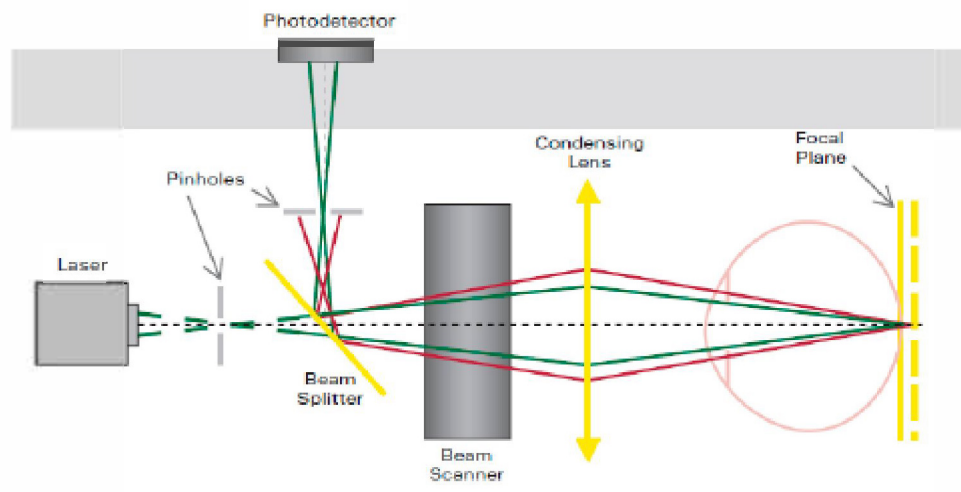
Figure 1.8 Schematic diagram of a confocal laser scanning ophthalmoscope.

(Picture from Rasta SH, Manivannan A, Sharp PF. Spectral imaging technique for retinal perfusion detection using confocal scanning laser ophthalmoscopy. J Biomed Opt. 2012 Nov;17(11):116005.).

inner nuclear layer appeared as light in OCT images (Fischer et al., 2009).

This technique has been used to examine real-time longitudinal changes in the retina of mutant mice with photoreceptor degeneration (Ruggeri et al., 2007, Fischer et al., 2009), and in mice with intravitreal injection of NMDA (Nakano et al., 2011). Spectral domain OCT was also employed to investigate degenerative changes in outer retinal layers in transgenic rabbits (Muraoka et al., 2012) and in rats with sodium iodate induced retinal lesion (Hariri et al., 2012). Although this imaging technique provides important information on the site of lesion within a confined area of the retina, information on whether the lesion is widespread throughout different areas of the retina and quantification of the damage across different retina quadrants is difficult. A few studies now using OCT to assess the retinal layer changes in rodents, but no study have combine the planar images by using confocal scanning laser ophthalmoscopy (CSLO) with the cross sectional image spectral domain optical coherence tomography at the same time. We report here a novel method for assessment of retinal lesion induced by sodium iodate in the adult rat based on confocal scanning laser ophthalmoscopy (CSLO) and OCT, which allows simultaneous take Spectralis HRA + OCT registers the CSLO and OCT images in the retina simultaneously evaluation of damage across the retinal layers and different quadrants of the retina.

Based on the literature review how can we perform a green tea study on oxidative stress model? Give an summary of reported green tea extract and catechins studies showed that the most effective and safe dosages of EGCG for their anti-oxidative effect and angiogenesis inhibition in different ocular disease models were usually from range 10 to 50 µM. In the physically normal situation, after drinking two cups of green tea, the EGCG level in plasma is 0.17 µM. In our previous

pharmacokinetics studies, we used 550 mg/kg green tea extract (Sunphenon®DCF-1), fed intra-gastrically to the adult Sprague-Dawley rats, equivalent to drink 10 cups of green tea. The maximum level of EGCG we measured was about 0.3 μM in plasma, 0.25 μmol/kg in the retina **(Figure 1.9)**. In plasma, retina, lens, cornea, the highest concentration level was within two hours after GTE administration.

According to the 8-isoprostane level results, the oxidative level was decreased in different ocular compartment after the 550 mg/kg GTE administration **(Figure 1.10)**. It is detectable that normal physical levels after the GTE administration can be able to produce anti-oxidative effects against oxidative stress. This effect might be attributing to the synergistic of the different catechins in this GTE. Moreover, the GTE may indirectly lower the oxidative level. So, we want to investigate the anti-oxidative properties of GTE, different catechin combinations and purified catechins EGCG in oxidative stress condition to verify their anti-oxidative effect.

Figure 1.9 Profiles of catechins in ocluar compartments. Figure shows the profiles of total catechins and their gallate esters (free and conjugated) changes in (a) plasma,(b) retina, (c) lens, and (d) cornea after 550 mg/kg GTE treatment (n = 6). The profiles in the compartments were divided into two groups according to the presence of gallate derivatives. Error bar represents standard derivation. (Picture from Chu KO, Chan KP, Wang CC, Chu CY, Li WY, Choy KW, Rogers MS, Pang CP. Green tea catechins and their oxidative protection in the rat eye. J Agric Food Chem. 2010 Feb 10;58(3):1523-34.)

(a) Plasma catechin group / Catechin gallate group

(b) Retina catechin group / Catechin gallate group

(b) Retina catechin group / Catechin gallate group

(c) Lens catechin group / Catechin gallate group

(d) Cornea catechin group / Catechin gallate group
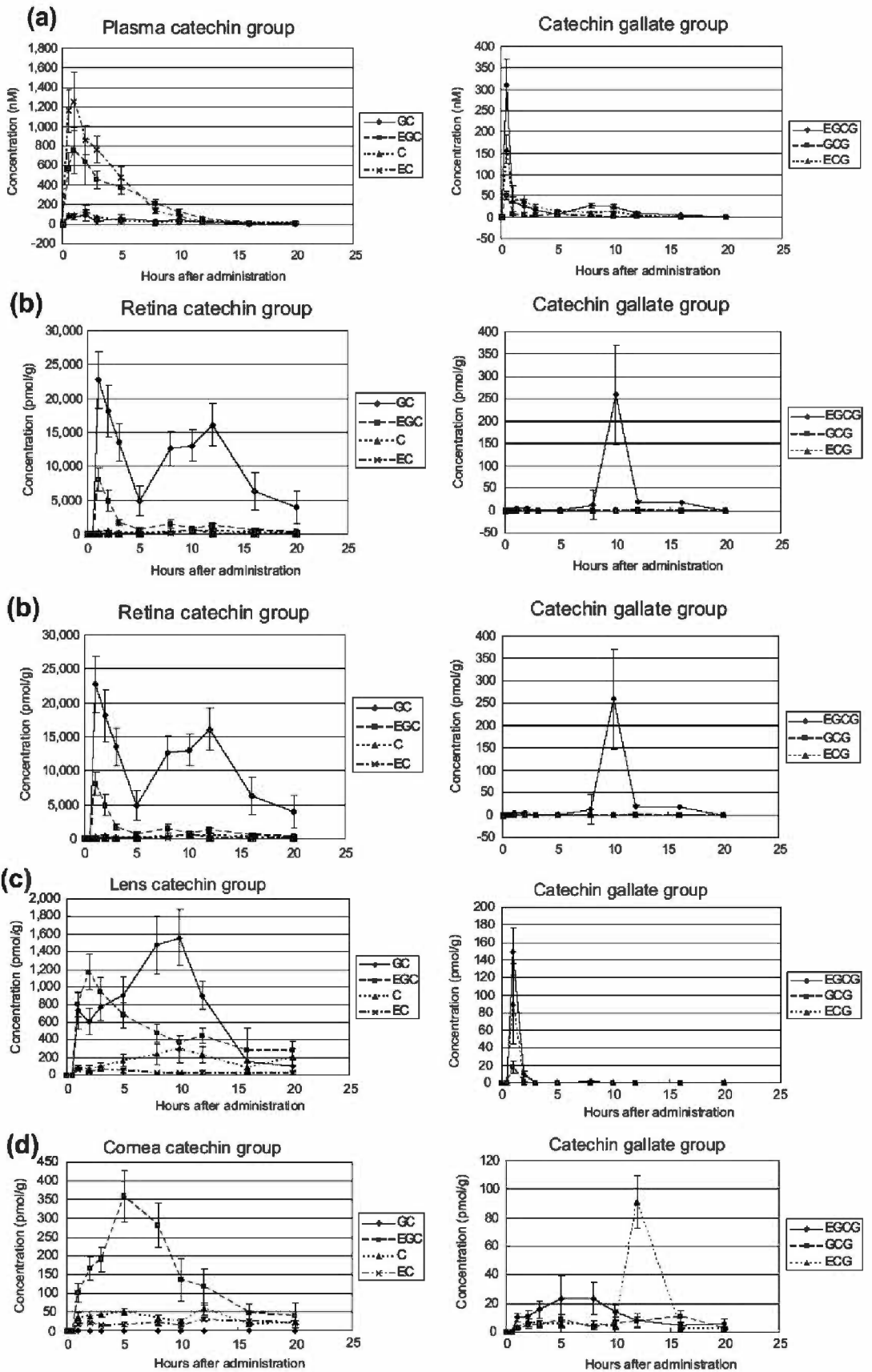
Figure 1.10 Profiles of 8-Isoprostane in different compartments. Shows the profiles of 8-iso-PGF2a in (a) plasma, (b) retina, (c) lens, and (d) cornea. We compared 8-epi-isoprostane levels at time zero to the first minimum level. c and d show that isoprostane levels in these regions rapidly and significantly reduced ($p < 0.001$, $n = 6$) and remained at low levels. b showed isoprostane level slowly and significantly decreased to a minimum level in the retina ($p < 0.05$, $n = 6$) but gradually increased back. No significant decrease in level was found in plasma (a). Error bar represents standard derivation. (Picture from Chu KO, Chan KP, Wang CC, Chu CY, Li WY, Choy KW, Rogers MS, Pang CP. Green tea catechins and their oxidative protection in the rat eye. J Agric Food Chem. 2010 Feb 10;58(3):1523-34.)

(a) Plasma

(b) Retina

(c) Lens

(d) Cornea

44
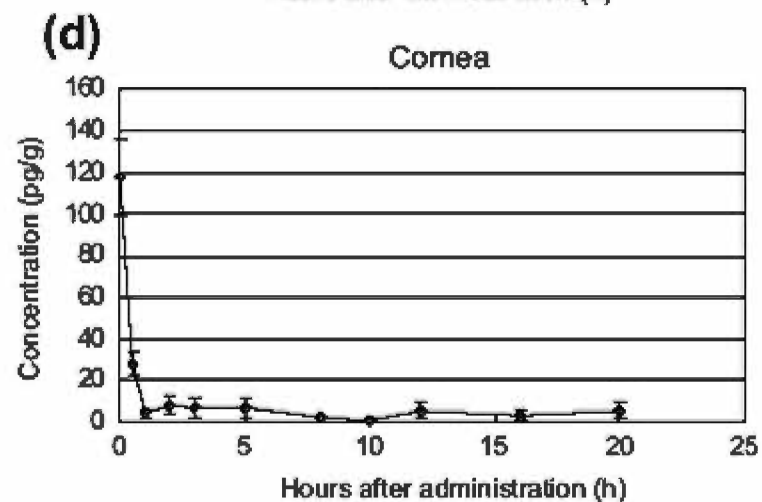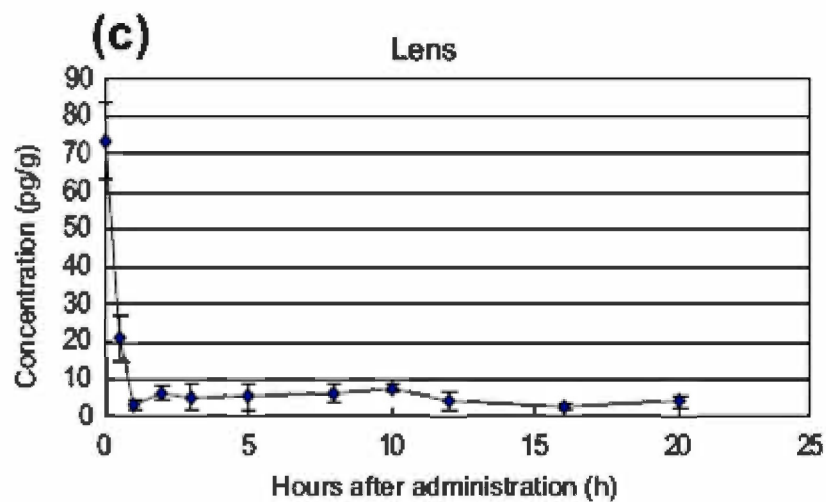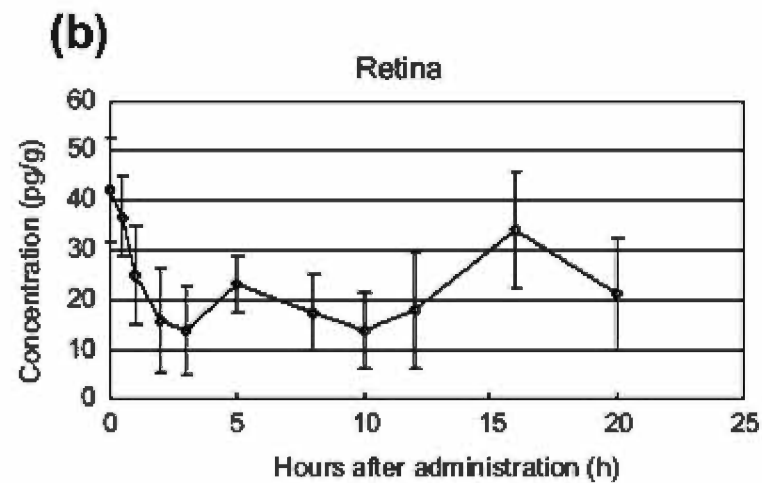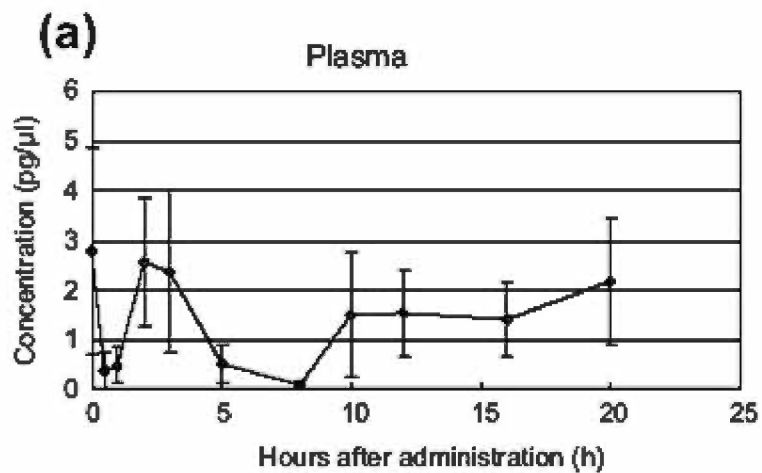
Chapter 2: Objectives and study design

The objectives of this research project

(1) To test the rat ocular uptake and distribution of GTE (Theaphenon®E) in plasma, vitreous, and retina.

(2) EGCG, catechins combination (EGCG, EC, EGC, and GC), catechins combination (GC, EGC, and EC), and the GTE preparation, Theaphenon®E, will be fed to the adult Sprague-Dawley rats in an attempt to against oxidative stress-induced retinal degeneration induced by sodium iodate.

Study design

(1) In healthy adult Sprague-Dawley rats, the rats were randomly assigned to 9 groups: viz. 0, 0.5, 1, 2, 4, 6, 10, 15, 20 hours. 550 mg/kg Theaphenon®E was suspended in 500µl water and intragastric feeding to each rat. The catechins contents in plasma, retina, and vitreous humor were analyzed by High Performance Liquid Chromatography with electrochemical detection (HPLC-ECD) after β-D-glucuronidase and sulfatase digestion.

(2) Adult Sprague-Dawley rat single-dose (25, 40, 50, 75 mg/kg) intravenous or intraperitoneal injection of sodium iodate, after 1, 4, 7, 14 days injection, the rats retinas were assessed by confocal scanning laser ophthalmoscopy (CSLO) and spectral domain optical coherence tomography (SD-OCT). Until Day 14, the rats were sacrificed for histological examinations of retinas.

(3) The 40 mg/kg sodium iodate treated rats were also administered intra-gastrically with 550 mg/kg Theaphenon®E, 387.8 mg/kg EGCG, 438.0 mg/kg catechins

combination (EGCG, GC, EGC, and EC), and 50.3 mg/kg catechins combination (GC, EGC, and EC), respectively. Controls were injected intravenously with normal saline or 40 mg/kg sodium iodate only. After in vivo examination of the retinas by CSLO and SD- OCT, the rats were sacrificed for histological analysis. Biochemical analyses included determination of superoxide dismutase (SOD), glutathione peroxidase (GPx), caspase 3 mRNA, with 8-Iso-PGF$_{2\alpha}$ as an oxidative stress marker to measure the oxidant status in retina.

Chapter 3: Materials and Methods

3.1 Experimental Materials

3.1.1 Animals

All rats were treated according to the guidelines of the Association for Research in Vision and Ophthalmology (ARVO) Statement on the Use of Animals in Ophthalmic and Vision Research. This study protocol was approved by the Animal Experimentation Ethics Committee, The Chinese University of Hong Kong. Adult Sprague-Dawley rats, weighing 200g to 250g, and aged 9 weeks, were obtained from the Laboratory Animal Service Center, The Chinese University of Hong Kong. The animals were housed in standard conditions, maintained at $22\pm1^{\circ}C$, $40\pm10\%$ humidity and 12 hour: 12 hour dark-light cycle. Standard rodent chow and water were provided *ad libitum*. For each study group, at least 3 rats were used for the experiments.

3.1.2 Chemicals

Sodium iodate (Sigma-Aldrich, MO, USA); ketamine (35 mg/kg; Ketaset; Fort Dodge Animal Health, Fort Dodge, IA, USA); xylazine (5 mg/kg; TranquiVed; Vedco, Inc., St. Joseph, MO, USA); 0.9% sodium chloride solution (Baxter company, USA); Paraformaldehyde (Sigma-Aldrich company, USA); (-)-epicatechin (EC), (-)-gallocatechin (GC), (-)-epigallocatechin (EGC), (-)-epigallocatechin gallate (EGCG), purchased from Chengdu Biopurity Phytochemical, China; green tea extract Theaphenon®E obtained generously donated from Dr. Yukihiko Hara (Department of Environmental Physiology, Shimane University Faculty of Medicine, Japan, 99% purity by TLC/high performance liquid chromatography),

Theaphenon®E is a trademark of green tea polyphenol preparation, will have a chance to be accepted as a high-grade tea catechin powder, the content EGCG is 70.5%; 8-Isoprostaglandin F2R-D4 (8-iso-PGF2R-D4), 8-iso-PGF2R, and other prostaglandin metabolites were from Cayman (Ann Arbor, MI); Bis-(trimethylsilyl) trifluoroacetamide (BSTFA), pentafluorobenzyl bromide (PFBBr), N,N-diisopropylethylamine, and dodecane were purchased from Sigma; Butylated hydroxytoluene (BHT) was from Calbiochem (La Jolla, CA); Triphenylphosphine was from Aldrich (Milwaukee, WI). All the primers were purchased from Invitrogen.

3.2 Methods

3.2.1 Normal rat treated with green tea extract (Theaphenon®E)

Nine groups of Sprague-Dawley rats, each group had six rats. They were weighed and fasted overnight before the GTE administration. GTE tablets were powdered and suspended in 0.5 mL of sterile water. Previous studies on the pharmacokinetics of catechins in rats have used a wide range of EGCG dosages from 25 to 500 mg/kg (Chen et al., 1997, Nakagawa and Miyazawa, 1997). In this study, we used 550 mg/kg GTE (Theaphenon®E), which is similar to our previous studies (Chu et al., 2006, Chu et al., 2007, Chu et al., 2010). The doses of catechins were comparable to most publications. The rats were randomly assigned to 9 groups: viz. 0, 0.5, 1, 2, 4, 6, 10, 15, 20 hours. The rats from each time point were fed 0.5 mL of GTE (Theaphenon®E) suspension by a feeding tube **(Figure 3.1)**. The rats were anesthetized with 35 mg/kg ketamine and 5 mg/kg xylazine by intraperitoneal injection (i.p.), and sacrificed at different time points after GTE (Theaphenon®E) administration. Rats of time zero were immediately sacrificed after feeding. The negative controls were fed 0.5 mL of water.

The eyes were enucleated. The retina and vitreous were dissected immediately. Retinas were washed in ice-cold saline, and then were snap-frozen in liquid nitrogen and stored at -80 °C. Plasma was obtained from peripheral whole blood after centrifugation at 3000 rpm at 4 °C for 10 min and stored at -80 °C (Chu et al., 2004).

3.2.2 Tissue and plasma preparations for catechins measurement

The tissue preparation followed by a published fully validated procedure (Chu et al., 2004). The retina weighed and homogenized in 0.25 mL of methanol/ethyl acetate (2:1) and 0.25mL of 0.3Msodium dithionite with 0.1%w/vNa$_2$EDTAin ice. After centrifugation at 10000g at 4 °C, the supernatant was purged by nitrogen to remove the organic solvents and reduce the volume to about 0.2 ml.

Then 0.25 ml of 0.4M phosphate buffer (pH 6.8) and 20 μl of a mixture of β-D-glucuronidase (2500U) and sulfatase (1U) were added to digest the conjugated catechins by incubation the mixture at 37 °C for 45 min.

The thawed plasma or vitreous humor was mixed with 40 μl of ascorbate-EDTA buffer solution, 40 μl of 0.4M NaH$_2$PO$_4$ buffer (pH 7.4), and 20 μl of a mixture of β-D-glucuronidase (250U) and sulfatase (1U). After purging by nitrogen and incubation at 37 °C for 45 min, all the samples were snap-cooled in ice before to add 1ml of 0.05MNaH$_2$PO$_4$ buffer (pH 7.0), solid phase was eluted by 10 ml of a methanol/ethyl acetate (2:1) mixture at 35 °C into a tube containing 20 μl of 2% ascorbate-EDTA to against oxidation.

After evaporated, it was dissolved into 100 μl of a mixture containing 10% acetonitrile and 0.06% trifluoroacetic acid in 0.05 M phosphate buffer (pH 3.0) and filtered for analysis by High-performance liquid chromatography (HPLC).

3.2.3 Pharmacokinetic data Analyses

All of the statistical analyseswere performed by SPSS 18.0. The pharmacokinetic parameters of catechins were analyzed by WINNONLIN Professional version 4.01.The parameters, MRT_{inf}, maximum peak time (Tmax), maximum concentration (Cmax), area under curve (AUC), terminal elimination rate (λz), oral clearance (Cl/F), and volume of distribution (Vz), were assessed by non-compartmental models.

3.2.4 Sodium iodate application

Sodium iodate (Sigma-Aldrich, MO, USA) was dissolved in sterile normal saline at a stock concentration of 4% (w/v). Single dose intra-venous (i.v.) injection of sodium iodate was applied to the rat tail vein. The rats were divided into 6 groups: normal saline (n=3); 75 mg/kg sodium iodide as control groups (n=3), the high dose of sodium iodide were used to compare the ionic strengths of sodium iodate with sodium iodide, to deduce whether the tissue damage is due to the oxidative effect of the iodate rather than the osmosis pressure; 25 mg/kg sodium iodate (i.v., n=6), 40 mg/kg sodium iodate (i.v., n=12); 50 mg/kg sodium iodate (i.v., n=3, i.p., n=3) and 75 mg/kg sodium iodate (i.v., n=3, i.p., n=3) as experimental groups. Before sodium iodate injection, the rats were anesthetized by intraperitoneal (i.p.) injection with a mixture of 35 mg/kg ketamine and 5 mg/kg xylazine. Afterwards, returned to the animal colony and kept under standard cycle lighting until further CSLO and OCT assessments.

3.2.5 Sodium iodate with catechins and GTE (Theaphenon®E) application (high dose)

The dosage of catechins was according to the proportion of each catechins in GTE
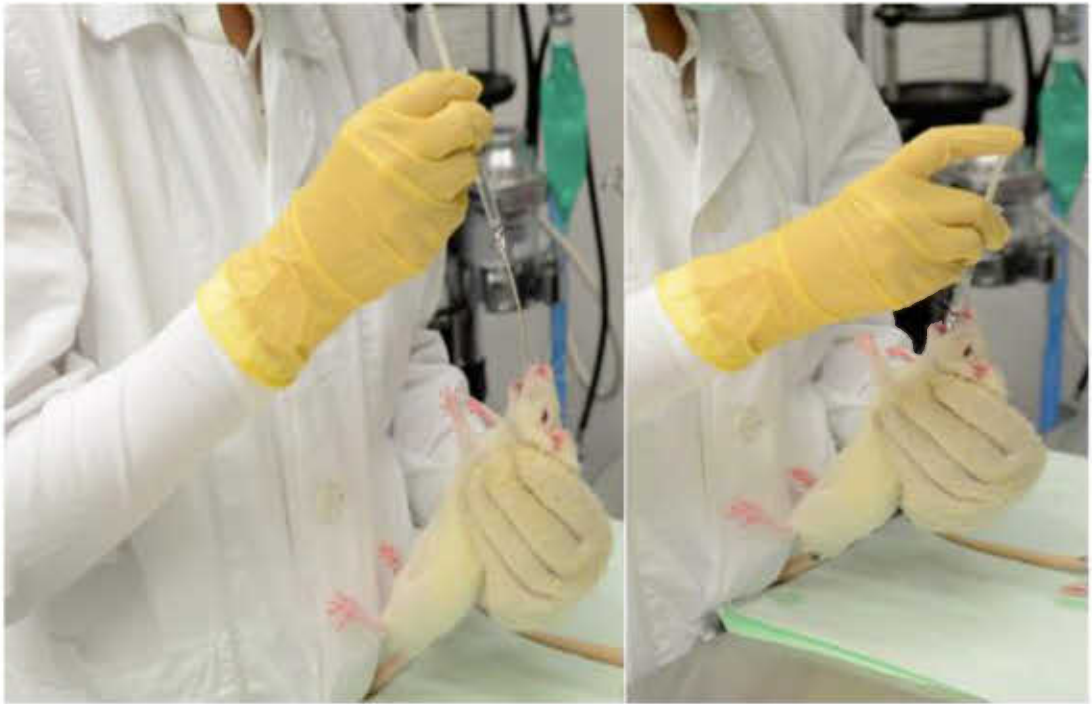
Figure 3.1 Intra-gastric fed the sterile water to the normal rat as negative control.

Theaphenon[®]E (EGCG: 70.53%, EGC: 4.61%, EC: 3.88%, GC: 0.64%). The dosage of Theaphenon[®]E was 550 mg/kg; so, EGCG was 387.8 mg/kg, 850 µmol/kg; catechins combination (EGCG, GC, EGC, and EC) was 438.0 mg/kg with EGCG (387.8 mg/kg, 850 µmol/kg), GC (3.53 mg/kg, 12 µmol/kg), EGC (25.4 mg/kg, 83 µmol/kg), EC (21.4 mg/kg, 74 µmol/kg); catechins combination (GC, EGC, and EC) was 50.3 mg/kg with GC (3.53 mg/kg, 12 µmol/kg), EGC (25.4 mg/kg, 83 µmol/kg), EC (21.4 mg/kg, 74 µmol/kg). Assume each 200 ml cup of tea contains approximately 200 mg catechins, including 88 mg EGCG, equal to 1.3 mg/kg EGCG, so 550 mg/kg Theaphenon E is equivalence to 300 cups of green tea of consumption for one time (Sutherland et al., 2006).

The experimental groups were divided into six groups, each with five animals. Group I: Negative control, i.v. injected with saline; Group II: Positive control, single i.v. injected with 40 mg/kg sodium iodate; Group III: Single i.v. injected with 40 mg/kg sodium iodate and oral intake of 550 mg/kg Theaphenon[®]E; Group IV: Single i.v. injected with 40 mg/kg sodium iodate and oral intake of 387.8 mg/kg EGCG; Group V: Single i.v. injected with 40 mg/kg sodium iodate and oral intake of 438.0 mg/kg catechin combination (EGCG, GC, EGC, and EC); Group VI: Single i.v. injected with 40 mg/kg sodium iodate and oral intake of 50.3 mg/kg with catechin combination (GC, EGC, and EC). All the catechins and GTE were fed intragastrically 12 hours and 1 hour before sodium iodate injection.

3.2.6 Sodium iodate with catechins and GTE (Theaphenon[®]E) application (low dose)

The lower dosage of catechins was also according to the proportion of each catechins in GTE Theaphenon[®]E (EGCG: 70.53%, EGC: 4.61%, EC: 3.88%, GC:

0.64%). The low dosage of Theaphenon®E was 100 mg/kg; so, EGCG was 70.5 mg/kg, 154 µmol/kg; catechins combination (EGCG, GC, EGC, and EC) was 79.6 mg/kg with EGCG (70.5 mg/kg, 154 µmol/kg), GC (0.64 mg/kg, 2.2 µmol/kg), EGC (4.61 mg/kg, 15 µmol/kg), EC (3.88 mg/kg, 13.4 µmol/kg); catechins combination (GC, EGC, and EC) was 9.1 mg/kg with GC (0.64 mg/kg, 2.2 µmol/kg), EGC (4.61 mg/kg, 15 µmol/kg), EC (3.88 mg/kg, 13.4 µmol/kg).

The experimental groups were also divided into six groups, each with five animals. Group I: Negative control, i.v. injected with saline; Group II: Positive control, single i.v. injected with 40 mg/kg sodium iodate; Group III: Single i.v. injected with 40 mg/kg sodium iodate and daily oral intake of 100 mg/kg Theaphenon®E; Group IV: Single i.v. injected with 40 mg/kg sodium iodate and daily oral intake of 70.5 mg/kg EGCG; Group V: Single i.v. injected with 40 mg/kg sodium iodate and daily oral intake of 79.6 mg/kg catechins combination (EGCG, GC, EGC, and EC); Group VI: Single i.v. injected with 40 mg/kg sodium iodate and daily oral intake of 9.1 mg/kg catechins combination (GC, EGC, and EC). The catechins and GTE were fed intragastrically 12 hours and 1 hour before sodium iodate injection and daily oral intake until 14 days post sodium iodate injection.

3.2.7 In vivo imaging (Retinal examination by confocal scanning laser ophthalmoscopy and spectral-domain optical coherence tomography)

Confocal scanning laser ophthalmoscopy (CLSO) and spectral-domain optical coherence tomography (OCT) were used for in vivo imaging (HRA2; Heidelberg Engineering GmbH, Dossenheim, Germany). The commercially available model of CSLO was used to image the fundus of the retina. The HRA2 is installed with two laser sources (488 nm and 795 nm, barrier filters at 500 nm and 810 nm). The digital

pixel resolution is 5-10μm/pixel. The field of view ranges between 15° × 15° and 55°× 55°. The focus range is between -24 and +40 diopters. A dual-beam simultaneous imaging with an infrared CLSO provides a planar visualization of the retina. A 55° wide field lens was added to the camera, in order to have a wider view to study the changes of the fundus. So, from optic disc to the ambitus, at least around 60% of the total retina area can be monitored by the CSLO. The scan rate of the CSLO was 16 frames per second with image size ranges between 384x384 pixels and 1536x1536 pixels. Eye-tracking (a retinal recognition technology enabling the same retinal location being "locked on") was activated during imaging. Fifteen images at the same location of the retina were captured, and then automatically averaged by the built-in software to augment the signal-to-noise ratio, and the fundus photos were displayed on the computer screen simultaneously (Li et al., 2011, Liu et al., 2012).

The Spectralis OCT parameters were modified according to the technical advice from the manufacturer to adapt OCT imaging in rats. The length of reference arm was adjusted to match the length of the sample arm scanning the rat eye by altering configurations at the software level. Thus, retinal fundus photograph and OCT images could be simultaneously captured on the exact retinal focus, which ensures the high quality of OCT imaging in rats. In each retina, 4 different square regions, the superotemporal, inferotemporal, inferonasal, and superonasal quadrants around the optic nerve head were scanned separately by the volume scan protocol, which consists of 19 evenly distributed B scans (1024 A scans for each B scan) covering a 20°×15° area of the retina (Hee et al., 1995, Leung et al., 2008a). The Spectralis HRA + OCT registers the CSLO and OCT images in the retina simultaneously. No any photobleaching or phototoxicity was induced by the laser during the image, and there

was no detectable change in the morphology fundus even imaging at the same laser intensity for 30 minutes.

The images were captured on each rat before (Baseline) and after sodium iodate injection (Day 4, 7 and 14). The imaging procedure was performed with one technician gently holding the animal and another operating the CSLO and the OCT. The platform could be manually rotated around the longitudinal axis of the body or in the horizontal plane. Each rat was placed on a custom-made platform and the head and body were fixed. Systemic anesthesia was applied but contact lenses were not required. Prior to imaging, rats were anesthetized as described and pupils were dilated by topical 1% tropicamide. Because cornea transparency is one of the key factors affecting the quality of the image, so during imaging, one drop sterile saline was applied to the cornea to maintain media clarity. This in vivo imaging technique provides real-time morphometric of living rat retinas which is not possible with conventional histological analysis. The setup with an animal in place is shown in **Figure 3.2**.

In vivo images were captured by CSLO at baseline, day 4, day 7, and day 14 after sodium iodate injection, were exported to a computer for hyper-reflective blots counting by using Photoshop (11.0; Adobe Systems Incorporated, San Jose, CA). In each retina, 4 different square regions with clearly visualized, each photos measuring 400μm ×400 μm of the retina were analyzed. The dark blots in four different quadrants in each eye were counted manually before and after the injection performed by a blinded observer.

3.2.8 Eyeball collection and fixation
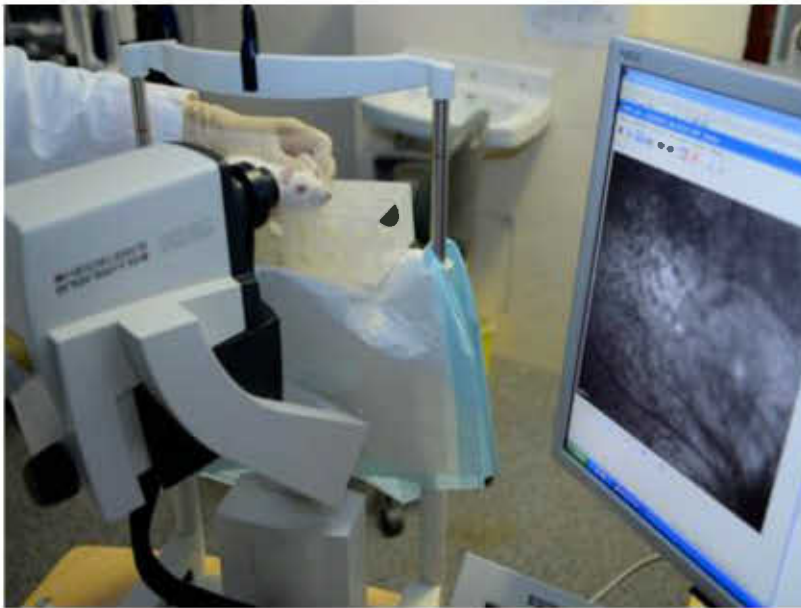
Figure 3.2 *In vivo* **imaging on sodium iodate treated rats with confocal scanning laser ophthalmology (CSLO).** The CSLO (HRA2, Heidelberg Engineering, GmbH, Dossenheim, Germany) was used for assessing the sodium iodate-treated retina imaging. A 55 degree wide field lens was added to the camera to increase the field of view. Fifteen images at the same location of the retina were captured, and then automatically averaged by the built-in software to augment the signal-to-noise ratio, and the fundus photos were displayed on the computer screen simultaneously.

At sodium iodate post-injected on Day 14, after captured the CSLO and OCT images, the rats were performed perfusion, and then got the eyeball for the further histological analysis, the chest cavity was carefully opened, and a 19-gauge perfusion cannula was perfused through the left ventricle with Phosphate Buffered Saline (PBS) first, and then performed with 4.0% paraformaldehyde in PBS buffer at PH 7.4 to remove erythrocytes in the retina. Eyes were enucleated, fixed in 10% neutral buffered formalin for at least 24 hours.

3.2.9 Dehydrate processing, embed and sectioning

After fixation in formalin, the eyes rinsed in PBS for 3 times, the eyeball was transferred to plastic cassette with proper label. The samples were dehydrated through a series of graded ethanol baths with increasing concentration (30%, 70%, 95% and 100% ethanol) in a processing machine (Shandon Excelsior, Thermo), then cleaned in xylene. After the sample was dehydrated, it was infiltrated with paraffin. The dehydrated tissue was then embedded (with the open edge facing downwards) in a wax block using the Embedding Center (EG 160, Leica, Germany). A mold that suitable to the size of the rat eye was chosen before the embedding procedure.

Paraffin sectioning was done with microtone (RM2135, Leica, Germany) and 5 μm in thickness section were obtained. The eyeball was cut along the pupil to optic nerve head (PO position). Each piece of section was extended with 30% alcohol followed by floating on 40°C water bath for 10 minutes and collected on the glass slide (HistoBond, Marienfeld). The sections stored at room temperature were dried thoroughly and kept until staining.

3.2.10 Histochemical staining (haematoxylin and eosin)

The paraffin sections were placed on a 60°C oven for 30 minutes for wax melting and also have a good attachment of tissue on the slide. Then de-waxing in xylene solution and rehydrated using a graded series of alcohol baths from absolute to 95% and 70% ethanol concentration, and then wash in running tap water for 2 minutes.

For haematoxylin and eosin (H&E) staining, the section was immersed in haematoxylin solution (Biocare Medical) for 10 minutes for nuclei staining. After rinsing in running tap water for 2 minutes, the staining was differentiated by immersing the section in 1% acid alcohol for 2 seconds, rinsed immediately in running tap water and then put in Scott's tap water for 2 minutes until blue coloration appeared. The sample was then put in aqueous eosin for 10 minutes in order to stain the cytoplasm.

After staining, the sections were washed with running water, and then dehydrated through a series of ethanol baths 70%, 95%, absolute ethanol 1 minute for each, and then cleared in xylene. Finally the section were mounted with Canada Balsum and dried in the room temperature and labeled properly.

3.2.11 Image acquisition

The mounted slide was put under the light microscope (Leica, Wetzlar, Germany) equipment with SPOT RT color system (Diagnostic Instruments, Serling Heights, MI, USA). The whole retinal layer were clearly assessed and captured for further analysis.

In paraffin sections, morphological analyses including measurements of thickness of inner/outer segments (IS/OS) of photoreceptors, outer nuclear layer (ONL), inner nuclear layer (INL) and inner plexiform layer (IPL) were performed at 300μm from the optic nerve head (posterior hole) using Image J (version 1.46e; NIH, Bethesda,

MD). The INL cell density fixed at 1000 μm^2 area 300μm from the optic nerve head (posterior hole) determined using Image J software.

3.2.12 Target gene expression in different pathways

3.2.12.1 Retina collection

After the high dose of the EGCG, catechins combination (EGCG, GC, EGC, and EC), catechins combination (GC, EGC, and EC), green tea extract Theaphenon$^®$ E 12 hours and 1hour oral treated before 40 mg/kg sodium iodate intravenous injection, 24 hours after sodium iodate injection, the rats were scarified by barbiturate overdose. Eyes were enucleated. The retinas were dissected, stored at -80 °C immediately until RNA extraction.

3.2.12.2 Total RNA extraction and purification

Total RNA was extracted from fresh-frozen retina using 500μL Trizol reagent (Carlsbad CA, USA), incubated for five minutes at room temperature (RT), and then vortexed frequently, added 100 μL of chloroform to the Trizol, and vortexed for 15 seconds, centrifuged at 15,000xg for 10 minutes at 4°C to separate phases. Completely aspirate the supernatant and purified with an mRNA isolation kit (Qiagen, Valencia, CA) added 1 volume of 70% ethanol to the homogenized lysate, and mix well by pipetting then put to the RNeasy column with spinning at 8000 rcf for 15 seconds at room temperature. The flow-through was discarded. The column-bound RNA was then washed with 500 μL RW1 buffer twice and centrifuge for 8000 rcf for 15 seconds to wash the spin column membrane (RNeasy extraction kit) and discard the flow-through. Add 500 μl Buffer RPE to the RNeasy spin column. Close the lid gently, and centrifuge for 15 s at 8000 rcf to wash the spin column membrane.

Discard the flow-through, added 500 μl Buffer RPE to the RNeasy spin column. Close the lid gently, and centrifuge for 2 min at 8000 rcf to wash the spin column membrane. Place the RNeasy spin column in a new 2 ml collection tube (supplied), and discard the old collection tube with the flow-through. Close the lid gently, and centrifuge at full speed for 1 min. Place the RNeasy spin column in a new 1.5 ml collection tube (supplied). Add 30–50 μl RNase-free water directly to the spin column membrane. Close the lid gently, and centrifuge for 1 min at 8000 rcf to elute the RNA.

The concentration and the quantity (absorbance at 260nm wavelength / absorbance at 280 nm wavelength) of the purified RNA was determined by Nanodrop ND-1000 UV-Vis spectrophotometer (Nanodrop technologies, Wilmington, DE, USA) and Nanodrop 3.1.0 software, with the RNase-free water as the reference to measure the RNA concentration and labeled on each sample. The RNA samples were immediately stored at -80 °C until reverse transcription.

3.2.12.3 Reverse transcription

1μg of the purified RNA was used to synthesize cDNA by using SuperScript ^{TM} III cDNA synthesis kit (Invitrogen), according to the manufacturer's instructions. RNA was diluted in RNase-free water by using 1 μl of dNTP mixture (10mM, Roche, Basel, Switzerland), 1 μl random primer (250ng/ μl; Qiagen). The volume of the mixture was made up to 13 μl and incubated in 65 °C for 5 minutes, after then, immediately incubated on ice for 2 minutes. The mixture was then made with 5x Frist-Strand Reaction Buffer (Invitrogen), 1 μl $_{DL}$-DTT (0.1 M), 1 μl RNase OUT ^{TM} recombinant RNase inhibitor and 1 μl SuperScript ^{TM} III reverse transcriptase. After the reagent mixed well, the reaction condition was set to 25 °C for 5 minutes for

primer annealing, 50 °C for 60 minutes for strand elongation, 70 °C for 15 minutes for enzyme denaturation, and finally at 4 °C in a thermal cycler (BioRad). The synthesized cDNA was collected and stored at -80 °C until PCR analysis.

3.2.12.4 Real- time polymerase chain reaction (PCR)

Gene-specific primers for all tested genes are presented in **Table 3.1** All PCRs were analyzed by the LightCycler real-time PCR instrument from Roche. Thermal cycling conditions comprised an initial denaturation step at 95°C for 3 min followed by 45 cycles at 95°C for 30 sec and an annealing temperature at 60°C for 30 sec. All samples were run in triplicate, and each well of PCR contained 20µl as a final volume, including 1µl of cDNA, 10 µM gene-specific primers, 2X SYBR Green I (Roche). GAPDH was used as a housekeeping gene. Negative samples were run for each RT-PCR consisting of no RNA in the reverse transcriptase reaction and no cDNA in the PCR. The mathematical method described by Pfaffl was used to evaluate the relative expression ratio for all genes compared with GAPDH (Pfaffl, 2001).

3.2.13 Assay for 8-Iso-PGF$_{2\alpha}$ in retina

3.2.13.1 Retina collection

After the high dose of the EGCG, catechins combinations (EGCG, GC, EGC, and EC), catechins combinations (GC, EGC, and EC), green tea extract Theaphenon®E 12 hours and 1hour oral treated before 40 mg/kg sodium iodate intravenous injection, 24 hours after sodium iodate injection, the rats were scarified by barbiturate overdose. Eyes were enucleated. The retinas were dissected, stored at -80 °C immediately, until lipid extraction.

Table 3.1 Sequence of the primer.

Gene	Primer name	Sequence (5'>3')	Length (nt)	Tm (℃)	Amplicon size	Reference
GAPDH	eRt-Gapdh-F	GTGCCAGCCTCGTCTCATA	19	60.09	190	NM_017008.3
	eRt-Gapdh-R	GTTGAACTTGCCGTGGGTAG	20	60.03		
SOD	eRt-Sod1-F	GGATGAAGAGAGGCATGTTGG	21	59.63	122	NM_017050.1
	eRt-Sod1-R	TACGGCCAATGATGGAATGC	20	59.6		
GPx	eRt-Gpx3-F	TTCGGACACCTCAGACGG	18	59.54	149	NM_022525.3
	eRt-Gpx3-R	GGCAGTCTGTCTTGGACTTC	20	59.11		
Casp3	eRt-Casp3-F	AGTCTGACTGGAAAGCCGAA	21	59.63	122	NM_017050.1
	eRt-Casp3-R	ATAGTAACCGGGTGCGGTAG	20	59.6		

3.2.13.2 Extraction of tissue lipids

The protocol was based on published validated methods (Morrow and Roberts, 1999, Morrow et al., 1999). To measure levels of 8-Iso-PGF$_{2\alpha}$ in tissue phospholipids, the phospholipids must first be extracted from the tissue sample. To weigh 0.05 to 1 g of retina was added 20 ml of ice-cold Folch solution, with chloroform/methanol (2:1, v/v), containing 0.005% butylated hydroxytoluene (BHT) in a 50 ml centrifuge tube. The tissue is then homogenized with a blade homogenizer for 30 s, and the mixture is sealed under nitrogen at room temperature for 1 h. Four milliliters of 0.9% NaCl are then added and the solution is vortexed and centrifuged at 800g for 10 min. After centrifugation, the upper aqueous layer is discarded and the lower organic layer is carefully separated from the intermediate semisolid proteinaceous layer.

3.2.13.3 Hydrolysis of lipid extracts

The organic phase containing the extracted lipids, then transferred to a 50 ml centrifuge tube and evaporated to dryness under a stream of nitrogen. Four milliliters of methanol containing 0.005%BHT and Four milliliters 15% NaOH were then added to the residue. The mixture was vortexed and incubated at 37 °C for 30 min to hydrolysis and release of the F2-IsoPs. The mixture is then acidified to pH 3 with 5 M HCl. Dilution of the methanol in the solution with water to 5% or less is necessary to ensure proper column extraction of 8-Iso-PGF2α in the subsequent purification procedure.

3.2.13.4 Purification and derivatization

20 µl of 10 pg/µl D4-isoprostane as the internal standard, was Added to the

mixture, vortexed and applied to a C18 Sep-Pak column (Waters Associates, Milford, MA) washed with 10 ml pH 3 water and cyclohexane. The sample and subsequent solvents were eluted through the Sep-Pak using a 10 ml sterile plastic syringe. The column was then washed 10 ml of water (pH3) and 10 ml of heptane. The F2-IsoPs are eluted with 10 ml of ethyl acetate/heptane (50/50, v/v). The ethyl acetate/heptane eluated from the C18 Sep-Pak was then dried over sodium sulfate, applied to a silica Sep-Pak (Waters Associates) that was prewashed with 5 ml of ethyl acetate, then washed with 5 ml of ethyl acetate followed by elution of the F2-IsoPs with 5 ml of ethyl acetate/methanol (50:50 v/v) and then evaporated under a stream of nitrogen. Add 40 µl 10% pentafluorobenzyl bromide (PFBB) and 20 µl 20% Diisopropyl Ether (DIPE) 30 minutes at room temperature. Dry reagents under nitrogen and resuspend in 10-20 µl ethyl acetate. Thin layer chromatograph to 13 centimeter in a solvent with chloroform/ ethanol (93:7), visualize the thin layer chromatography (TLC) standard by spraying with 10% phosphomolybdic acid/ethanol and heating, then scape silica from the TLC, place silica in 1.5 ml tube and add 1 ml ethyl acetate, votex 30s and pour off ethyl acetate into another tube, dry the organic layer, add 50 µl N, O-bis-(trimethylsilyl) trifluoroacetamide (BSTFA), dry the reagent under nitrogen. Add 20 µl dodecane readily injection for Gas chromatography–mass spectrometry (GC-MS).

3.2.14 Statistical analysis

Mann-Whitney U-test was used to compare the mean between different experimental groups and the controls. Data were expressed as mean±standard error of the mean (SD). All analyses were performed using PASW Statistics 18 (SPSS Science, Chicago, IL), and comparisons were considered as significance different

when $p < 0.05$.

Chapter 4: Results

4.1 Pharmacokinetic study of catechins distribution in the normal rat eye

The catechin concentration versus time curves in plasma appeared as a single peak, however, in retina and vitreous the profile appeared as multiple peaks **(Figure 4.1)**. Some catechins sustained at high level even after 20 hours of GTE administration, for example, EGCG and EC in retina. No catechins were detected in any of the plasma, vitreous, and retina in the negative control group. Also, shapes of the profiles of catechins and catechin gallates were in general similar in all compartments. Whereas, the profiles between catechins and catechin gallates within the same tissue we different.

Comparison catechins profiles in plasma between Theaphenon®E and Sunphenon® DCF-1 (our previous data), the Cmax of catechins are generally no difference from Sunphenon ® DCF-1 results except EGCG is significantly higher in Theaphenon® E. The exposure level (AUC) of EGCG is higher but GC is lower in Theaphenon® E. The elimination rate (λz) of C, EC, EGCG, EGCG, and ECG are higher in Theaphenon E. Therefore, the mean residence time of C, EGCG, and ECG are shorter **(Table 4.1)**. In the retina, the Cmax and AUC level were higher, with 784 nmol/kg and 5228 nmol/kg. EGCG was the dominant constitute and maintained to 20 hours. Low level of ECG was found in Theaphenon®E which was absent in Sunphenon®DCF-1 **(Table 4.2)**. High level of GC present in the vitreous humor, with Cmax ~ 4492 nM, AUC ~ 47534, Tmax is 5.2 hour. EGCG was the dominate gallates derivative, with Cmax~2224, AUC ~20612, Tmax ~9.4 hour **(Table 4.3)**.

The order of dominance of catechins levels in Theaphenone was EGC>EC>C>GC E, however, in Sunphenon®DCF-1, EC>EGC>C>GC. The order of dominance of

galloyl catachins was the same in both GTE, ie. EGCG>ECG>GCG>CG. Catechins were found extensively absorbed at short time, within 30 minutes after intra-gastric administration **(Table 4.4)**.

Figure 4.1 Profiles of total catechins and catechins gallate. Normal rat treated with 550 mg/kg GTE (Theaphenon®E) n=6. The profiles in each group divided into two groups according to the presence of gallate derivatives. Error bars represent mean ± SD.

Catechin as a group   Catechin gallate as a group

(A) Plasma

Catechin profile in plasma — Catechin gallate profile in plasma

(B) Retina

Catechin profile in retina — Catechin gallate profile in retina

(C) Vitreous humor
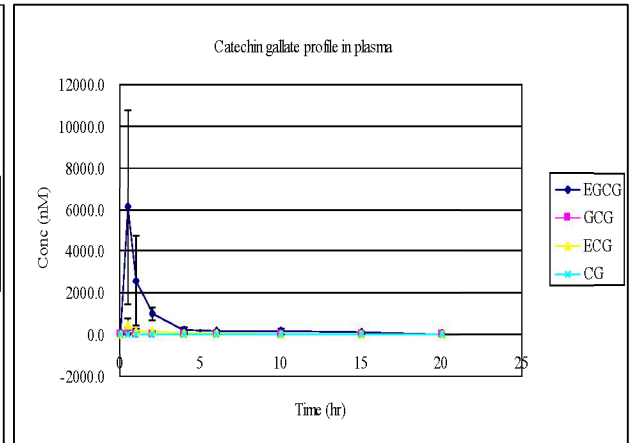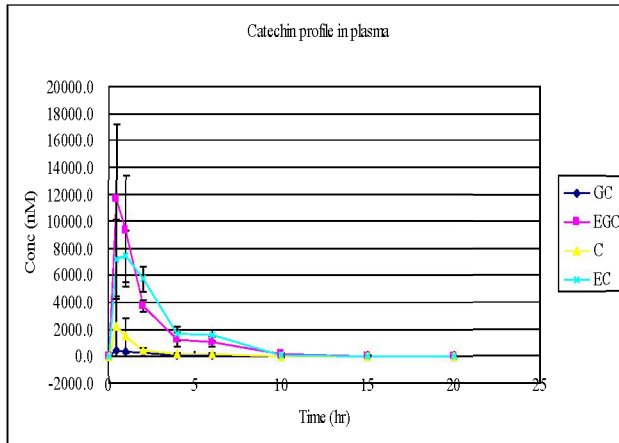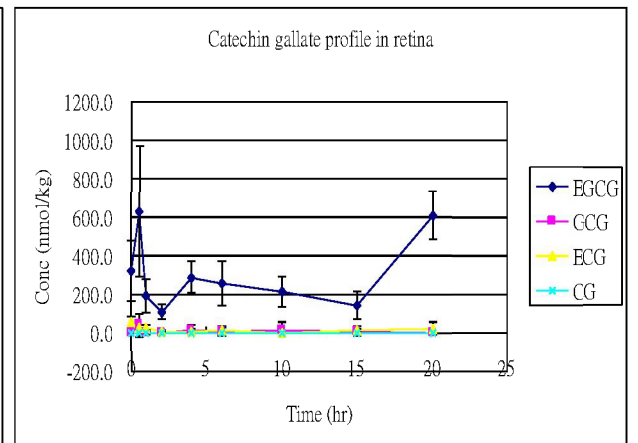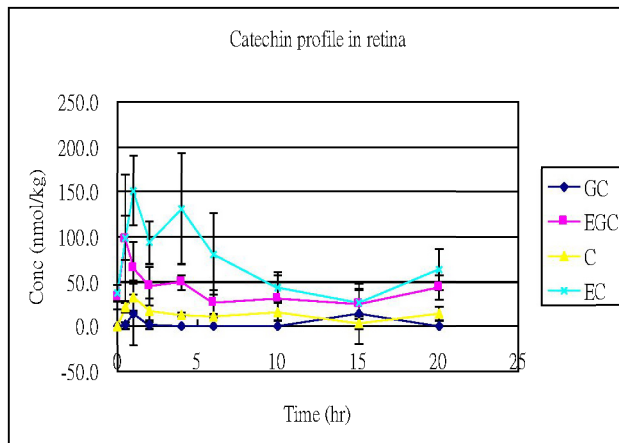
Catechin profile in vitreous humor — Catechin gallate profile in vitreous humor

Table 4.1 Pharmacokinetic parameters of catechins in plasma 20hours after a single dose of Theaphenon®E treated to the normal rats

Plasma from Theaphenon®E

PK Parameter	GC Mean	SD	EGC Mean	SD	C Mean	SD	EC Mean	SD	EGCG Mean	SD	GCG Mean	SD	ECG Mean	SD	CG Mean	SD
λ_z (1/hr)	0.27	0.03	0.39	0.04	0.37	0.08	0.40	0.06	0.23	0.02	1.25	0.38	0.21	0.04	1.48	1.04
$\lambda_z1/2$ (hr)	2.59	0.30	1.79	0.19	1.95	0.46	1.74	0.22	3.10	0.27	0.59	0.16	3.37	0.54	0.75	0.56
Tmax (hr)	0.92	0.58	0.67	0.26	0.83	0.26	0.80	0.27	0.67	0.26	0.50	0.00	0.70	0.27	0.63	0.25
Cmax (nmol/L)	530.8	200.2	13718.4	4947.7	2989.5	1990.1	9142.7	1912.0	6686.8	4437.1	131.3	91.7	443.8	352.3	1.5	0.8
AUCINF (hr*nmol/L)	1725.6	125.5	25106.6	1472.9	4323.6	826.2	26668.7	975.7	8731.2	2726.7	89.7	41.1	976.1	228.4	1.6	0.5
Vz/F (L)	5.48	0.47	1.88	0.27	1.48	0.43	1.53	0.20	106.80	45.99	30.51	18.07	96.88	18.91	138.71	95.73
Cl/F(L/hr)	1.48	0.11	0.73	0.04	0.53	0.10	0.61	0.02	23.47	8.45	32.89	13.08	20.21	4.56	135.84	33.67
MRTINF (hr)	3.97	0.37	2.51	0.46	2.75	0.53	2.85	0.16	3.38	0.68	0.77	0.20	4.10	0.81	1.37	0.78

Plasma from Sunphenon®DCF-1

PK Parameters	GC Mean	SD	EGC Mean	SD	C Mean	SD	EC Mean	SD	EGCG Mean	SD	GCG Mean	SD	ECG Mean	SD	CG Mean	SD
λ_z (1/hr)	0.24	0.01	0.39	0.06	0.11	0.01	0.29	0.03	0.03	0.02	0.12	0.00	0.11	0.02	-	-
Tmax (hr)	1.17	0.76	1.17	0.76	0.83	0.29	1.17	0.76	1.00	0.87	2.33	2.31	1.17	0.76	-	-
Cmax (nmol/L)	880.0	410.0	7000.0	3100.0	1130.0	220.0	9800.0	1900.0	630.0	400.0	40.0	40.0	490.0	420.0	-	-
AUCINF (hr*nmol/L)	3858.5	986.8	31000.0	4600.0	5200.0	700.0	37000.0	7300.0	3300.0	1400.0	160.0	90.0	1600.0	600.0	-	-
Vz/F (L)	58.9	17.0	4.8	1.2	38.7	5.3	6.9	1.1	7111.1	149.7	3014.2	681.3	351.7	44.8	-	-
Cl/F(L/hr)	13.9	4.1	1.9	0.5	4.1	0.7	2.0	0.4	23.2	0.8	357.8	87.1	40.4	11.3	-	-
MRTINF (hr)	4.0	0.2	3.1	0.0	6.7	0.1	3.0	0.3	24.6	2.4	7.6	0.1	4.6	0.7	-	-

Table 4.2 Pharmacokinetic parameters of catechins in retina 20hours after a single dose of Theaphenon$^{®}$E treated to the normal rats

Retina from Theaphenon®E

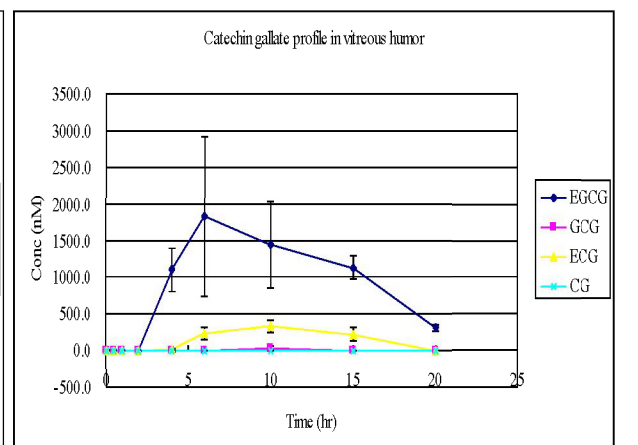| PK Parameter	GC Mean	SD	EGC Mean	SD	C Mean	SD	EC Mean	SD	EGCG Mean	SD	GCG Mean	SD	ECG Mean	SD	CG Mean	SD
λz (1/hr)	-	-	0.04	0.03	0.04	0.01	0.06	0.02	0.04	0.02	-	-	0.09	0.03	-	-
$\lambda z 1/2$ (hr)	-	-	27.72	20.31	16.68	5.17	11.85	4.35	18.28	7.14	-	-	8.37	2.20	-	-
Tmax (hr)	5.0	6.7	0.70	0.27	0.80	0.27	3.20	2.17	7.92	9.60	5.50	6.84	1.52	2.99	-	-
Cmax (nmol/kg)	61.0	43.5	118.2	55.6	356.7	150.3	174.5	45.8	784.4	195.9	59.0	54.8	63.5	15.5	-	-
AUCINF (hr*nmol/kg)	166.3	213.7	722.0	146.1	4331.1	1413.5	1304.1	194.8	5227.8	575.4	209.1	213.8	253.0	43.4	-	-
Vz/F (L)	-	-	364.5	47.2	12.9	3.8	142.6	25.2	555.2	65.9	-	-	743.5	188.9	-	-
Cl/F(L/hr)	-	-	13.7	8.8	0.6	0.2	8.9	2.1	23.5	7.8	-	-	62.8	11.5	-	-
MRTINF (hr)	-	-	39.9	29.2	25.3	7.9	17.1	6.8	24.9	8.9	-	-	14.6	3.6	-	-

Retina from Sunphenon®DCF-1

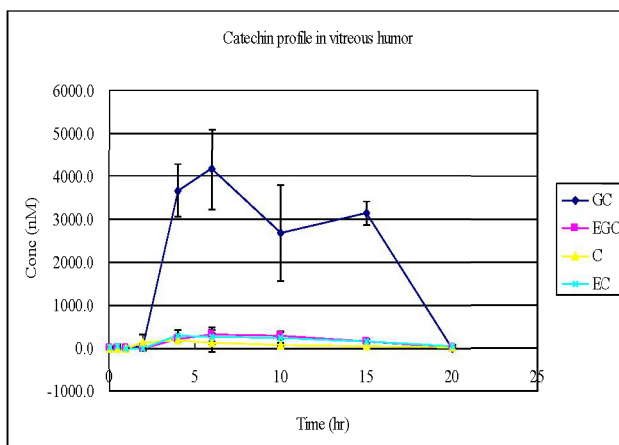| PK Parameters	GC Mean	SD	EGC Mean	SD	C Mean	SD	EC Mean	SD	EGCG Mean	SD	GCG Mean	SD	ECG Mean	SD	CG Mean	SD
λz (1/hr)	0.188	0.045	0.20	0.05	0.25	0.01	2.43	0.15	0.41	0.04	-	-	-	-	-	-
Tmax (hr)	1	0.1	1.20	0.10	3.70	4.10	10.20	0.20	10.10	0.10	2.00	0.10	-	-	-	-
Cmax (nmol/kg)	22729.4	4229.4	8020.8	1658.5	492.7	235.2	608.0	112.0	259.1	67.2	3.2	1.9	-	-	-	-
AUCINF (hr*nmol/kg)	206683.5	48654.4	26793.3	8889.2	4904.4	2704.0	1463.1	296.3	652.4	193.3	4.4	2.7	-	-	-	-
Vz/F (L)	-	-	-	-	-	-	-	-	-	-	-	-	-	-	-	-
Cl/F(L/hr)	0.8	0.2	7.2	2.3	19.6	7.1	181.7	40.1	395.9	112.4	-	-	-	-	-	-
MRTINF (hr)	10.5	1.9	7.2	1.7	11.0	0.7	9.7	0.1	10.6	0.2	-	-	-	-	-	-

Table 4.3 Pharmacokinetic parameters of catechins in vitreous humor 20hours after a single dose of Theaphenon®E treated to the normal rats

Vitreous humor from Theaphenon®E

PK Parameter	GC		EGC		C		EC		EGCG		GCG		ECG		CG	
	Mean	SD	Mean	SD	Mean	SD	Mean	SD	Mean	SD	Mean	SD	Mean	SD	Mean	SD
λz (1/hr)	0.02	0.01	0.11	0.09	0.11	0.06	0.10	0.03	0.08	0.02	-	-	-	-	-	-
$\lambda z1/2$ (hr)	30.8	9.8	11.2	9.5	7.5	3.4	7.5	1.6	9.4	2.2	-	-	-	-	-	-
Tmax (hr)	5.2	1.1	8.0	2.3	4.0	2.0	6.4	2.2	9.4	3.7	10	0	10.16667	2.857738	6	5.656854
Cmax (nmol/L)	4492.0	443.5	404.1	102.5	321.7	69.5	436.8	102.5	2224.4	805.4	33.9245	31.02043	369.6002	73.9796	3.123333	5.117391
AUCINF (hr*nmol/L)	47534.3	3108.8	3632.2	381.2	1682.6	815.1	3428.0	534.4	20612.0	3929.4	158.935071	145.5895	3376.303	557.6921	8.053	13.0685
Vz/F (L)	0.7	0.1	41.3	15.5	11.1	3.9	42.7	11.5	95.6	32.1	-	-	-	-	-	-
Cl/F(L/hr)	0.02	0.00	3.62	1.76	1.17	0.61	3.98	0.61	6.91	0.77	-	-	-	-	-	-
MRTINF (hr)	47.2	14.0	19.9	12.2	13.2	3.2	13.3	2.0	16.1	3.2	-	-	-	-	-	-

Vitreous humor from Sunphenon®DCF-1

PK Parameters	GC		EGC		C		EC		EGCG		GCG		ECG		CG	
	Mean	SD	Mean	SD	Mean	SD	Mean	SD	Mean	SD	Mean	SD	Mean	SD	Mean	SD
λz (1/hr)	0.166	0.01	0.04	0.00	0.11	0.03	0.07	0.00	0.06	0.01	0.04	0.01	0.22	0.04	-	-
Tmax (hr)	3.2	0.2	0.50	0.10	4.30	1.60	5.00	0.20	3.10	0.20	3.50	0.20	2.00	0.20	-	-
Cmax (nmol/L)	110.6	22.1	15.9	7.0	96.5	23.3	20.5	10.6	15.4	2.7	20.9	9.9	14.0	5.1	-	-
AUCINF (hr*nmol/L)	1634.2	332.2	79.2	30.2	1404.9	251.2	205.8	97.4	109.5	27.4	172.7	70.3	100.8	47.1	-	-
Vz/F (L)	193.6	47	11326.4	3403.5	139.8	21.7	3630.6	1362.4	14096.0	4220.5	3920.2	1318.4	2842.8	1094.4	-	-
Cl/F(L/hr)	32	6.9	460.2	132.0	14.5	4.0	239.1	84.3	788.9	169.0	160.6	44.9	609.8	201.1	-	-
MRTINF (hr)	11	0.2	23.1	1.0	15.1	4.8	15.9	0.8	19.0	2.3	26.8	2.6	10.2	0.2	-	-

Table 4.4 Comparison catechins profile in different ocular tissues

Compartment	Theaphenon E	Sunphenon DCF-1
Plasma	Cmax: No difference except EGCG higher	Cmax: EGCG lower
	Exposure level (AUC): EGCG higher, GC lower	Exposure level (AUC): EGCG lower, GC higher
	Elimination rate (λz): C, EC, EGCG, EGCG, and ECG are higher.	Elimination rate(λz): C, EC, EGCG, EGCG, and ECG are lower.
	Mean residence time: C, EGCG, and ECG are shorter	Mean residence time: C, EGCG, and ECG are longer
	Order of dominance of catechins: EGC>EC>C>GC	EC>EGC>C>GC
	Order of dominance of galloyl catachins: EGCG>ECG> GCG>CG	Order of dominance of galloyl catachins: EGCG>ECG> GCG>CG
	Tmax: within 30 minutes	Tmax: within 1 hour
Vitreous humor	GC was the dominate compound.	GC was the dominate compound.
	EGCG was dominate gallates derivative	EGCG was not dominate
	EGC higher Cmax & AUC: 404 nM, 3632	EGC Cmax & AUC: 15.9 nM, 79.2
	Higher Cmax in EC & EGCG: 436, 2224 nM	Lower Cmax in EC & EGCG: 20.5, 15.4 nM
	Higher AUC in EC & EGCG: 3428, 20612	Lower AUC in EC & EGCG: 205, 109
Retina	EGCG dominated in retina maintained to 20 hour	EGCG dominated in retina
	GC, EGC, EC are significant lower	GC, EGC, EC are dominant
	Low level of ECG is found	ECG is absent

4.2 Establishment of a retinal degeneration model on sodium iodate treated rat

## 4.2.1 Fundus examination by confocal scanning laser ophthalmoscopy (CSLO) in living rat retinas

Retinal lesions were induced in Sprague-Dawley adult rats with single intravenous injection of 25, 40, 50, 75 mg/kg sodium iodate, and single intraperitoneal injection of 50, 75 mg/kg sodium iodate. The retina was examined using CSLO before the sodium iodate injection (Day 0) and after sodium iodate injection on Day 4, 7, 14.

In the single intravenous treated group, with 40 (n=12), 50, 75 mg/kg (n=3) sodium iodate treated rats, in these retinal images, typical appearance of the retinal vessels and optic nerve head was readily recognizable. No obvious change was visible in the retina of these animals before sodium iodate injection (Day 0) and 4 days after injection (Day 4) **(Figure 4.2 A-B)**. However, a dramatic change started to appear at 7 days post sodium iodate injection (Day 7), which was characterized by the presence of many small dark blots in the retina **(Figure 4.2 C)**.   These dark blots were more obvious in the retina when examined on Day 14 **(Figure 4.2 D)**. Whereas with 25 mg/kg (n=6) sodium iodate injection, the distribution of the dark blots were limited to certain regions in part of the retina until Day 14 **(Figure 4.3 C-D)**. In the group with 50, 75 mg/kg (n=3) intraperitoneal injection, 75 mg/kg sodium iodate cause the retinal appeared dark blots from day 7, the retina covered with small dark blots throughout the retina until day 14 **(Figure 4.3 E-H)**. However, with 50 mg/kg intraperitoneal injection, the dark spots only appeared from day 14. In control animals that had injected either with saline (n=6) **(Figure. 4.2 E, 4.3 A-B)** or 75 mg/kg sodium iodide (n=3) **(Figure. 4.2F)**, no such changes were observed in the retina until Day 14.

Figure 4.2 40 mg/kg sodium iodate-induced retinal lesions under infra-red confocal scanning laser ophthalmoscopy (CSLO). Montages retinal images generated by CSLO. A-D: Typical changes in the retina of a rat injection intravenously with 40 mg/kg sodium iodate. Hyper-reflective structures or blots (white arrows) were detected in all retinal quadrants 7 and 14 days after injection. E-F: Retina in control animals 14 days after injection of saline or 75 mg/kg sodium iodide. OD: Optic disk. Superior is up and temporal to the right in these images. Scale bar is 200 μm.

Figure 4.3 Sodium iodate-induced retinal lesions under infra-red confocal scanning laser ophthalmoscopy (CSLO). Montages retinal images generated by CSLO. A-B: Retina in control animals 7 days and 14 days after injection of saline. C-D: Changes in the retina of a rat injection intravenously with 25 mg/kg sodium iodate. Hyper-reflective structures or blots (white arrows) were detected in part of the retinal quadrants 7 and 14 days after injection. E-H: Typical changes in the retina of a rat injection intravenously with 50, 75 mg/kg sodium iodate. Hyper-reflective structures or blots (white arrows) were detected in all retinal quadrants 7 and 14 days after injection. OD: Optic disk. Superior is up and temporal to the right in these images. Scale bar is 200 μm.
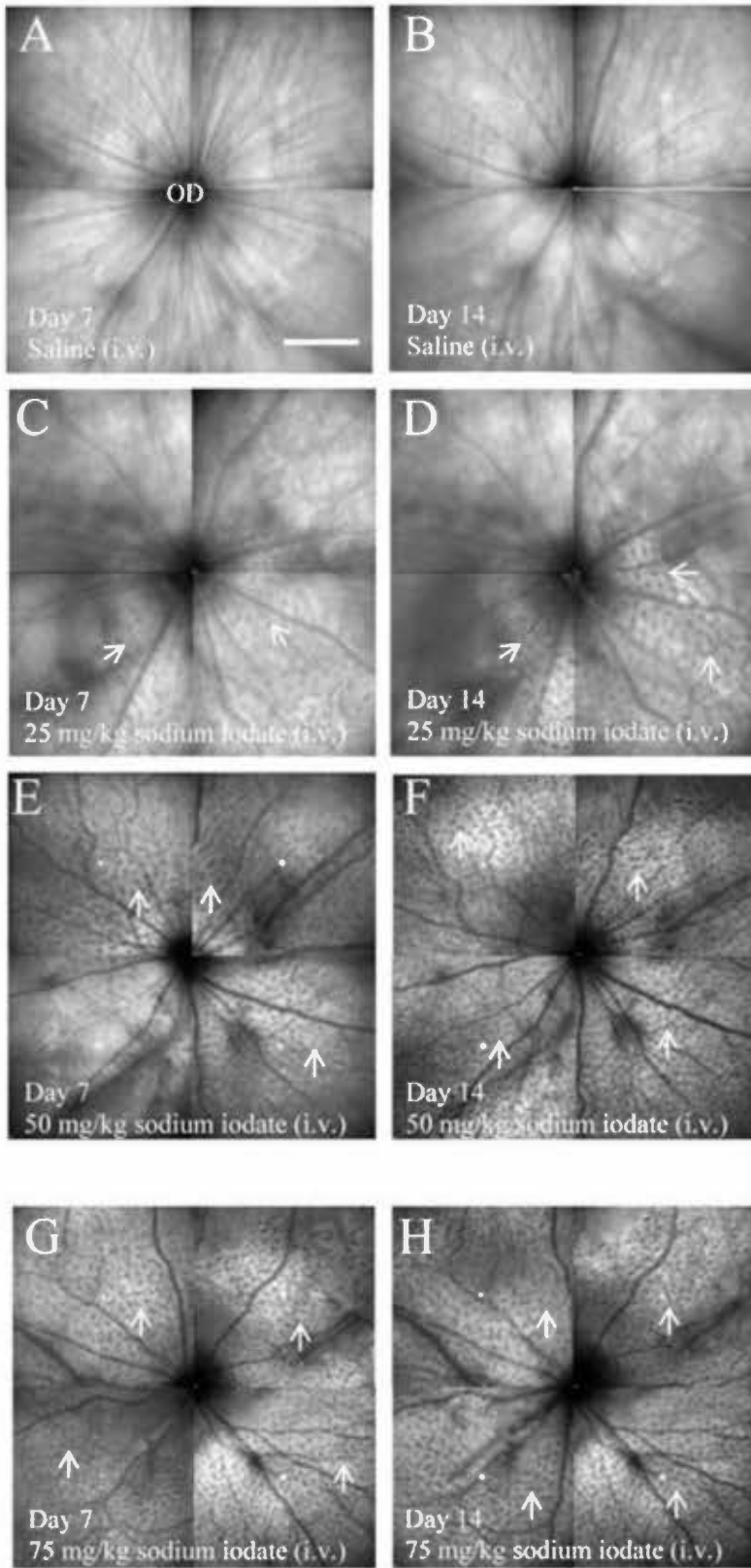
4.2.2 Outer nuclear layer thickness assessed by spectral –domain optical coherence tomography (SD-OCT)

Cross-sectional images of the retina were also taken from these animals using spectral domain OCT at the same time with CSLO. Images from Day 0, animals showed a typical laminated layer of the intraretinal (**Figure 4.4 A**), which was observed also in the retina 4 days after 40 mg/kg sodium iodate injection (**Figure 4.4 B**). Structure changes were first detected at Day 7, which were characterized by appearance of dome-shaped hyper-reflective areas in outer layers of the retina, corresponding to the position of the outer nuclear layer (ONL) and inner/outer segments of photoreceptors (IS/OS) (**Figure 4.4 C**). The photoreceptor outer segment structure disappeared and the IS/OS low reflective band is replaced by hyper-reflectivity regions in part of the retina and has become irregular in shape.

Retinal layers in inner regions of the retina were relatively unaffected, in terms of thickness and reflectivity. These abnormalities were more obvious and increased in number in optical sections of severe irregularity in the retina 14 days after injection (**Figure 4.4 D**), representing lesions induced by 40 mg/kg sodium iodate that are known to confine preferentially to outer retinal layers(Machalinska et al., 2010, Muraoka et al., 2012). Such abnormalities were not observed in control animals injected with saline (**Figure 4.4 E**) or sodium iodide (**Figure 4.4 F**).

Further analyses of images collected by CSLO (n=3) and their corresponding cross-sectional images by OCT with 40 mg/kg sodium iodate intravenous treated showed a high spatial correlation of the dark blots in the planar image of the retina with hyper-reflective regions in the ONL (**Figure 4.5 A and B**), suggesting that degenerative changes in the outer retinal layers in the cross sectional images can be visualized readily by CLSO images of the retina.

Figure 4.4 Sodium iodate-induced retinal lesions under spectral-domain optical coherence tomography (OCT). Cross-sectional OCT images of the retina in adult rats treated with 40 mg/kg sodium iodate, i.v. A-D: typical appearance of retinal layers in OCT images. Obvious degenerative profiles (white arrows) in photopigment layer and outer nuclear layer were first observed at Day 7 and became more prominent at Day 14. This damage was not observed in control retinas 14 days after injection of saline (E) or sodium iodide (F). INL: inner nuclear layer; ONL: outer nuclear layer; IS/OS: photopigment layer. Scale bar is 200 μm.
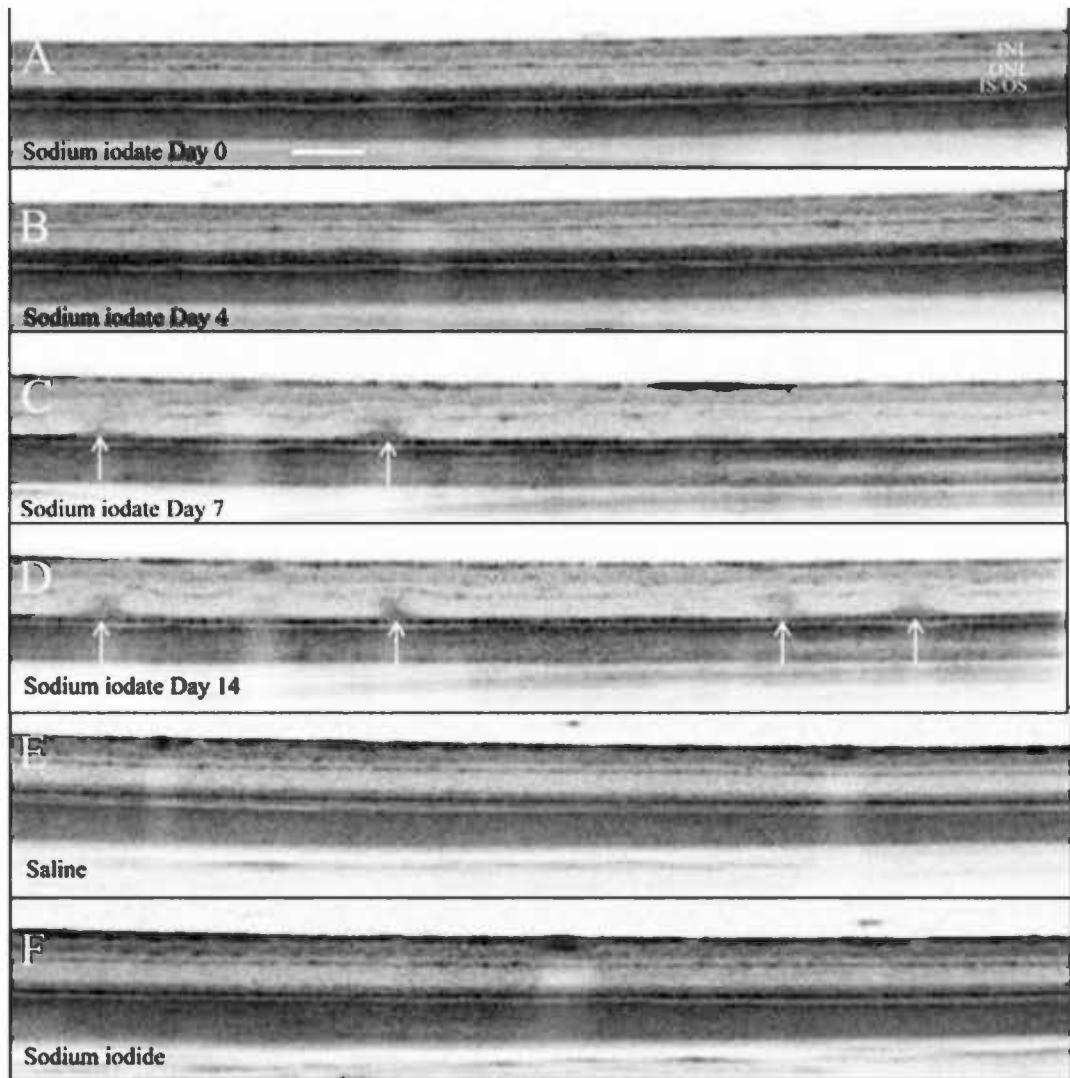
A
Sodium iodate Day 0

B
Sodium iodate Day 4

C
Sodium iodate Day 7

D
Sodium iodate Day 14

E
Saline

F
Sodium iodide

Figure 4.5 Hyper-reflective blots in CSLO images are in register to degenerative profiles in OCT images. CSLO and OCT images collected from superotemporal quadrant of a retina 7 days after injection of 40 mg/kg sodium iodate. The HRA+OCT captures the CSLO and OCT images from the retina simultaneously. A: CSLO images depicting scan lines (white lines) that cut across regions without hyper-reflective blot (line 1 and 2), and regions that contain blots (white solid arrows) (line 3 to 6). Hyper-reflectivity was also observed in the blood vessels (white empty arrow). B: Cross-sectional OCT images correspond to the 6 locations in A. Note the location of blood vessel in the vitreal surface (black empty arrow in Panel 1) and the degenerative profiles (solid white arrows) in ONL (Panel 3-6) that are in complete register with the blots in CLSO image of this retina. Scale bar in A is 50 μm, in B 100 μm.

Sodium iodate Day 7
40 mg/kg
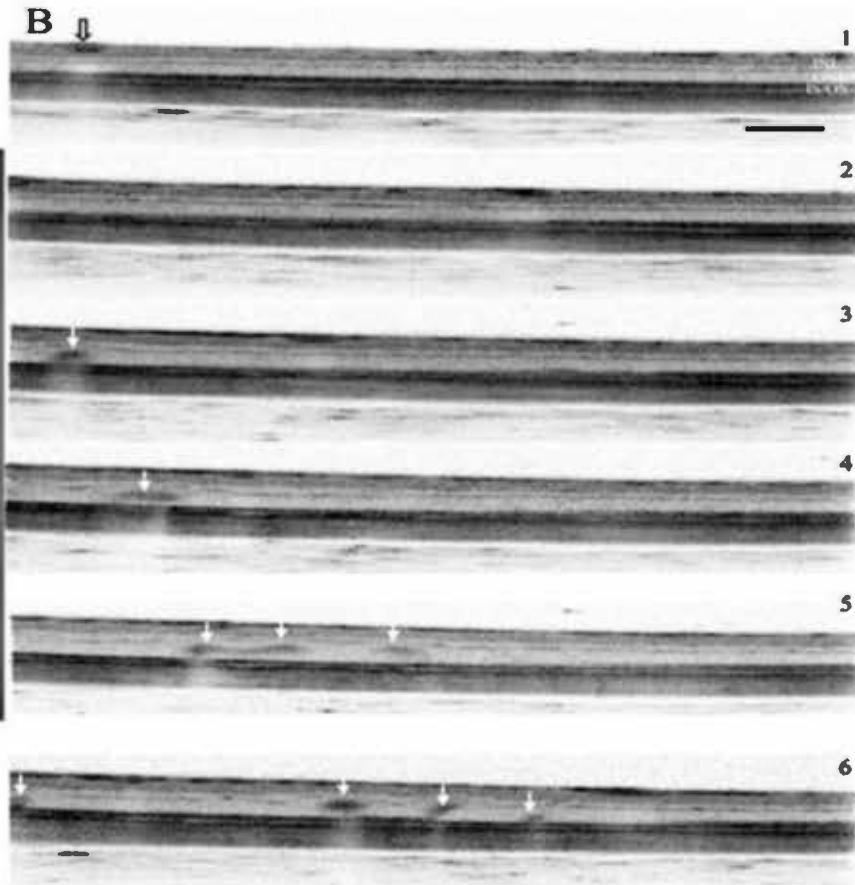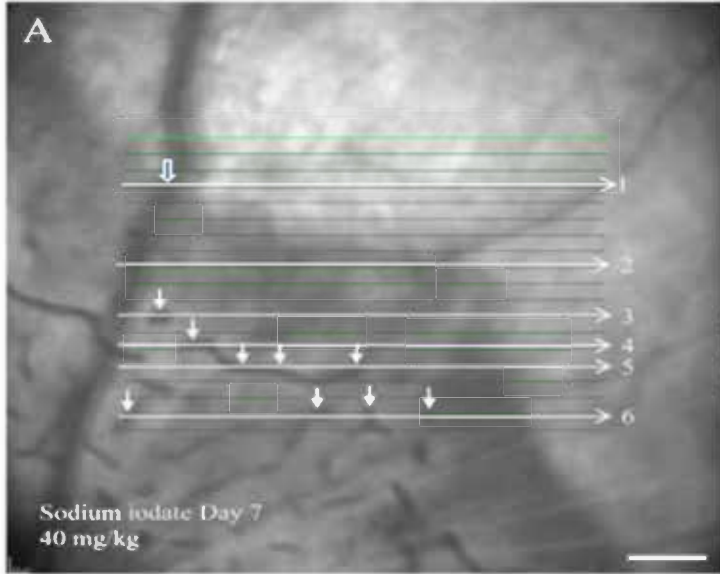
4.2.3 Dose effect of sodium iodate

We examined the change in blot number in response to different doses of sodium iodate by using CSLO. The quantitative analyses showed a dose dependent increase in blot number at 7 and 14 days after sodium iodate injection (i.v.). The response is progressive in animals injected with 25 or 40 mg/kg sodium iodate i.v. and is more acute in those received higher doses 75 mg/kg sodium iodate (**Figure 4.6**). Moreover, animals with injection of 50 mg/kg sodium iodate administered intraperitoneally showed a milder response than those with similar dose given intravenously (Day 7: 666.5±33.2-fold; Day 14: 2.07±42.6-fold, $p<0.05$), and the dark blots only started from day 14.

4.2.4 Histopathology of sodium iodate-induced lesion in the rat retina

To further investigate the relationships of the structural changes in infra-red CSLO and OCT images, we investigated the histological changes in paraffin sections of the retina after intravenous injection of 40 mg/kg sodium iodate. Morphological analyses showed that there was no detectable change in cellular arrangement in the retina 1 day (n=3) and 4 days post sodium iodate injection (n=3) (**Figure 4.7 B and C**). The retinal layers were readily identified as in the normal controls (n=3) (Figure 11A). Obvious lesions were found in the retina start from Day 7 (n=3), which appeared as massive degeneration of IS/OS of pigments and focal reduction of photoreceptor cells in ONL (**Figure 4.7 D**), producing irregular profiles of folding in the outer retinal layers. The inner retinal layers, including ganglion cell layer (GCL), inner plexiform layer (IPL) and inner nuclear layer (INL), are relatively spared. Similar abnormalities were observed in the retina 14 days post-injection (n=3), but with a further increase in folding and a reduction in retinal thickness (**Figure 4.7 E**).

Figure 4.6 Dose dependent effect of sodium iodate on blot number in the retina.
The number of blots in CSLO images increased with increasing dose of sodium iodate. Comparison of the number at Day 14 with Day 7 showed significant between animals injected i.v. with 25 or 40 mg/kg of drug when with those injected with 75 mg/kg, the maximum dose tested. $*P < 0.05$, Mann- Whitney U tests; mean ± SD. For counting the number of dark blots the image tool UTHSCSA (version 2.0) was used. i.v.: intravenous injection.
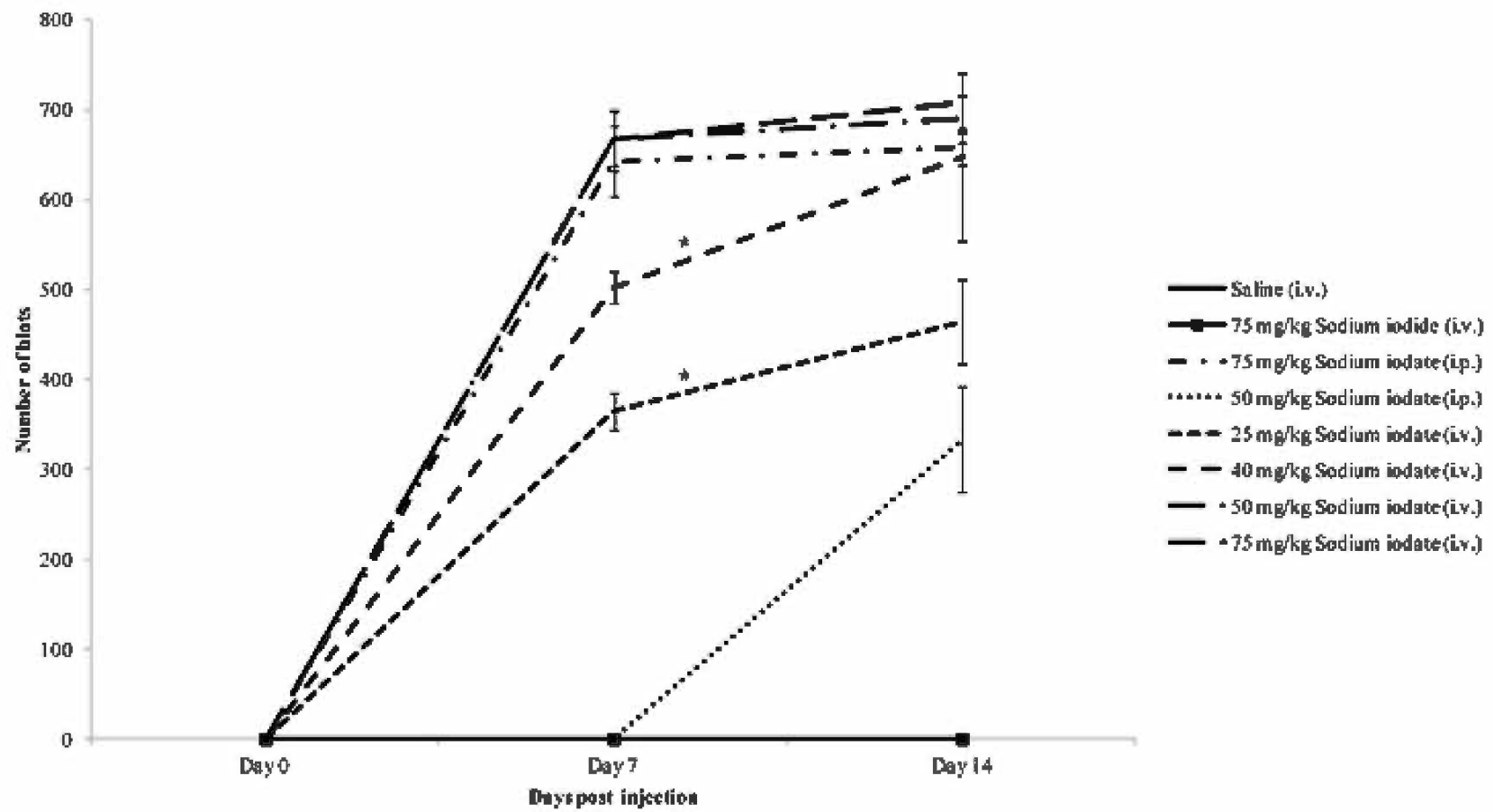
Figure 4.7 Temporal changes in retinal lesion after sodium iodate injection.
Paraffin section of the rat retina stained with Hematoxylin and Eosin in A: saline control, observed at 21 days; B-F: on different day after injection of 40 mg/kg sodium iodate. The retinal layers are clearly depicted in the control retina and in retinas 1 day and 4 days after sodium iodate injection. Disruption of the outer retinal layers (arrows) was detected at day 7 and the lesions became more severe at Day 14 and Day 21. Note the progressive increase in folding in the outer retinal layers and thinning out retinal thickness at the end of the examined period. GCL: ganglion cell layer; IPL: inner plexiform layer; INL, inner nuclear cell layer; OPL: outer plexiform layer; ONL, outer nuclear layer; IS/OS: Inner and outer segment of photoreceptor; RPE: retinal pigment epithelium. Scale bar is 100 μm.

Figure labels (A): IPL, INL, OPL, ONL, IS/OS, RPE
Control

(B): Day 1, 40 mg/kg sodium iodate (i.v.)

(C): Day 4, 40 mg/kg sodium iodate (i.v.)

(D): Day 7, 40 mg/kg sodium iodate (i.v.)

(E): Sodium Iodate Day 14
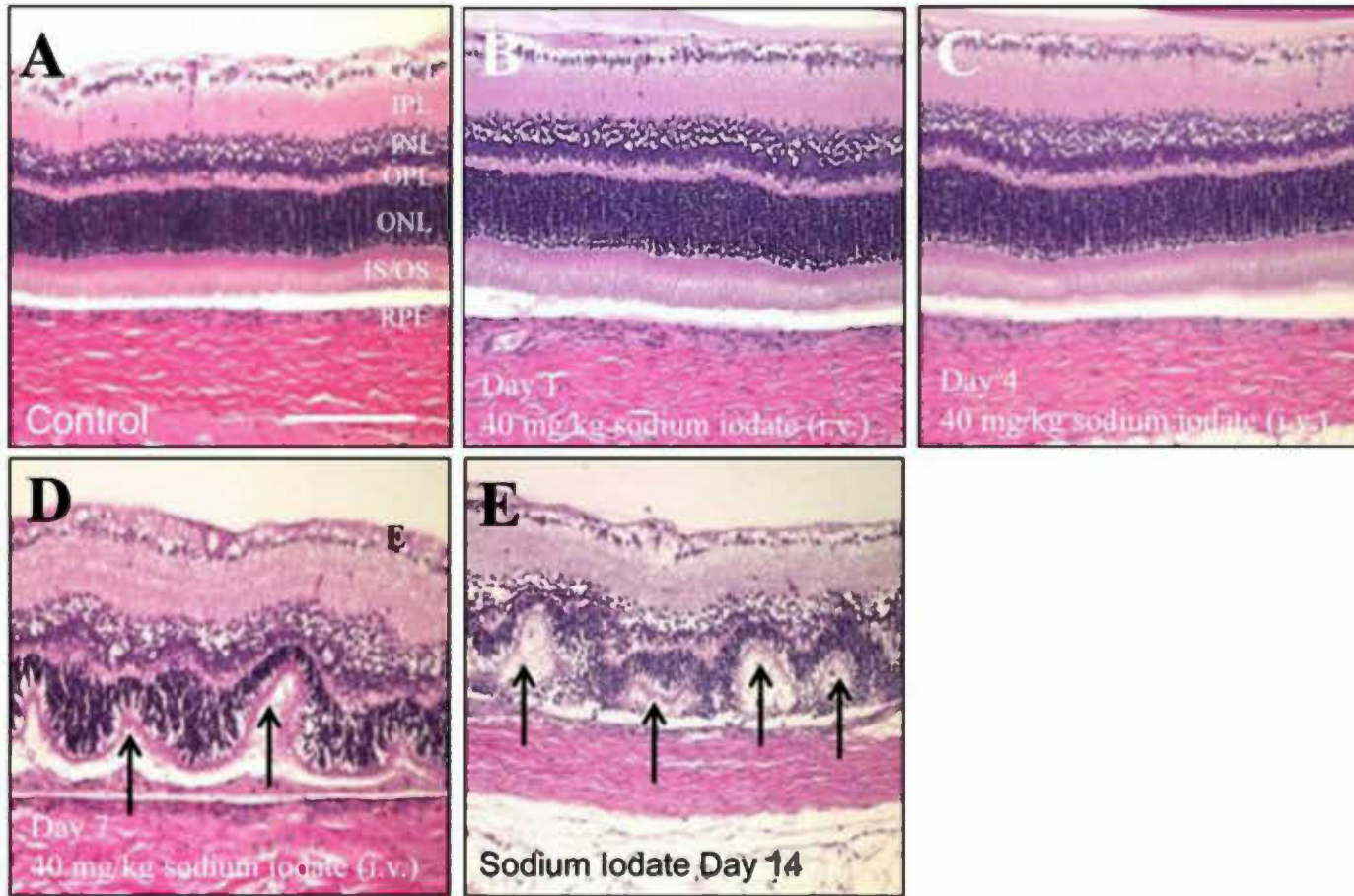
In another experiment, we investigated the morphological changes in retinal sections 14 days after intravenous injection of different dosages of sodium iodate. Sodium iodate at 25 mg/kg (n=3), the lowest dosage we examined, could generate obvious degeneration in outer retinal layers and a reduction in thickness of the retina, when compared with the control injected with saline (n=3) (**Figure 4.8 A and B**). Higher doses (40 or 50 mg/kg) produced further degenerative changes in the retina. At 75 mg/kg (n=6), the highest dose we tested, there was massive disruption of all retinal layers (**Figure 4.8 E**).

Quantitative analyses of morphological changes in these histological sections showed a significant dose dependent reduction in thickness of IS/OS and ONL, and in number of row of cells in ONL in animals with intravenous injection of sodium iodate (25-75 mg/kg) at 7 days and 14 days post-injection when compared with the saline control (**Figure 4.9 A-C**). However, in animals injected intraperitoneally with sodium iodate, significant reduction was observed only at the dose of 75 mg/kg but not at 50 mg/kg, indicating that intravenously injection is more effective in generating degeneration in outer retinal layers than intraperitoneal injection. Analyses of IPL and INL revealed a less severe damage when compared with the saline control, particularly at Day 7 (**Figure 4.10 A-C**). These findings indicate that sodium iodate has a selective effect on cellular structures in the outer retina within the first two weeks of injection.

The effects of sodium iodate on other organs were also determined in these animals. We found that sodium iodate at 25 (n=3) or 40 mg/kg (n=6) administered intravenously did not produce any obvious damage in the kidney and the liver (**Figure 4.11 B and E**), when compared with respective control that had received saline injection (n=6) (**Figure 4.11 A and E**). Obvious damage in cellular structures

Figure 4.8 Dosage effect of sodium iodate on retinal lesion. Representative micrographs showing responses of the retina to different doses of sodium iodate at day 14. A-B: saline control; C-H: sodium iodate at 25-75 mg/kg. Note the progressive changes of lesion that spread from photopigment layer at low dose to ONL and INL at higher doses.

intraperitoneal   Intravenous

Saline

25 mg/kg NaIO$_3$

50 mg/kg NaIO$_3$

75 mg/kg NaIO$_3$
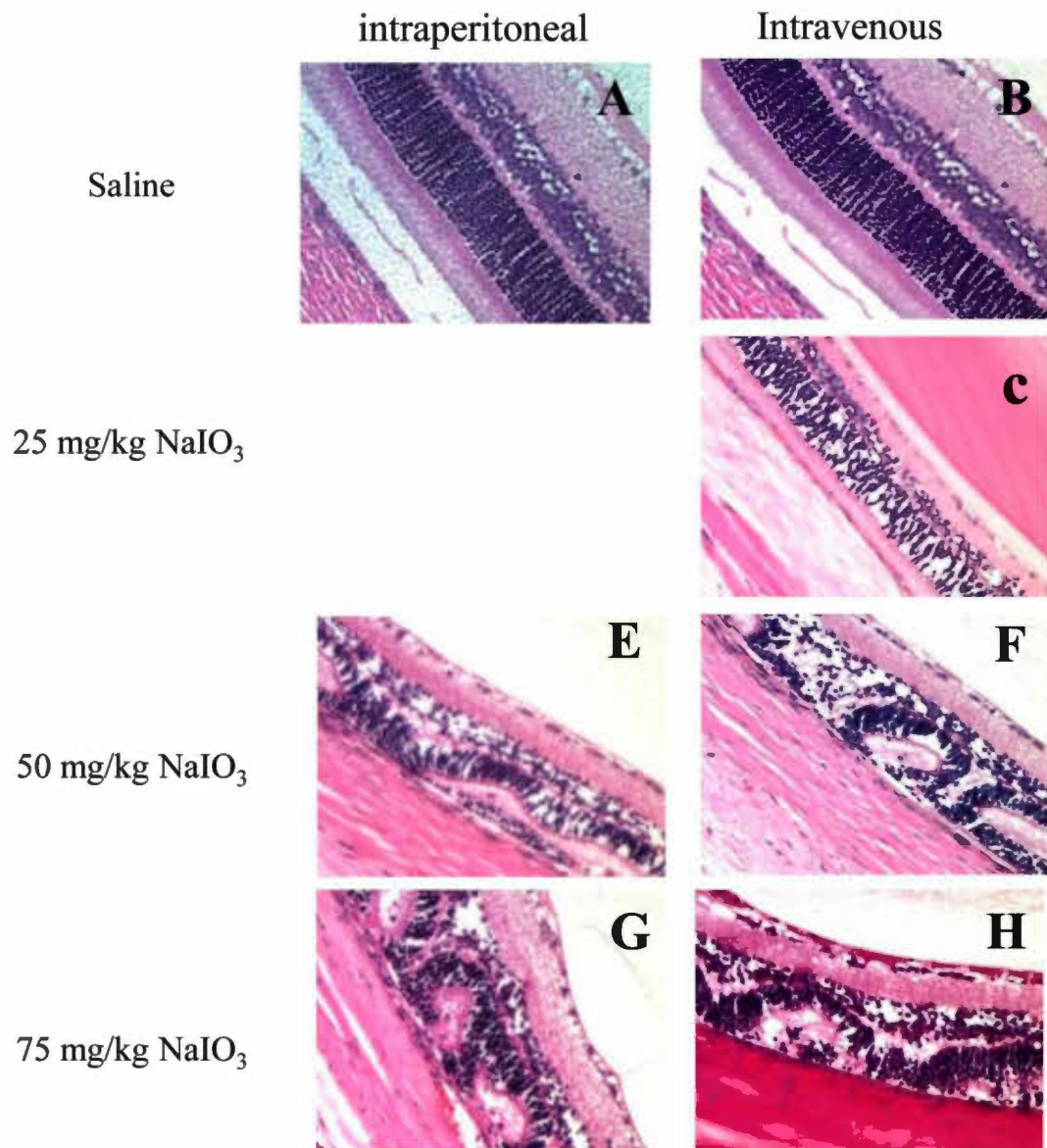
Figure 4.9 Quantitative analyses of outer retinal layers thickness and row number after sodium iodate insults. A: Dose dependent reduction in thickness of inner and outer segment of photoreceptor (IS/OS) in histological section of retina (n=3 in each group). Intravenous injection gave a more prominent effect than intraperitoneal injection at comparable dose of sodium iodate. B: Similar changes were observed in the outer nuclear layer (ONL). C: Counting of number of rows of photoreceptor nuclei in ONL confirmed the dose dependent response. $*P<0.005$, $**P <0.001$ when compared with saline control (Mann-Whitney U test). Each plot indicated the mean ± SD.

A IS/OS

B ONL

c ONL rows

Legend:
- Saline (i.v.)
- 75 mg/kg Sodium iodide (i.v.)
- 50 mg/kg Sodium iodate (i.p.)
- 75 mg/kg Sodium iodate (i.p.)
- 25 mg/kg Sodium iodate (i.v.)
- 40 mg/kg Sodium iodate (i.v.)
- 50 mg/kg Sodium iodate (i.v.)
- 75 mg/kg Sodium iodate (i.v.)
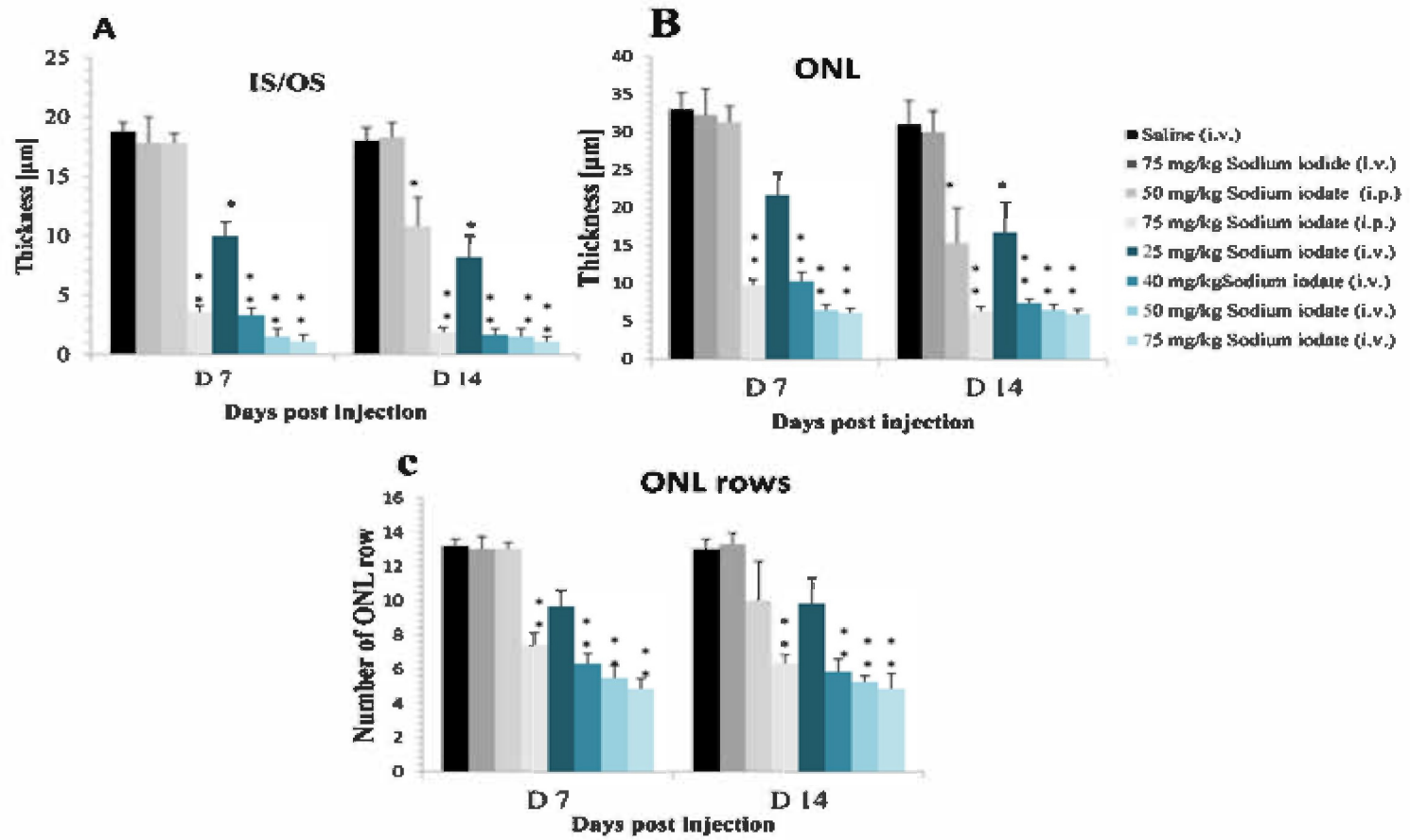
Figure 4.10 Quantitative analyses of changes in inner retinal layers after sodium iodate injection. A: Reduction in thickness of inner plexiform layer (IPL) was only obvious at Day 14, and again intravenous injection showed a more substantial effect than intraperitoneal injection at comparable dose of drug. B: Cell density counts showed a dose dependent reduction in inner nuclear layer (INL), which was particularly obvious at Day 14. $*P < 0.005$, $**P < 0.001$ when compared with saline control (Mann-Whitney U test). Legend is the same as that in Figure 4.9.

A IPL

B INL cell density

C INL
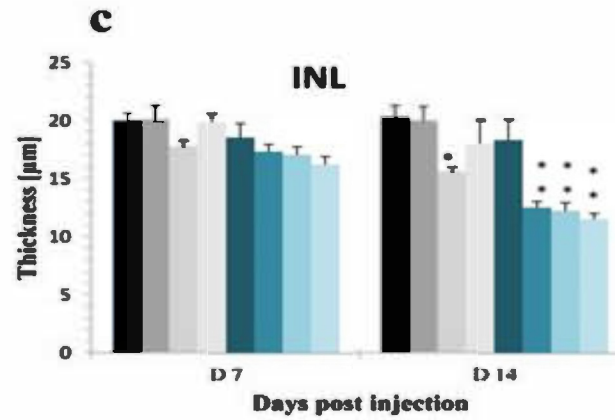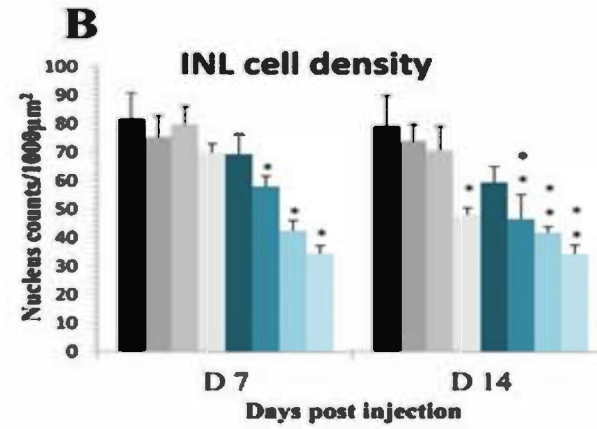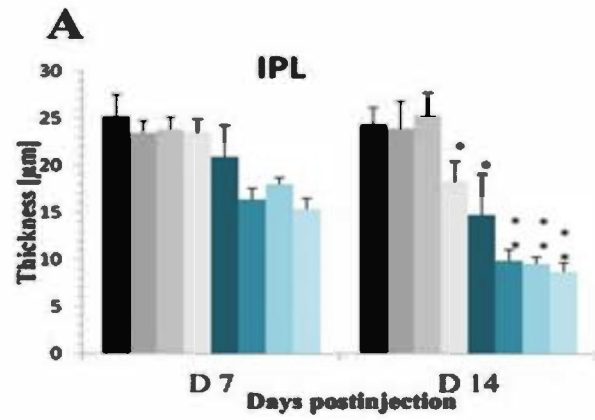
Figure 4.11 Histological assessment of liver and kidney in sodium iodate-treated rats. A.B: H&E staining of paraffin section of kidney in control (saline injected) C.D: treated with 25 mg/kg (i.v.) of sodium iodate 14 day after injection. E.F: treated with 40 mg/kg (i.v.) of sodium iodate 14 day after injection. G.H: treated with 50 mg/kg (i.v.) of sodium iodate 14 day after injection. I.J: treated with 75 mg/kg (i.v.) of sodium iodate 14 day after injection.
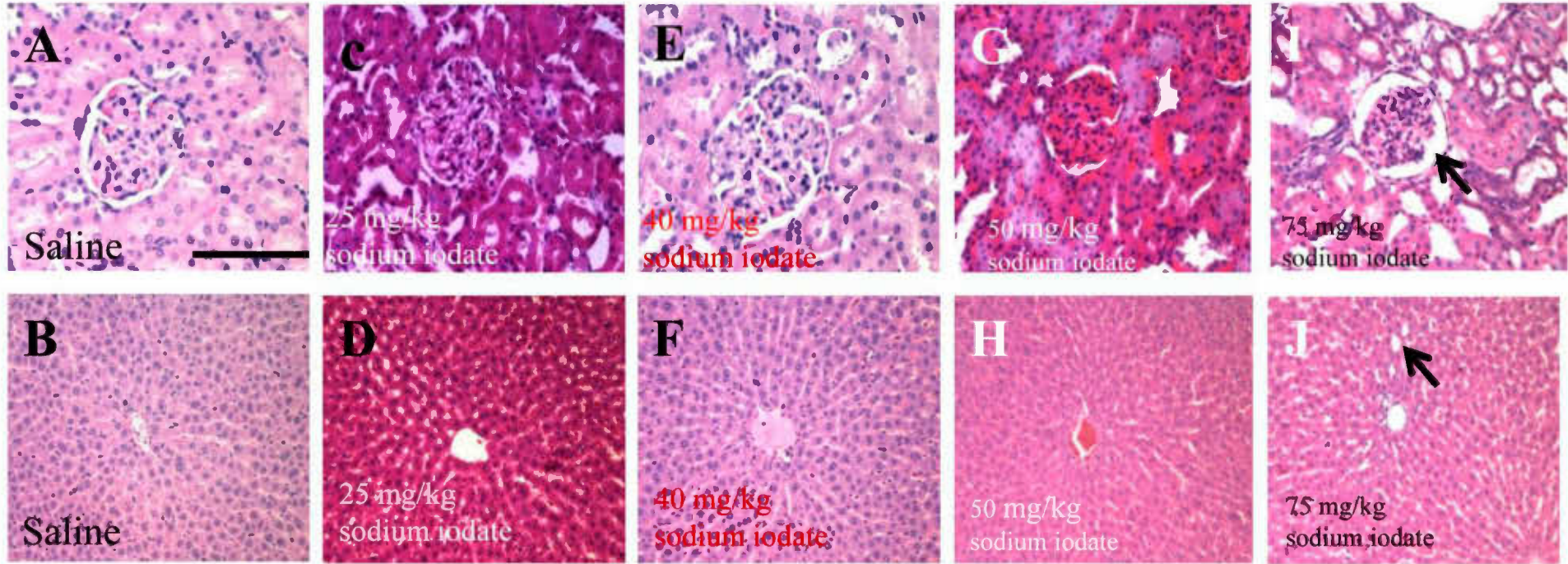
was observed at higher dose (75 mg/kg) (n=6) in both kidney and liver. The kidney with massive cell death and caused large gap space in the glomerulus, and also has extensive damage to the glomerulus and renal tubular. Massive death appearance in hepatocytes, more pyknotic cells but sinusoidal spaces are intact (**Figure 4.11 D and H**).

Moreover, while all animals with 40 mg/kg injection showed lesion in the retina, only about 50% with 25 mg/kg injection had retinal lesion, indicating that 40 mg/kg is the maximal dose that generates toxicity consistently to the retina but not other major organs.

4.2.5 Correlation of CSLO and OCT images with histology of retina

To investigate the anatomical basis of hyper-reflective blots in CSLO images, we selected several animals with injection of 25 mg/kg sodium iodate that produced a restricted distribution of dark blots in CSLO images of the living retina on Day 14. The rats were then sacrificed, their retinas were fixed, paraffin embedded and sectioned across the lesion regions. We found a correlation of the blot-rich regions with retinal regions that showed extensive damage in the outer retinal layers. In one specimen, the dark blots were confined to the inferior-nasal quadrant of the retina, whereas in histological section cutting across similar region of that retina lesions of the outer retinal layers were observed in nasal but not temporal hemiretina (**Figure 4.12 A-B**). In another retina, dark blots were found in a region surrounding the optic disk (**Figure 4.12 C**). Sections across this retina slightly inferior to the optic disk revealed obvious lesions in the central but not peripheral regions (**Figure 4.12 D**). The dark blots appeared in CSLO were corresponded to regions with lesion of outer retinal layers.

Figure 4.12 Hyper-reflective blots in CSLO images indicated location of outer retinal degeneration in histological section. A: In this rat CSLO revealed a localized sodium iodate induced lesion that is confined to inferior nasal quadrant of the retina. B: Sectioning of this retina at the level indicated in "A" (broken line) showed concomitant degeneration in outer retinal layers (black arrows) that is observed only in the nasal but not temporal retina in H&E preparation. C: In another rat, hyper-reflective blots were observed in central regions around the optic disk (white arrows). D: Histological section at the level indicated by the broken line in "C" showed a restricted damage (black arrows) in the central retina. Scale bar in A is 500 μm, applied also to C. Scale bar in B is 500 μm, applied to D.
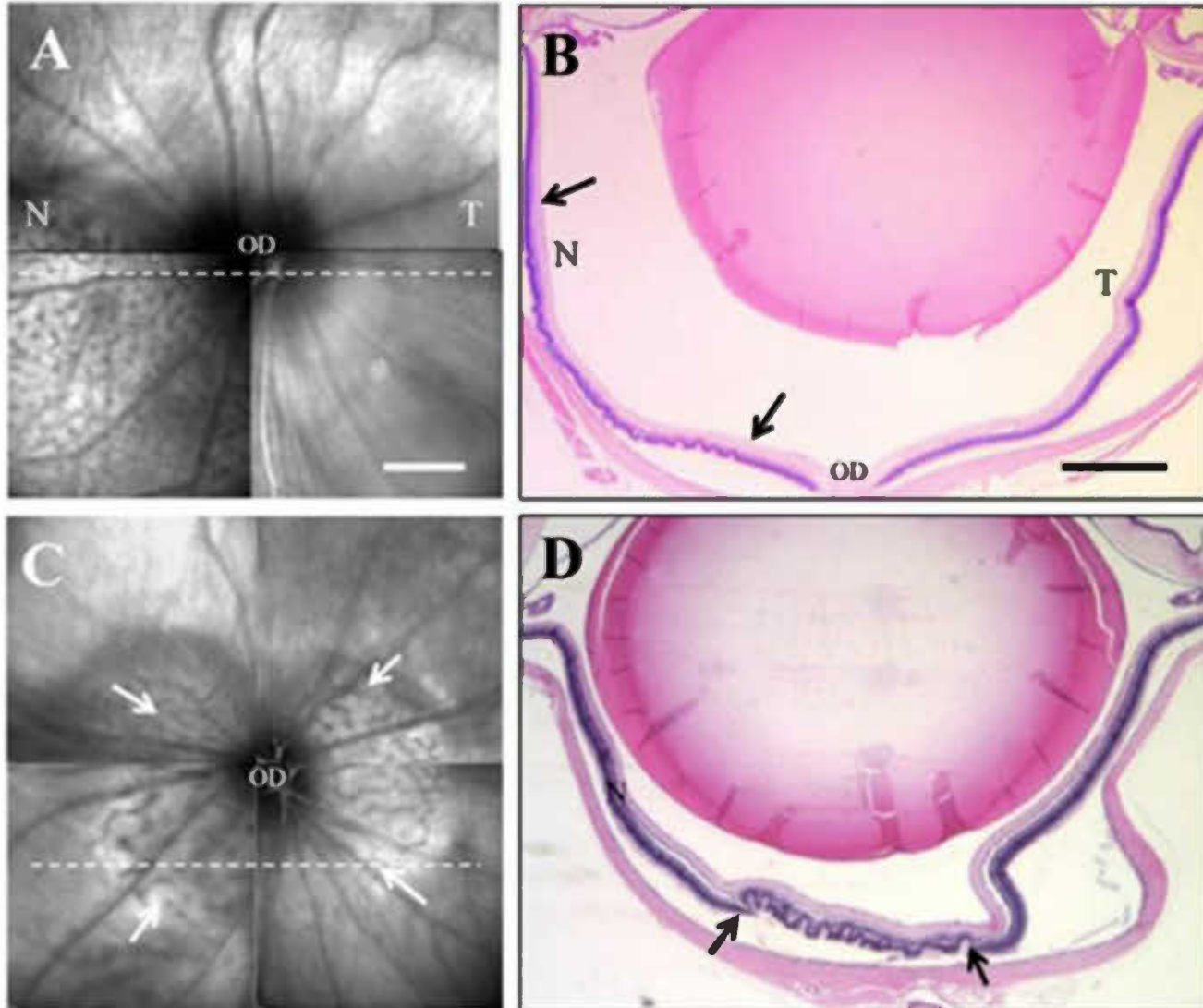
The highly organized laminated pattern in histological sections of normal retina was readily recognized in high resolution OCT images (**Figure 4.13 A-B**). In retina treated with 40 mg/kg sodium iodate, hyper-reflective structures found in the IS/OS layer and in the ONL in the OCT image are likely corresponding to the focal lesions observed in the paraffin section, which consist of degenerated photoreceptor pigments and folded layer of photoreceptor cells (**Figure 4.13 C-D**).

4.3 Catechins, catechin combinations and green tea extract attenuates sodium iodate - induced retinal degeneration (high dose)

4.3.1 Fundus examination by confocal scanning laser ophthalmoscopy (CSLO)

In fundus examination by CSLO, typical appearances of the retinal vessels and optic nerve head were well recognized. No obvious change was visible in the retina of control animals 14 days after saline injection (**Figure 4.14 A**). However, a dramatic change was observed in the retina 14 days after sodium iodate injection, which was characterized by the presence of many small dark blots throughout the four quadrants of the retina and hyper-reflectivity of retinal vessels (**Figure 4.14 B**). Worthily, with Theaphenon®E, EGCG, and catechins combination (EGCG, GC, EGC, and EC) treatments, the distribution of the dark blots was localized and restricted (**Figure 4.14 D-F**). However, in the catechins combination without EGCG (GC, EGC, and EC), the retina has no obvious change compare with the sodium iodate treated only retina.

The saline treated rats have no observable blots in the retina (**Figure 4.15**). For eyes treated with EGCG, catechins combination (EGCG, GC, EGC, and EC) and Theaphenon®E, prior to 40 mg/kg sodium iodate injection, the number of blots was significantly lower when compared with that of sodium iodate group at 14 days post
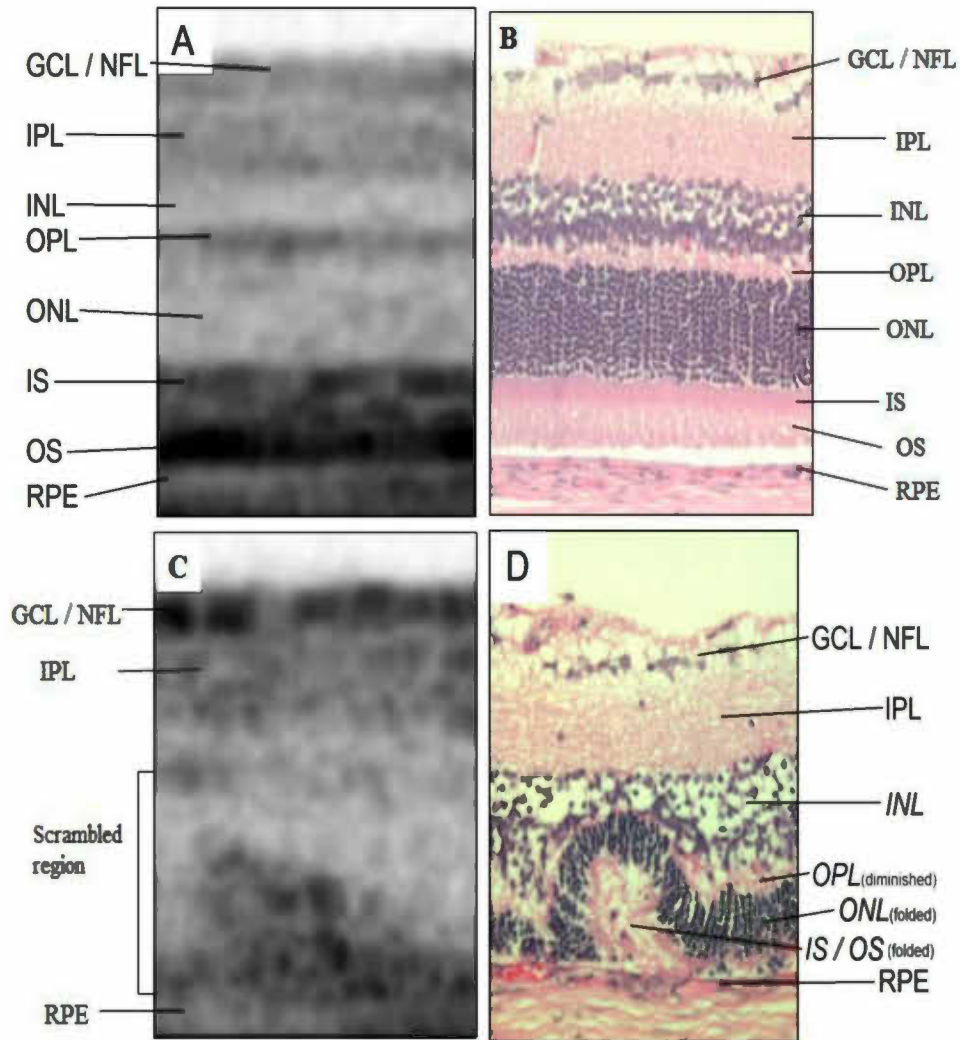
Figure 4.13 Histological correlation of retinal lesion in sodium iodate induced injury. A-B: Representative images of cross-sections of the retina under OCT and histological preparation. Note that all layers of the retina can be revealed by the live imaging technique. C-D: Comparison of the images suggested that the degenerative profile in outer retinal regions shown in OCT image is likely corresponding to the disrupted photopigment layer and the folded outer nuclear layer. GCL/NFL: ganglion cell and nerve fiber layer; IPL: inner plexiform layer; INL, inner nuclear cell layer; OPL: outer plexiform layer; ONL, outer nuclear layer; IS/OS: Inner and outer segment of photoreceptor; RPE: retinal pigment epithelium. Scale bar is 50 μm.

Figure 4.14 Retinal lesions under infra-red confocal scanning laser ophthalmoscopy (CSLO). All the retinas were 14 days after sodium iodate injection. A: Saline injection. B: 40 mg/kg sodium iodate injection. Hyper-reflective structures or blots (white arrows) were detected in all retinal quadrants. C: Catechins combination (GC, EGC, and EC) with sodium iodate treated. Dark blots were detected in all retinal quadrants. D-F: Dark blots were limited to certain regions (white arrows). Scale bar is 200 μm.
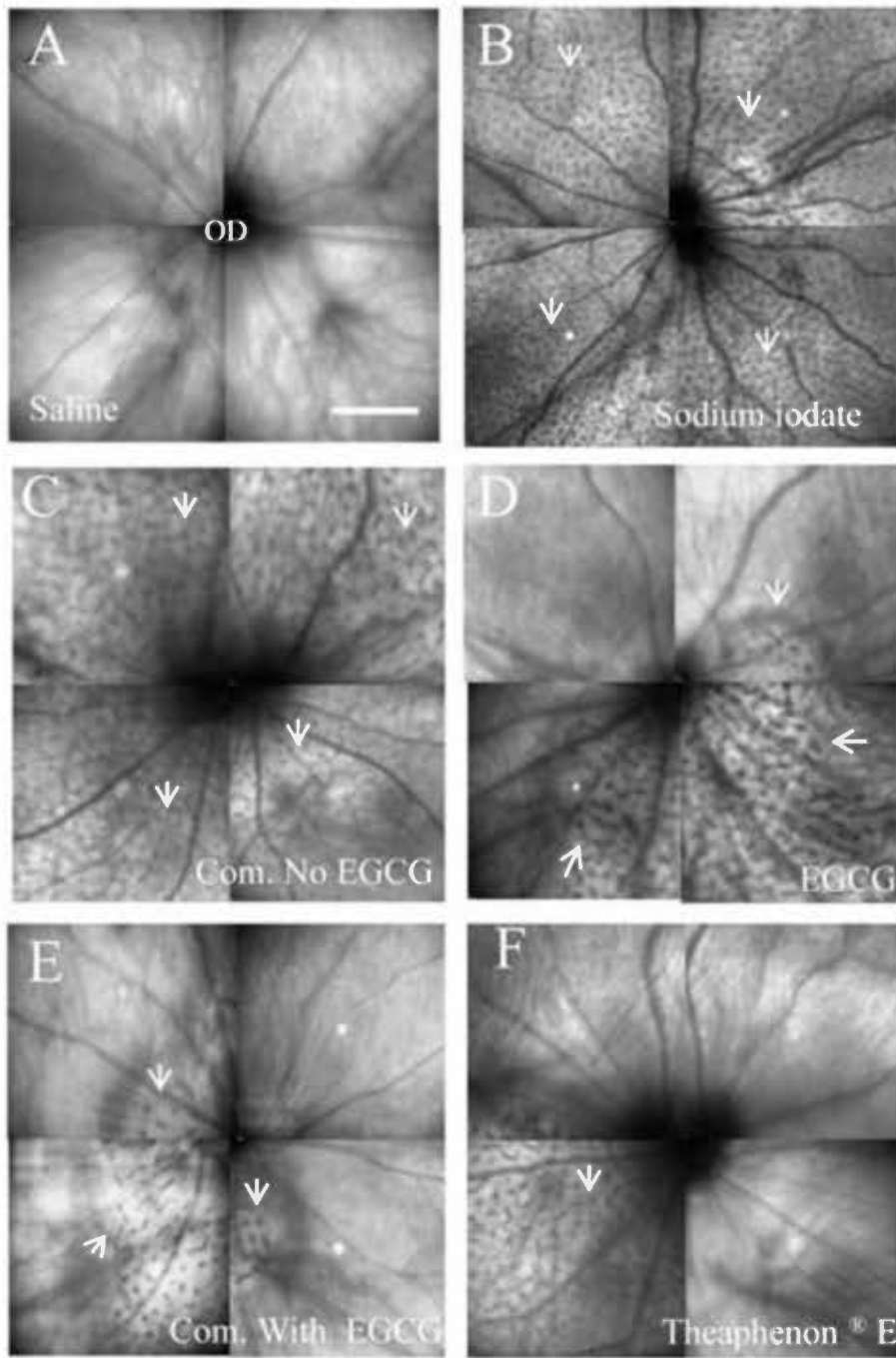
OD: Optic disc
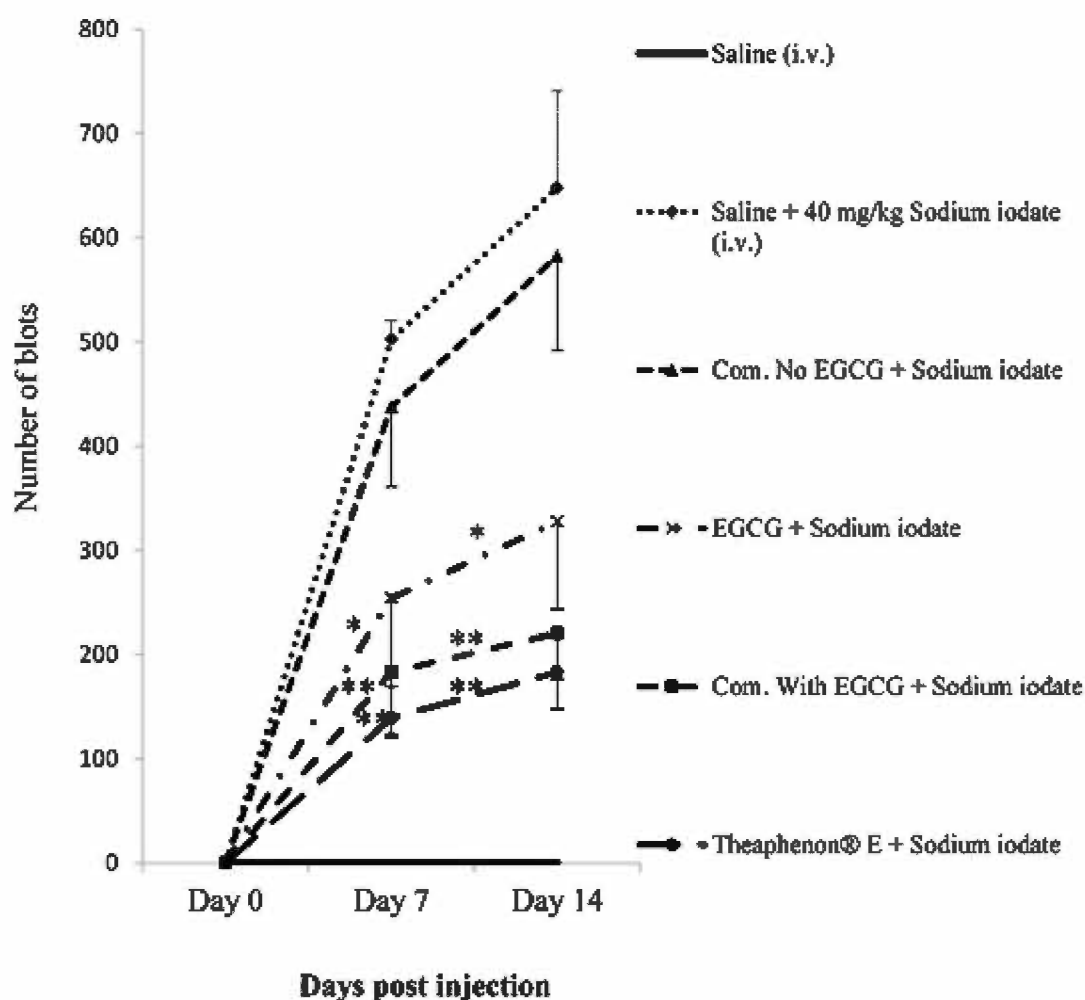
Figure 4.15 The number of blot in the retina. The number of the blots in CSLO images decreased after EGCG, catechins combination (EGCG, GC, EGC, and EC), Theaphenon® E treated. Comparison of the number at Day 7 and Day 14 with 40 mg/kg sodium iodate treated only. * $P < 0.05$, ** $P < 0.01$, Wilcoxon Rank sum tests; mean ± SD. For counting the number of dark blots the image tool UTHSCSA (version 2.0) was used. i.v.: intravenous injection.

injection. However, the eyes treated with catechins combination without EGCG have no significant protective effect against sodium iodate-induce retinal dark blots.

4.3.2 Outer nuclear layer thickness assessed by spectral –domain optical coherence tomography (SD-OCT)

Figure 4.16 shows an analysis of measuring the thickness of the ONL from different treatment of experiments groups where it can be seen that the 40 mg/kg sodium iodate caused the thinning of the ONL and these were significantly counteracted by catechins combination (EGCG, GC, EGC, and EC), EGCG, and Theaphenon®E. And the layer became thicker than the only sodium iodate treated retinas.

4.3.3. Catechins reduced sodium iodate-induced retinal degeneration in histological preparations

We have previously shown that when 40mg/kg sodium iodate was injected, the alignment of nuclei in the ONL and the rod outer segments were irregular, shortened and disorganized (**Figure 4.17 B**). The cell density in INL decreased. **Figure 4.17 D-F** shows with administrated the EGCG, catechins combination (EGCG, GC, EGC, and EC), and Theaphenon®E, the retina became more flatten, reducing the loss of nuclei. **Figure 4.18** represents a comparison between the catechins treated and untreated eyes, the proportion of total retinal length exhibiting irregular ONL alignment to total retinal length measured on Day 14 after the sodium iodate injection. Importantly, proportion of retinal length exhibiting irregular ONL alignment was significantly less in EGCG, catechins combination (EGCG, GC, EGC, and EC), and Theaphenon®E treated eyes than the sodium iodate treated only eyes.
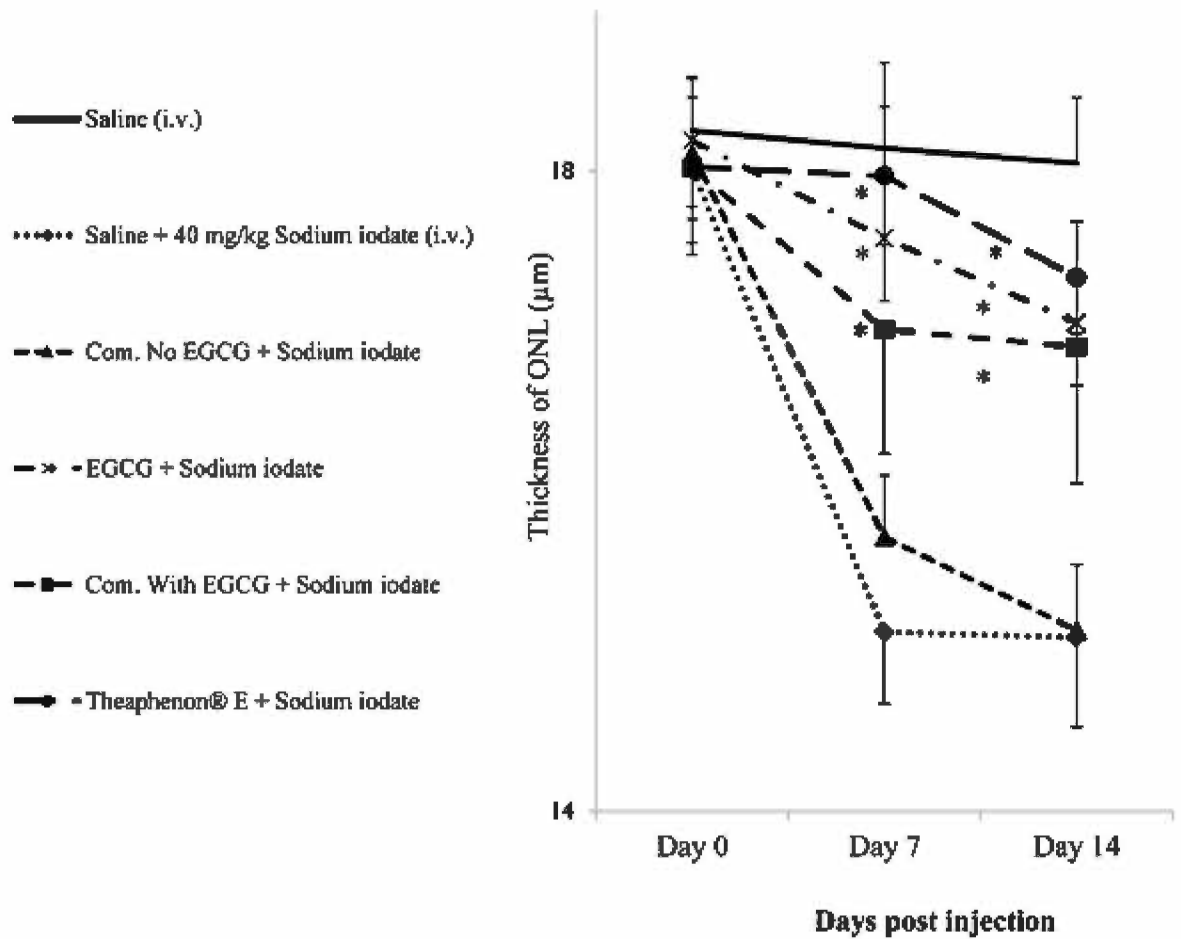
Figure 4.16 ONL thickness under spectral-domain optic coherence tomography (OCT). Graphs show results for ONL thickness in OCT images. The ONL thickness decreased in 40 mg/kg sodium iodate treated retina compare to saline injection after 14 days, after EGCG, catechins combination (EGCG, GC, EGC, and EC), Theaphenon®E treated, the ONL thickness increased significantly when compare to 40 mg/kg sodium iodate treated group. * $P < 0.05$, Mann- Whitney U test (Mean ± SD).

Figure 4.17 Catechins attenuate retinal changes in retinal lesion after sodium iodate injection. Paraffin section of the rat retina stained with Hematoxylin and Eosin in A: saline control; B: 40 mg/kg sodium iodate injection after 14 days; C-F: on different drug treatment with sodium iodate injection after 14 days. The retinal layers are clearly depicted in the control retina. Disruption of the outer retinal layers (arrows) was detected and the lesions were severe. Note with the EGCG, catechins combination (EGCG, GC, EGC, and EC) treated, the number of the folded retina decreased, with Theaphenon®E, the retina nearly to be normal. GCL: ganglion cell layer; IPL: inner plexiform layer; INL, inner nuclear cell layer; OPL: outer plexiform layer; ONL, outer nuclear layer; IS/OS: Inner and outer segment of photoreceptor; RPE: retinal pigment epithelium. Scale bar is 200 μm. All the images were taken 300 μm from the optic disk.

A Saline

50μm

B Saline + 40 mg/kg sodium iodate

C Com. No EGCG + Sodium iodate

D EGCG + Sodium iodate

E Com. With EGCG + Sodium iodate

F Theaphenon ® E + Sodium iodate
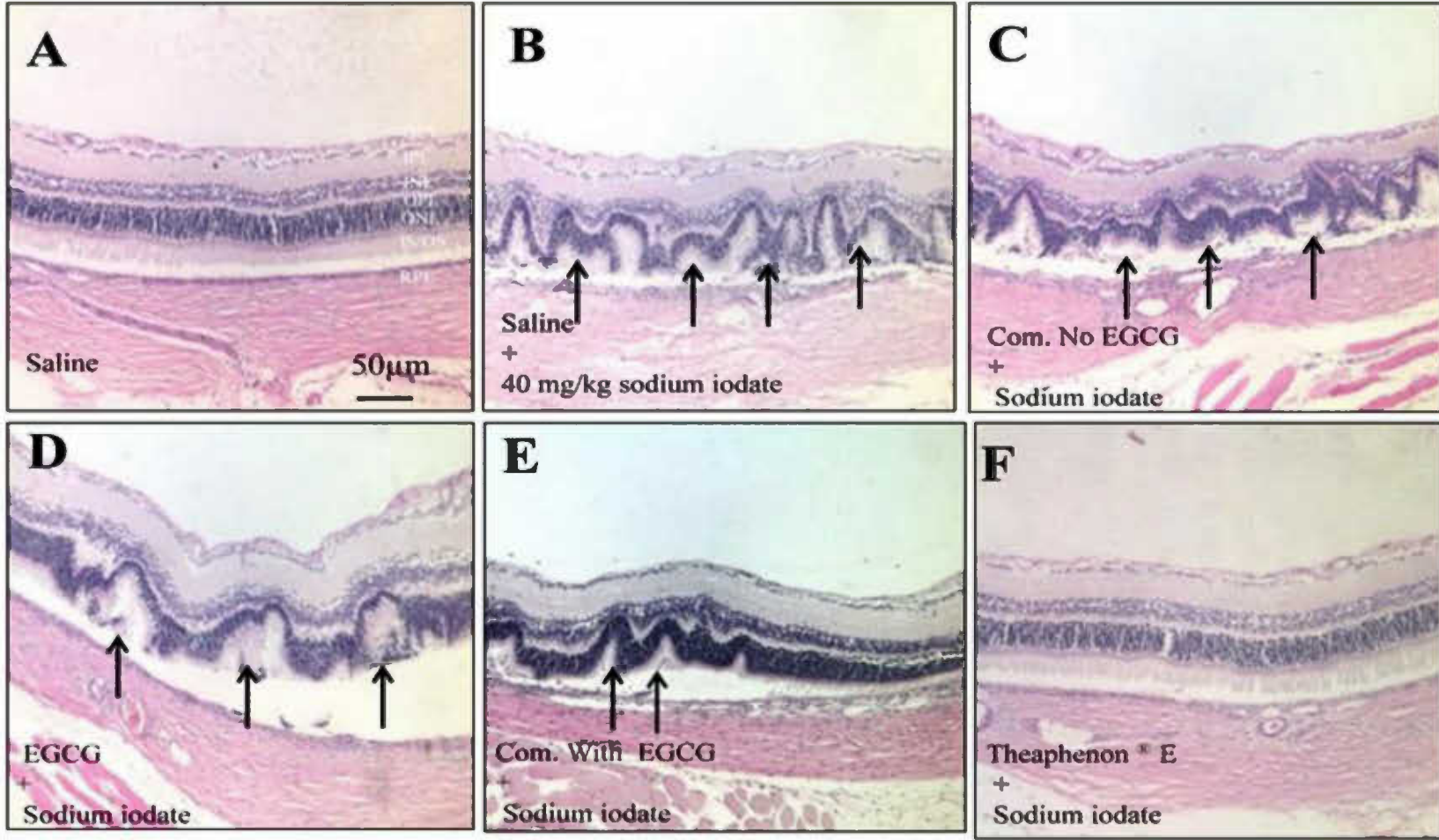
Figure 4.18 The proportion of the folded retina in the histological preparations.

The proportion of retinal length exhibiting irregular ONL alignment to total retinal length, Image J (version 1.46e; NIH, Bethesda, MD) was used. The proportion of the folded retina is defined the length of the folded retina divided by the total length of the whole retina in histological slices. The eyeballs were sections vertically through the optic nerve (superior-inferior). * P < 0.05, Mann- Whitney U test (Mean ± SD). i.v.: intravenous injection.
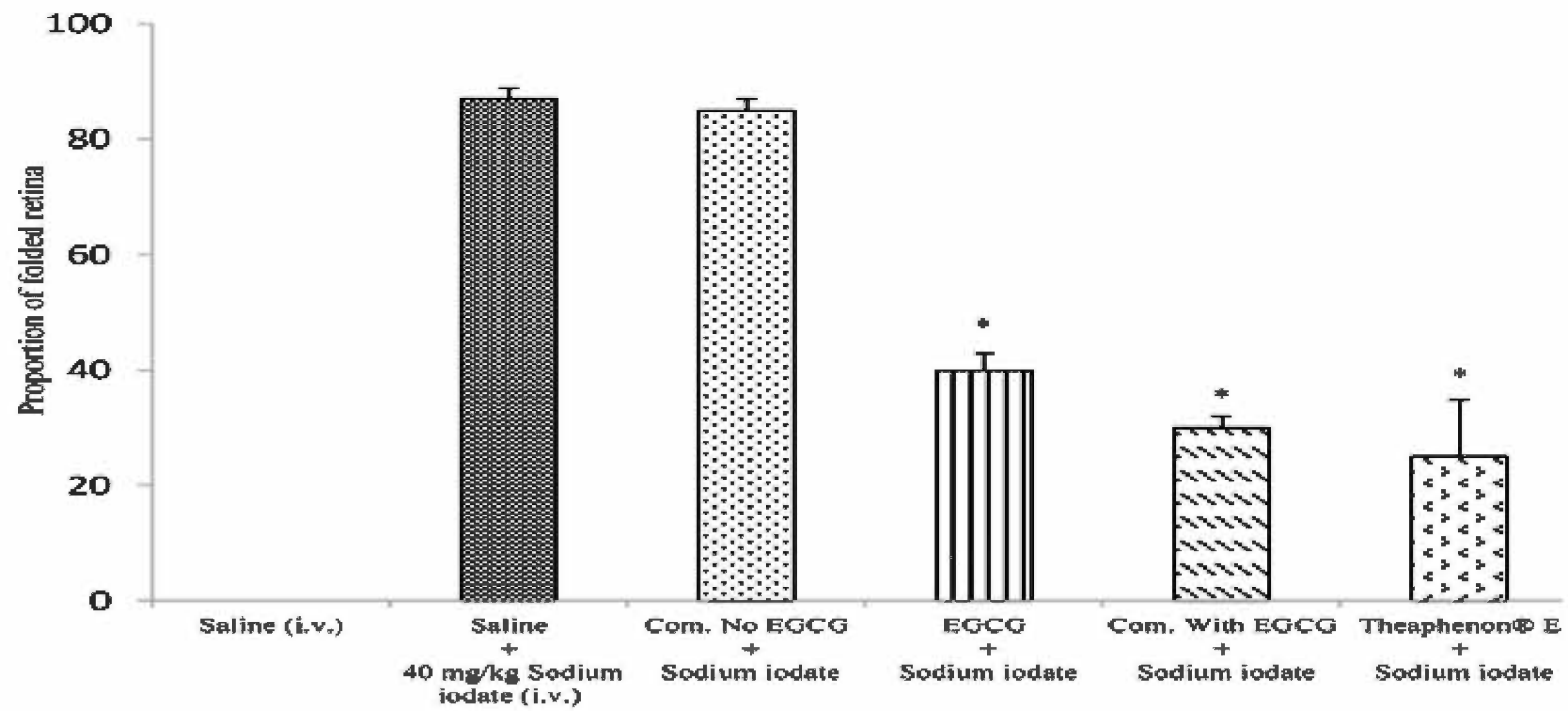
However, the sodium iodate effect wasn't counteracted by the catechins combination (GC, EGC, and EC). The finding that sodium iodate caused reduction of ONL compared with saline treated retinas is consistent with SD-OCT and histological preparations.

4.3.4 Determination of mRNA level in retina by real time-PCR

After 40 mg/kg sodium iodate injection without any treatment followed by 24 hours, the expression of mRNA levels of Superoxide dismutase (SOD), Glutathione peroxidase (GPx) and caspase-3, normalized to GAPDH, were significantly increased. In contrast, for eyes with EGCG, catechins combination (EGCG, GC, EGC, and EC) and Theaphenon$^{®}$E treated, the increased expression mRNA level of SOD, GPx and capase-3 were blunted (51.5%, 58.3%, 47.3%; 51.0%, 28.8%, 20.7%; 10.3%, 8.6%, 11.7% of sodium iodate treated only group with $P < 0.05$). The effect caused by the catechins combination (GC, EGC, and EC) on the mRNA levels of SOD, GPx and capase-3 were slightly attenuated, although the difference were not statistically significant. (**Figure 4.19**)

4.3.5 Quantification of 8-iso-PGF$_{2a}$ level in retina

The levels of 8-iso-PGF$_{2a}$ in the retina are shown in **Figure 4.20** were nearly 10 times increased in 40 mg/kg sodium iodate treated only group than in saline treated group. Importantly, the 8-iso-PGF$_{2a}$ levels were strongly attenuates by EGCG, catechins combination (EGCG, GC, EGC, and EC), and Theaphenon$^{®}$E treatment. However, the 8-iso-PGF$_{2a}$ level was slightly against by the catechins combination (GC, EGC, and EC), but no statistically significant.

Figure 4.19 The SOD, GPx, Caspase 3 mRNA level in retina.

The mRNA levels in retina normalized with GAPDH. It can be seen that sodium iodate caused significant increasing on the mRNA level compare to the saline group. These changes were all significantly blunted by treated with EGCG, Theaphenon® E. The catechins combination decrease the mRNA level but not statistical significant. * P < 0.05, Mann- Whitney U test (Mean ± SD). i.v.: intravenous injection.

A

B

C
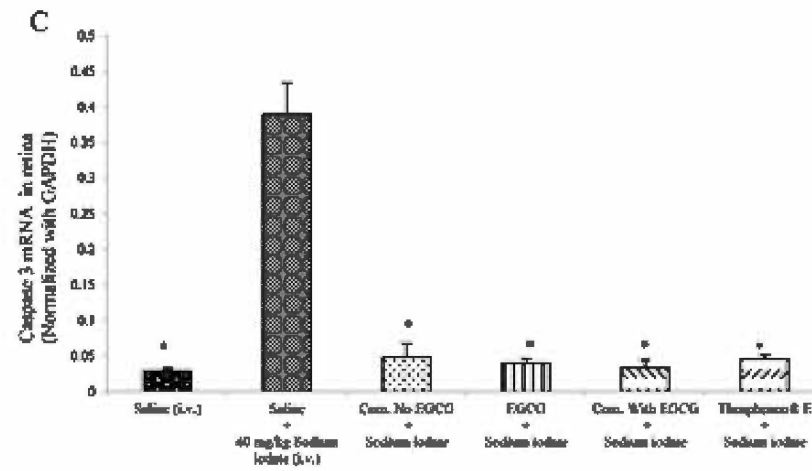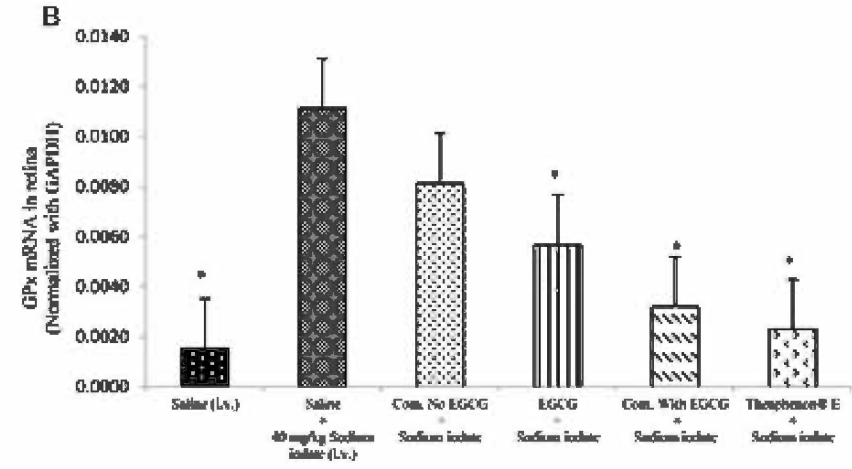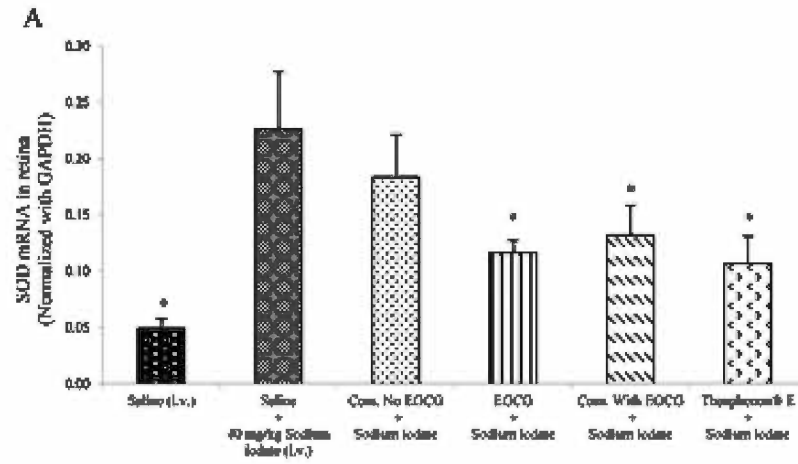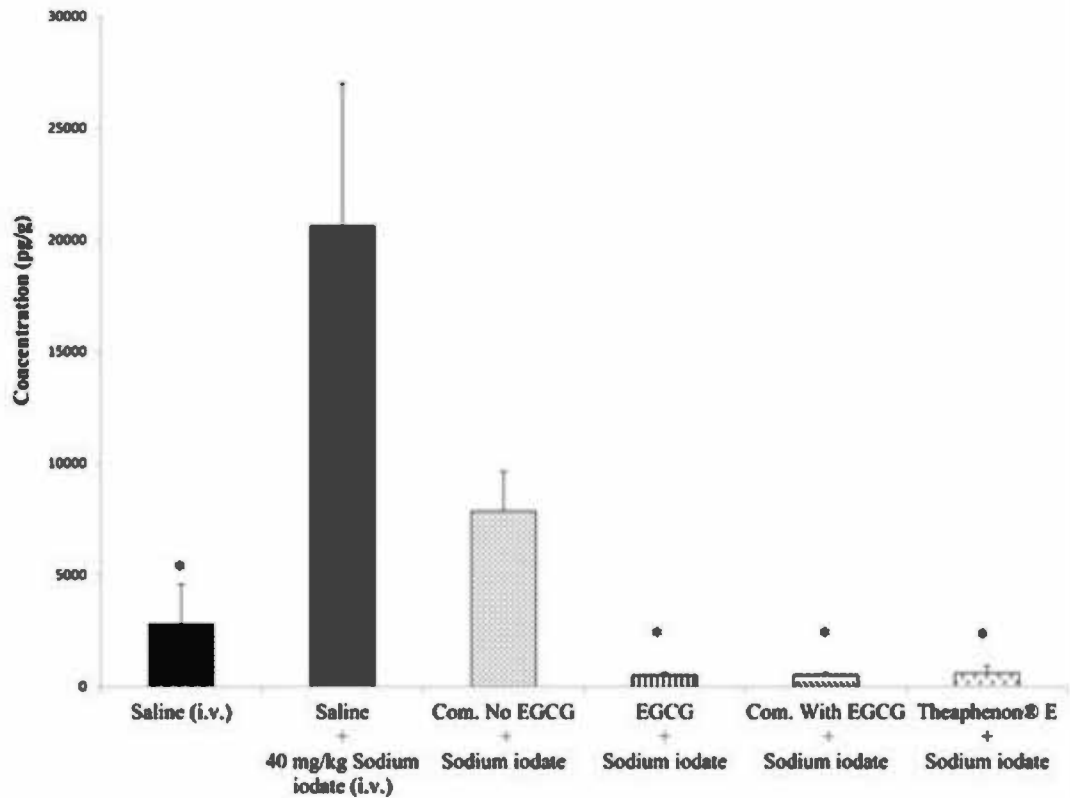
Figure 4.20 The 8-iso-PGF$_{2a}$ concentration in retina. 24 hours post injected sodium iodate, the 8-iso-PGF$_{2a}$ concentration in retina was dramatically increased compare to control, these were significantly blunted by EGCG, catechins combination (EGCG, GC, EGC, and EC), Theaphenon$^{®}$E treated. * $P < 0.05$, Mann-Whitney U test (Mean ± SD). i.v.: intravenous injection.

4.4 Low dose of green tea extract, EGCG, and catechins combinations has no protective effect on sodium iodate-induced retinal degeneration

After 40mg/kg sodium iodate post 14 days intravenous injection, the retinal lesions were induced throughout the rat retinal appeared as usual. However, with 100 mg/kg Theaphenon E, 70.5 mg/kg EGCG, 79.6 mg/kg catechin combination with EGCG treated, the number of the dark blots significantly decreased, but with 9.1 mg/kg catechin combination without EGCG treated, we can't find any significant changes by the CSLO in terms of the number or the reflectivity of dark blots in the retina (**Figure 4.21 and 4.22**).

In the morphometric evaluation of the retina, compare to the 40 mg/kg sodium iodate treated retinas, after these drugs treated, the alignment of nuclei in the ONL was irregular, a wavy folded retina was apparent in which the outer retinal were shortened and disorganized in both catechins drug treated and only 40 mg/kg sodium iodate treated eyes (**Figure 23**).

Figure 24 represents a comparison between the different compose of catechins with 40 mg/kg sodium iodate treated and only with 40 mg/kg sodium iodate treated eyes with respect to the proportion of total length of the retina exhibiting irregular and folded outer retinal alignment on 14 days post sodium iodate injection. However, the proportion of total retinal length display irregular and folded retinal length were not significantly less in the catechins treated eyes with the sodium iodate treated only eyes ($p>0.05$), indicating 100 mg/kg Theaphenon E, 70.5 mg/kg EGCG, 79.6 mg/kg catechin combination with EGCG, and 9.1 mg/kg catechin combination without EGCG has no significant preservation of retinal structure damaged by sodium iodate.

Figure 4.21 retinal treated by the low dose of the catechins captured by infra-red confocal scanning laser ophthalmoscopy (CSLO). All the retinas were 14 days after sodium iodate injection. A. Saline injection. B. 40 mg/kg sodium iodate injection. Hyper reflectivity blots (white arrows) were indicated in all retinal quadrants. C. Low dose of catechins combination (GC, EGC, EC) daily oral gavage feed with 40 mg/kg single intra-venous injection. Dark blots were detected in all retinal quadrants. D-F: Dark blots were appeared in all the quadrants of the retinas. Scale bar is 200μm.
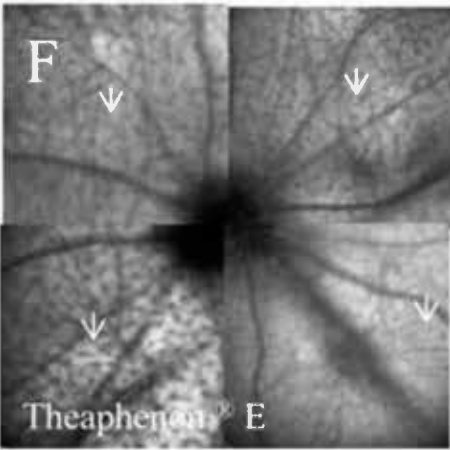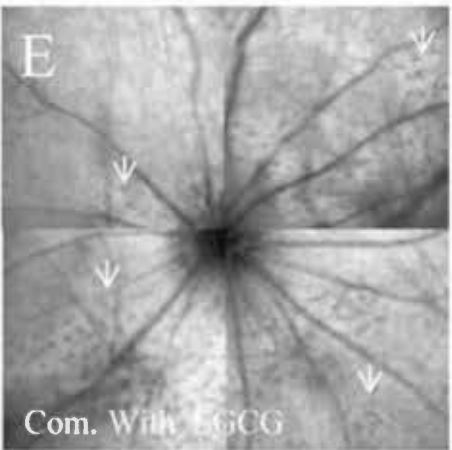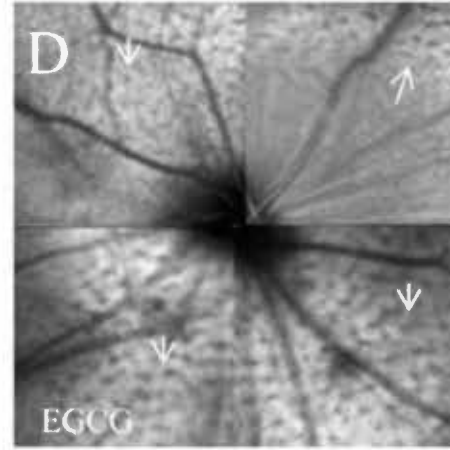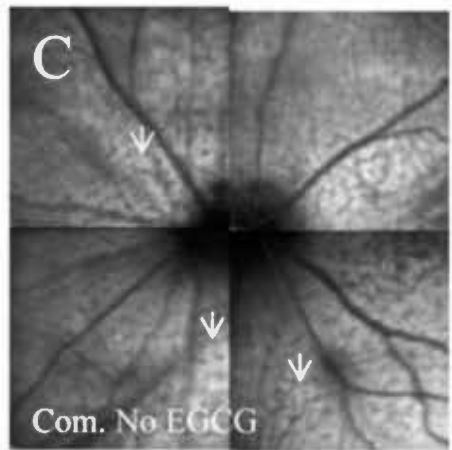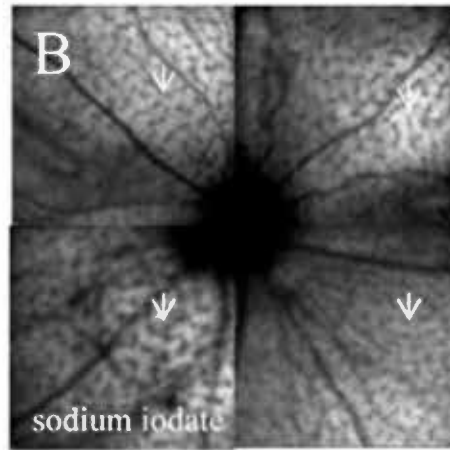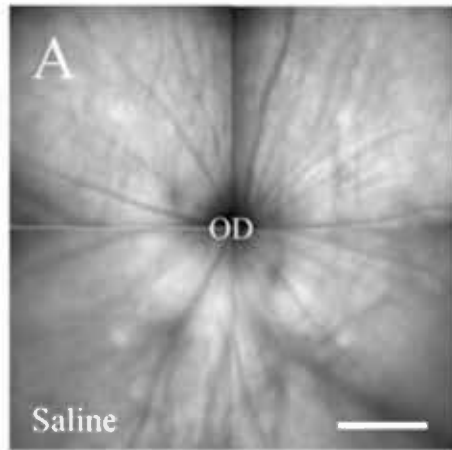
Figure 4.22 The number of the dark blot in the retina. The number of the blots in

CSLO images decreased after the low dose of the EGCG, catechins combination with

EGCG (EGCG, GC, EGC, and EC), and Theaphenon$^{®}$E treated. Comparison of the

number at Day 7 and 14 with 40 mg/kg sodium iodate treated only group. * $P < 0.05$,

Wilcoxon Rank sum tests; mean ± SD. For counting the number of dark blots the

image tool UTHSCSA (version 2.0) was used. i.v.: intravenous injection.
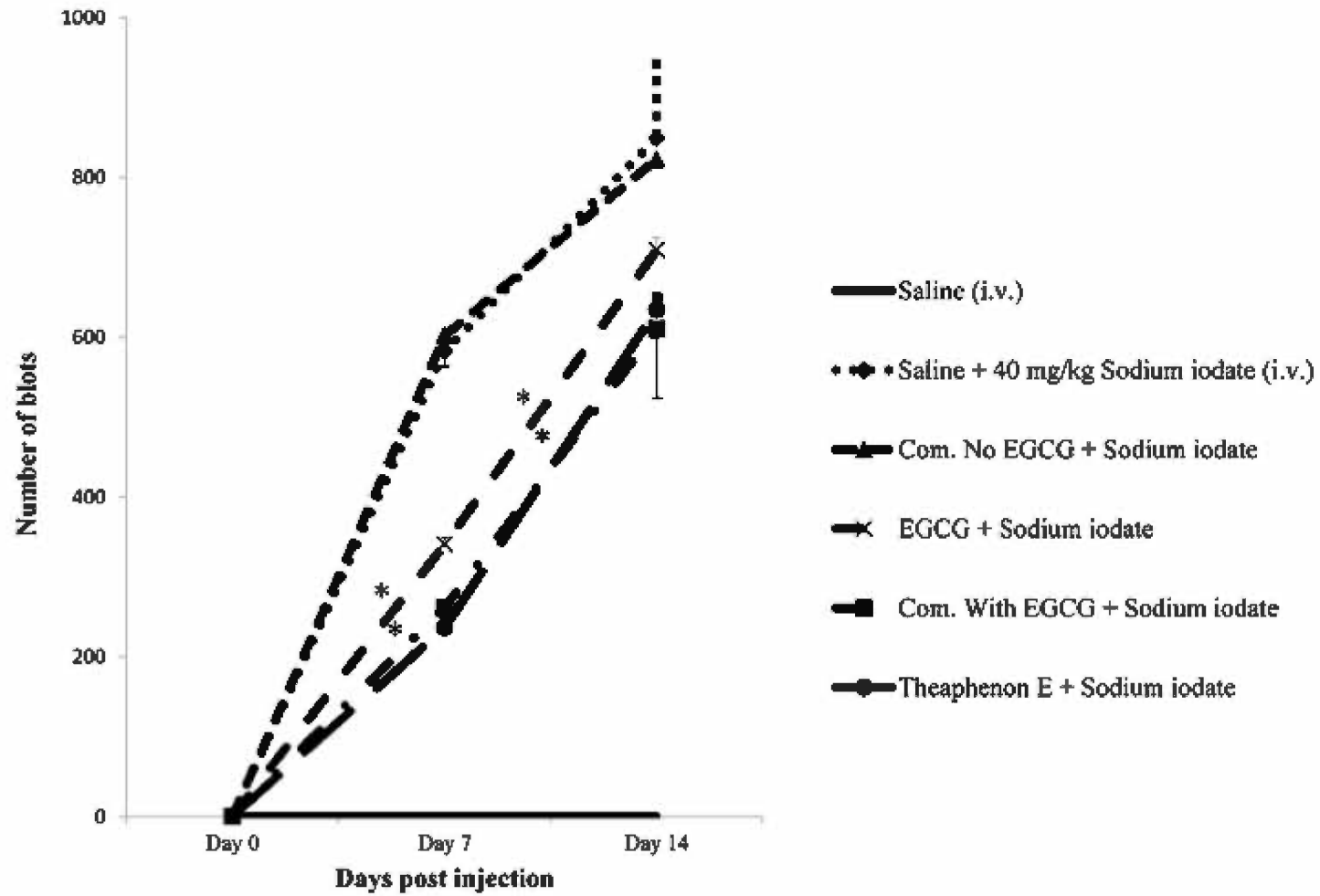
Figure 4.23 Low dose of catechins hasno protective effect in retinal damage induced by sodium iodate. Paraffin section of the rat retina stained with Hematoxylin and Eosin in A: saline control; B: 40 mg/kg sodium iodate injection after 14 days; C-F: on different low dose of drug daily treated with 40 mg/kg single intra-venous injection after 14 days. The retinal layers are clearly depicted in the control retina. Disruption of the outer retinal layers was detected and the lesions were severe. Note with the low dose of EGCG, catechins combinations without EGCG (GC, EGC, EC) combination (EGCG, GC, EGC, and EC) and Theaphenon[®]E treated, there was no detectable change. GCL: ganglion cell layer; IPL: inner plexiform layer; INL, inner nuclear cell layer; OPL: outer plexiform layer; ONL, outer nuclear layer; IS/OS: Inner and outer segment of photoreceptor; RPE: retinal pigment epithelium. Scale bar is 200 μm. All the images were taken 300 μm from the optic disk.

GCL
IPL
INL
OPL
ONL
IS/OS
RPE

A Saline   50μm

B Saline + 40 mg/kg sodium iodate

C Com. No EGCG (low dose) + Sodium iodate

D EGCG (low dose) + Sodium iodate

E Com. With EGCG (low dose) + Sodium iodate

F Theaphenon E (low dose) + Sodium iodate
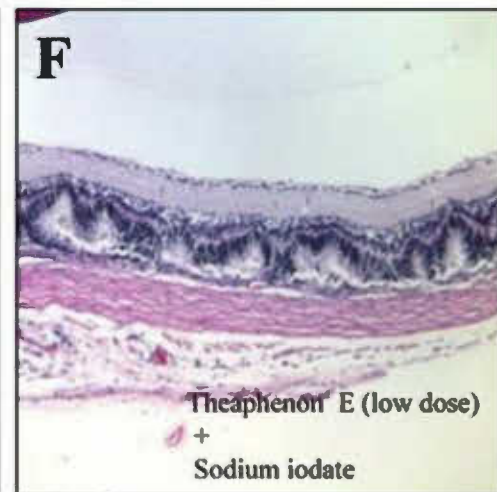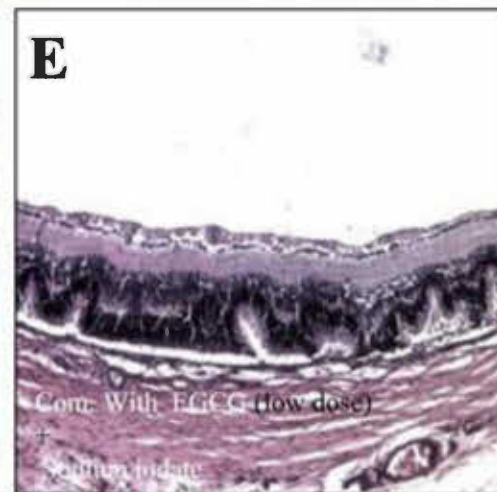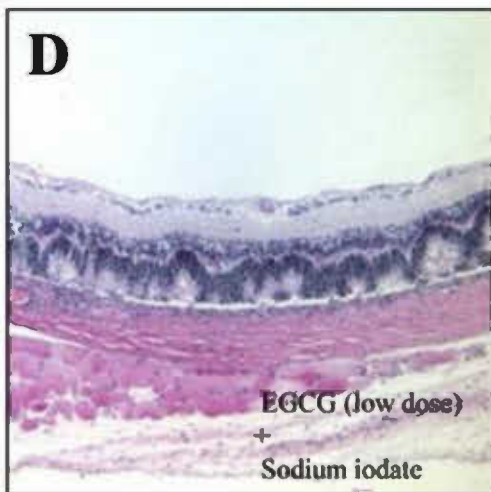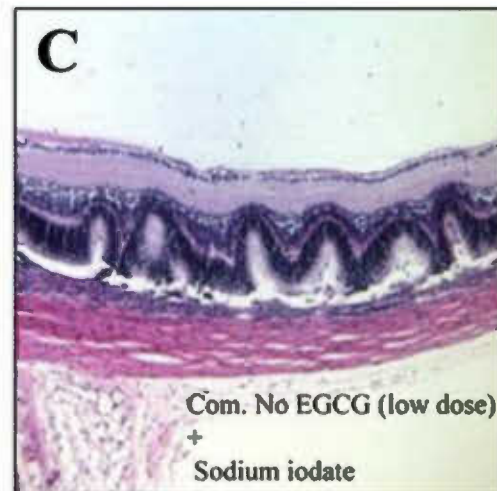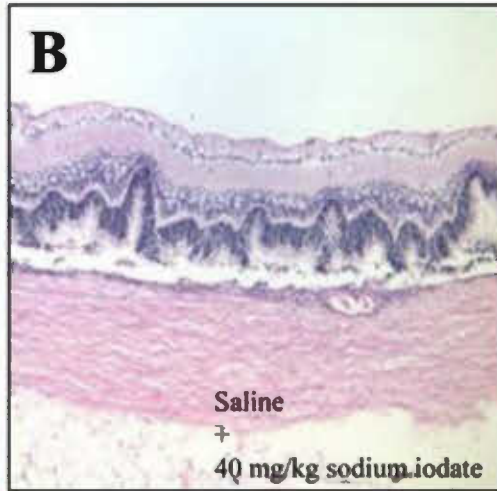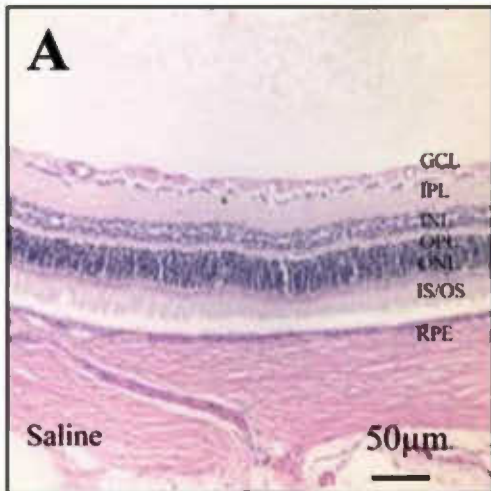
Figure 4.24 The proportion of the folded retina in the histological preparations.

The proportion of retinal length exhibiting irregular ONL alignment to total retinal length, Image J (version 1.46e; NIH, Bethesda, MD) was used. The proportion of the folded retina is defined the length of the folded retina divided by the total length of the whole retina in histological slices. The eyeballs were sections vertically through the optic nerve (superior-inferior). Compare to the control group, no significant was found in each treatment group. Mann- Whitney U test (Mean ± SD). i.v.: intravenous injection.
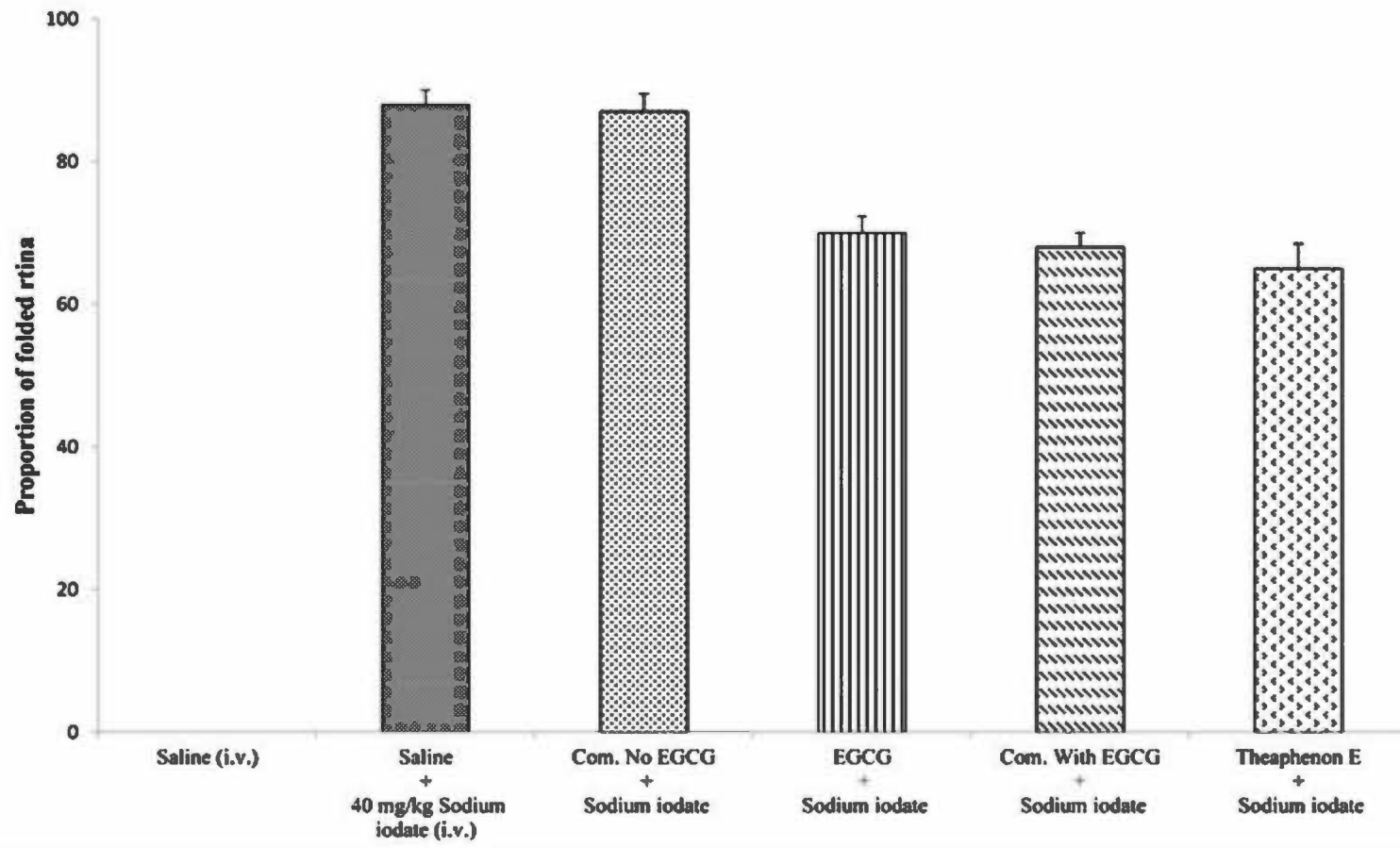
Chapter 5: Discussion

5.1 Pharmacokinetic study of catechins distribution in normal rat eye

Although many studies investigated the biological effect of catechins and GTE in the ocular, our pharmacokinetic study revealed the distribution of individual catechins after administration of GTE to the normal rat.

Multiple peaks were exhibited in the individual catechins profiles the retina and the vitreous humor **(Figure 4.1 B-C)**, it may be due to the catechins or the catechins metabolites recirculated or reabsorbed into the retina and the vitreous humor, so their levels were sustained during the measurement. This phenomenon was also observed in the previous GTE (Sunphenon®DCF-1) study (Chu et al., 2010). Similar shapes of the profiles among the catechins and catechin gallates indicated similar absorption mechanisms. Meanwhile, different profile suggested different absorption mechanisms. Different absorptions of catechins may involve catechins selectively binding with target protein in the ocular tissues rather than passive diffusion (Chen et al., 1997, Lin et al., 2007).

Some tissue may readily incorporate with catechins by specific mechanisms, as shown by the different profiles in that single peaks appeared in the plasma but multiple peaks in the retina and the vitreous **(Figure 4.1 A-C)**. Also, the presence of different catechins dominated in different tissues, indicating discriminative distributions in eye tissues.

In the further work, the metabolic studies should be performed in the interest of clearly understand the different absorption mechanism among the catechins. The metabolic studies not only focus on the catechins metabolites themselves but also

involve the metabolic environment in different eye tissues. This is crucial issue on drug application before clinical trial in order to against ocular oxidation.

5.2 Establishment of a retinal degeneration model on sodium iodate treated rat

5.2.1 Fundus examination by confocal scanning laser ophthalmoscopy (CSLO) and spectral domain optical coherence tomography (SD-OCT)

In the establishment of the sodium iodate model study, we have investigated the capability of Spectralis HRA + OCT to register the CSLO and OCT simultaneously of *in vivo* imaging on sodium iodate-induced retinal lesions in the adult rats. Clear and revealing in vivo CSLO and OCT images were obtained to image retinal structures in normal and diseases eyes.

In retinal degeneration, lesions are commonly sparse, which makes the histological analysis laborious and demanding, so the *in vivo* imaging combine with the CSLO has proven to be very effective to overall assessment and also as a pre-selection for other morphological studies, saving animals, time and finance, with the OCT at the same time, the extent of the lesions can be visualized in real time. The particular example in Figure 4.2-4.4 demonstrated the capability of detecting the intra-retinal (white arrows).

As we have shown in the results, CSLO and OCT are both useful for the morphology assessment and numerical quantification of the retinal changes and for the detection and analysis of appearance of lesions. The major findings we were able to obtain: (1) using infra-red CLSO hyper-reflective degenerative profiles can be recognized as dark blots in planar images of the retina after sodium iodate injection; (2) these profiles appeared at the time when lesions are observed in the IS/OS layer and ONL as revealed by OCT imaging; (3) distribution of these degenerative profiles

is well correlated with the lesion in outer retinal layers in histological sections; (4) these degenerative profiles show a dose dependent change in response to sodium iodate insult. These findings together provide a strong support that imaging of the retina with infra-red CLSO and spectral domain OCT simultaneously is an effective and reliable method to evaluate damages in outer retinal layers in living adult rats.

Our results showed that infra-red CSLO combined with OCT can be used to assess retinal lesion in living adult rats. The advantage of this method is that the retina can be monitored and viewed in planar and cross-sectional images in the same area at the same time, allowing assessment of the layer specific changes by OCT at defined location of the retina as revealed in the CSLO images, and visualization of abnormalities in a large area of the retina as shown in CSLO images with known and defined layer specific lesion.

However, the CLSO also have limitations, because the CLSO can assess around 60% of the total retina area, not the whole field of the retina. Since the membrane-rich less optically dense layers like the nerve fiber layers and the plexiform appeared as dark shade, but the less membrane-rich like the outer nuclear layer appeared as white in OCT images, in our findings, the cell death in ONL, and the folded rosettes formed the empty place. So, the dark blots and hyper-reflectivity in the CSLO and OCT might be the massive cell death formed rosettes empty space. Meanwhile, based on the literature review, only the Sprague-Dawley rats can be induced folded irregular retinal degeneration profile, the C57BL mice and Long Evans rats appeared in a regular cell apoptosis in ONL after sodium iodate administration, this indicating that the dark blot in CSLO only can be visualized in Sprague-Dawley rats, not in other species.

Previous *in vivo* imaging studies used spectral domain OCT as the tool to evaluate

degenerative changes in the retina. It is superior in providing high resolution cross-sectional views of the retina and has been used widely in assessment of retinal lesions in experimental and mutant rodents (Ruggeri et al., 2007, Fischer et al., 2009, Nakano et al., 2011). This technique has also been employed for assessing longitudinal changes in macular thickness and optic fiber layer thickness in human retina (Leung et al., 2008a, Leung et al., 2008b). Through analyses of images of the retina we found the appearance of hyper-reflective blots in the CSLO images corresponded to degenerative profiles in the photoreceptor and ONL of the retina.

Further analyses of retinas with distribution of blots restricted to certain areas showed a good correlation to lesion sites in the corresponding histological sections. Moreover, these blots are detected 7 days after injection of sodium iodate, coinciding with the time when obvious degenerative changes are observed in OCT images and histological preparations. These findings strongly support that the hyper-reflective blots observed under infra-red CSLO indicated degenerative profiles in the outer retinal layers. We showed further that changes in number of blots is dependent on the dose of sodium iodate, which again are supported by the morphometric analyses of outer retinal layers in histological sections. These dose dependent responses suggest that CSLO can be used as a reliable method to evaluation real-time longitudinal damage to the retina with outer retinal layer lesions. However, it remains to be determined whether this technique can be applied to degenerative changes in inner retinal layers and in other animals. To our knowledge this is the first study providing an in vivo technique to assess the retinal changes response to different sodium iodate doses.

5.2.2 Histopathology of sodium iodate induced lesion in the rat retina

We have reassessed the sodium iodate model of producing retinal lesions in

histology preparations. To this end, we studied the effects of different doses and post injection times on several aspects by using different techniques.

One important finding is that we have shown a characteristic pattern of degenerative changes in the retina after sodium iodate injection. By examining both changes in the outer retinal and inner retinal as well as intravenous or intraperitoneal injection we found that sodium iodate-induced structure changes are both dose and time dependent.

This lesion affects severely the photoreceptors in IS/OS layer and ONL, whereas changes in the IPL and INL are milder. This finding coincided with the previous reports documenting that the retinal pigment epithelium is the initial site towards to the sodium iodate toxic, with subsequently photoreceptor degeneration, which is conform to the mechanisms of the sodium iodate used as retinotoxic (Enzmann et al., 2006, Korte et al., 1984, Franco et al., 2009). The time course and the doses effect of the sodium iodate in response to the pathological changes in the IS/OS of photoreceptor, outer nuclear layer as well as the inner retinal layer changes. Over all, we performed for the first time the morphmetic analysis in different dosages in generating retinal lesions on both intravenous and intraperitoneal injections. Based on our results, we found that the minimum dose of sodium iodate to induce retinal lesions was 25 mg/kg. However, the retinal lesions could not be induced in every rat in 25 mg/kg sodium iodate group. Therefore, perhaps the 25mg/kg could be the marginal dosage that could induce the retinal lesions. For the 50 mg/kg sodium iodate i.p. injection, the dark patches appeared until Day 14, and the number of dark patches was even less than the 40 mg/kg i.v. injection **(Figure 4.6)**. For all the measurements, the effects of the i.p. injection at the same dose tended to be smaller than the i.v. injection.

The mechanism of sodium iodate induced retinotoxicity is not fully understood, but inhibition of lysosomal enzymes activities and iodate may bind to the melanosomes alter the ion composition and morphology play an important role, and the toxicity is associated with the iodate oxidizing properties (Sorsby and Reading, 1964). 30 minutes after intravenous iodate injection, the RPE, and subsequently the photoreceptor, can no longer be protected by glutathione, to elicit retinotoxic effect; the iodate dosage must exceed the capacity of endogenous radical scavenger systems.

The sodium iodate effect in the brain hasn't been investigated in our study, but reported studies showed, no effect of sodium iodate on the blood brain barrier (BBB) in doses that caused obvious changes of the blood retina barrier (BRB) (Ennis and Betz, 1986). The sodium iodate selectively affects the carrier D-glucose in the BRB but not in the BBB (Taarnhoj and Alm, 1992). The RPE may explain the difference between these two barriers, which is one part of the BRB, suggesting a selective toxic effect to the RPE consistent with earlier studies. The sodium iodate causes retinatoxicity happens not only in Sprague-Dawley rats but also in mice (Enzmann et al., 2006), rabbit (Clifton and Makous, 1973), sheep (Nilsson et al., 1977a), cat (Kiryu et al., 1992), and even in human retina (Singalavanija et al., 2000).

Enzmann et al., in 2006, injected 35, 50, 70 mg/kg sodium iodate in to the rat, assessed the retinal degeneration and visual function on 14, 21, and 28 days as well as 6 month post injection, a significant visual function defect with significantly lower swim speeds, and consistent with the anatomical observations, showed no functional and morphological recovery were found in these animal retinas even after 6 months treated with sodium iodate. So, sodium iodate causes permanent degeneration in retinal morphology and visual function (Enzmann et al., 2006).

5.2.3 Correlation of retina lesions in histological sections with SD-OCT

The acquired OCT images have high correlation with histology results. The Spectralis HRA + OCT system accomplished the goal of noninvasive in vivo imaging of the rat retina with high image quality and short examination time, suitable for routine high throughput reproducible applications. The OCT image provides a tool for precise spatial registration of the OCT cross-sectional images on the retina layers with histological sections.

The appearance of degeneration profiles in form of folding or rosettes as observed in our findings has been reported in histological preparation of the retina of Sprague-Dawley rats after injection of 40 mg/kg sodium iodate (Ohtaka et al., 2005). However, similar pattern of degeneration was not reported by Hariri et al (Hariri et al., 2012, Hariri et al., 2013). Who have utilized ultra-high resolution OCT to study degenerative changes after treatment of 40 mg/kg sodium iodate in Long Evans rats. In their findings, a progressive destruction of cellular structure is observed in the outer retinal layers, which appears to initiate at the interphase between the IS/OS of photoreceptors and the pigment epithelium as early as 1 hour after injection, producing a general and even thinning of the retina. The causes of these differences in pattern of degeneration are unknown. One possibility is the difference in sub-species of animal used. It might be worth noting the studies by Hariri et al. were done on pigmented rats, whilst those by Ohtaka et al. and the current study were performed on rats that lack ocular pigment.

The in vivo image is different from the traditional histology sections, is based on reflectivity. Retinal layers with much membrane and less optical dense are presented as a darker shade of gray, for example plexiform and nerve-fiber layers appeared as dark in OCT, retinal layers with more optically dense and less membrane are present

as light shade, like the outer nuclear layer, inner nuclear layer appeared as light in OCT images. To elucidate the unique hyper-reflectivity in the outer nuclear layer and the IS/OS of the outer photoreceptor layer, and the histological analysis was also conducted on the same retina, we detected the massive cell lose in the IS/OS of the photoreceptor and the folded of the retina, we speculate that these destructive structures of the retina in histological preparations cause the hyper-reflectivity seen in the outer photoreceptor layers. The consequence is since a large number of the outer nuclei decreased and appear as empty region, the IS/OS nearly disappeared, the region became less optical dense, so appeared as hyper-reflectivity, though further studies are needed to confirm this issue.

Consistency and safety are critical factors should be considered when performing systemic administrated sodium iodate-induced retinal damage as a drug feasible animal model for drug testing. The i.p. injected 75 mg/kg sodium iodate caused more severe damage to liver and kidney. So, we conclude that i.p. injection reduces the effective dose in the eye and cause more severe damage to other major organs. In animals injected intraperitoneally with sodium iodate, significant reduction was observed only at the dose of 75 mg/kg but not at 50 mg/kg, indicating that intravenously injection is more effective in generating degeneration in outer retinal layers. The chemo-kinetics of the animals is another important issue in the development of a drug testing model. Base on this study, the selected dose of sodium iodate for the drug testing is 40 mg/kg, which cause retinal lesions efficiently without causing any other systemic damages.

5.3 Treatment ability of catechins, catechins combination and green tea extract on sodium iodate treated rats

EGCG has been wildly studied for its anti-oxidative effect on ocular tissues. A more thoroughly and very impressive study on retina oxidative stress inhibited by EGCG has been done by Zhang B et al. They used EGCG intravitreal and/or intraperitoneal administered to attenuate photoreceptor degeneration induced by sodium nitroprusside generate nitric oxide, or light exposure to cause rat retinal damage. This conclusion was proved by a combination of using biochemical, eletrophysiological and histological methodologies. They also showed the inner rat retina is damaged by ischemia/reperfusion but protected by the intravitreal and or systemic injection of EGCG. The EGCG can be proved that it against oxidative stress-induced retinal degeneration both in inner and the outer part of the retina.

While a great number of the previous studies focus on the benefits of the EGCG, few studies has been performed to test the antioxidant effect of the purified catechins combination and the green tea extract Theaphenon$^®$E which contains a total catechin content to about 90% and even their biological effects. So the present experiments were performed to investigate specifically the anti-oxidative effect of Theaphenon$^®$E and the catechins combinations. There are a lot of good studies used the sodium iodate as an oxidant to cause retinal degeneration in order to test different drugs, sodium iodate induced retinal degeneration in rats was employed as an animal model to explore the capability of stem cells in differentiation into RPE and photoreceptors after transplantation into the subretinal space,(Enzmann et al., 2003, Gong et al., 2008) and investigate the protective effect of hepatocyte growth factor against retinal degeneration (Ohtaka et al., 2006). We also proved by ourselves that sodium iodate can work as a reliable model to cause the retinal lesions.

In our study, we performed not only EGCG, but also catechins combination with EGCG (EGCG, GC, EGC, and EC), catechins combination without EGCG (GC,

EGC, and EC) and a green tea extract Theaphenon®E. In the previous studies, initially EGCG was injected into the vitreous or by intraperitoneal (Zhang et al., 2007), but in our study the catechins were administered by oral gavage **(Figure 3.1)**, which is more relevant for the clinical use and avoid wound by the injection.

It is clearly shown in the present studies that EGCG, catechins combination (EGCG, GC, EGC, and EC), and Theaphenon®E are potent antioxidants. These data provide proof that damage to the retina caused by an insult of sodium iodate which involves oxidative stress can be blunted by only twice oral pretreatment of EGCG, catechins combination (EGCG, GC, EGC, and EC), and Theaphenon®E. This conclusion was reached by using CSLO, OCT, histological, and biochemical methodologies. It was impossible to make definite conclusions only from the histological preparations because of the variability of analyzing different areas of the retina, so we perform to measure the proportion of the folded retina divided by the whole length of the retina in a number of sections from different eyes. In order to prove sodium iodate was toxic to the retina and that could be counteracted with catechins and green tea extract were found by analyzing the whole of the retina either in terms of the histological or the biochemical.

5.4 Proposed mechanisms of catechins, catechins combination and green tea extract actions on sodium iodate treated rats

Apoptosis is a common pathway in the pathogenesis of photoreceptor degeneration in many kinds of retinal diseases (Shahinfar et al., 1991, Tso et al., 1994, Chang et al., 1993). In rats with photoreceptor degeneration, the number of positive TUNEL- labeling nuclei was significantly reduced in the catechins-treated eyes than in untreated eyes (Zhang and Osborne, 2006, Costa et al., 2008). On the

basis of the negative TUNEL signals indicated RPE cell death induced by sodium iodate take place through necrosis (Flage, 1983, Kiuchi et al., 2002). Therefore, the RPE protection seen in our histological study **(Figure 4.17 D-F)** suggests that EGCG, catechins combination (EGCG, GC, EGC, and EC), and Theaphenon®E could suppress RPE necrosis.

In apoptosis, DNA is broken down in a defined manner for detection by the apoptosis marker, such as caspase-3. The finding that intravenous injection of sodium iodate caused elevation of the capase-3 level in retina suggested that sodium iodate induced the photoreceptors to die by apoptosis. There are two main pathways lead to apoptosis, the intrinsic pathway is mediated by mitochondria, the extrinsic pathway is triggered by membrane biochemical interfere to secondarily affect mitochondria. So, the mechanisms about protecting photoreceptors in the catechins-treated rats could be: First, Due to apoptosis plays a pivotal role in photoreceptor degeneration in sodium iodate treated animals, these could be suppressed by the anti-apoptotic effect of the catechins. Second, catechins-mediated survival of RPE cells could protect the photoreceptors against degeneration base on the RPE was preserved to a greater degree in the catechins treated eyes. Third, since the photoreceptor membranes have unusually high concentrations of docosahexaenoic acid nearly 50% of the total fatty acid pool, and especially prone to free radical damage, like the sodium iodate-induced retinal degeneration is primarily mediated by extrinsic pathway. Interestingly, sodium iodate also caused an upregulation of caspase-3, thus supporting that it is inducing photoreceptor cell death by apoptosis rather than necrosis.

Sodium iodate is a known toxin to induce selective RPE damage by oxidative stress, and consequently retinal degeneration (Kim et al., 2008, Zhao et al., 2011).

SOD as major antioxidant enzymes, it can remove superoxide to against oxidative stress. The hydroperoxides formed as the result of SOD activity is quenched by GPx (Gandhi and Abramov, 2012). In this study, a significantly high expression of the SOD and GPx was observed in sodium iodate treated retinas might be due to their increased utilization for scavenging ROS. However, the catechism comprising the ortho-hydroxyl group in the B-ring and galloyl moiety in the C-ring could react directly with superoxide may reduce the formation of H_2O_2 and in addition it possesses a direct scavenging effect on H_2O_2 (Gokulakrisnan et al., 2010).

Biochemical analysis of the whole retina by the real-time PCR confirmed the CLSO, OCT and histological data that EGCG, catechins combination with EGCG, green tea extract significantly attenuates the increasing level of oxidative stress in retina produced by sodium iodate.

8-Isoprostane is the well characterized compound belonging to the F2-isoprostanes, a group of stable Prostaglandin F2α isomers derived from the non-enzymatic oxidation of arachidonic acid (Roberts and Morrow, 1997). It is the free radical peroxidation of arachidonic acid independent of the action of cyclooxygenase. For this reason, 8-isoprostane has been deemed as an ideal marker of oxidative stress, it is directly represent the oxidative stress. The 8-isoprostane provides a sensitive measurement for the oxidative status. So, after 24 hours injection of sodium iodate, it triggered the oxidative situation, the 8-isoprostane level 10 times increased, but co-treated with EGCG, catechins combination with EGCG and the green tea extract Theaphenon®E, the 8-isoprostane level dramatically decreased, indicating strong anti-oxidative effect of EGCG, catechins combination with EGCG and Theaphenon® E, but the catechins combination without EGCG (GC, EGC, and EC) has no significant effect on the 8-isoprostane level, that might because only small amount of

the GC, EGC, EC in this combination, the doses might be too low.

Enhancement of the RPE and photoreceptor survival could improve visual prognosis in patients with retinal degeneration, such as retinitis pigmentosa and early AMD. So, daily intake catechins may have benefit.

This study provides a combination of structural and biochemical evidence to show that the retinal degeneration is particularly affected by oxidative stress but orally administered EGCG, catechins combination (EGCG, GC, EGC, and EC), and Theaphenon®E could blunt this process. These data again proved our previous conclusion that orally administered GTE Theaphenon®E, the catechins must have reached the retina in sufficient amounts, to protect the retinal degeneration from a detrimental insult of oxidative stress. This might be of clinical relevance for the treatment of ophthalmic disorders. Many studies showed that EGCG can be consumed and tolerated at high doses. In our previous study, we orally administered 550 mg/kg GTE (Theaphenon®E) to the normal rats, showed distribution of individual catechins in each plasma, vitreous humor and retina. EGCG presents at high levels in the plasma, retina and, vitreous at 6686.8±4437.1 nM, 784.4±195.9 nmol/kg, and 2224.4±805.4 nM respectively. In addition, GC was dominantly present in vitreous humor; EGC and EC were appeared as high level in plasma and retina.

Many studies on the antioxidant effect of green tea only focus on EGCG; however, based on our pharmacokinetic study, we want to combine the EGCG, EC, EGC, and GC as a mixture to study their antioxidant effect. Use of a mixture, such as Theaphenon®E, was better than use of pure catechins because synergic effects on antioxidation and bioavailability. The EGCG and the Theaphenon®E formulations containing the same amount of EGCG, but the Theaphenon®E have more potent effect may due to other small amount of catechins. Our results indicated green tea

consumption could benefit the eye against oxidative stress.

We also indeed have the data showed that 550 mg/kg of green tea extract Sunphenon®DCF-1 equivalent to 10 cups of green tea, was intragastric feeding to the Sprague-Dawley rats. The maximum level of EGCG was in plasma, retina, lens and cornea were 0.3μmol/Kg, 0.25μmol/Kg, 0.15μmol/Kg, and 0.09μmol/Kg respectively. The duration of high concentration peak was within two hours. Our experimental design using very high levels of levels of catechism and GTE, producing the efficacy results, however, these can be artifacts due to non –specific interactions between the signaling molecules and oxidants. But, according to the 8-isoprostane level and the SOD, GP, and Capase-3 data, we have shown that the oxidative stress level was decreased after the EGCG, catechins combination with EGCG, and GTE administration. It is clearly necessary in the future to determine whether oxidative stress-induced retinal damage can be blunted by the oral intake of specific amounts of catechins combination or green tea extract in order to provide an insight of the potential use of these drugs in patients.

To examine the safety of EGCG, catechins combinations, and green tea extract Theaphenon®E, after administrated to the rat, we observed the rat behavior every day. They appeared as normal except the catechins combination with EGCG (EGCG, GC, EGC, and EC) after 24hours drug administration, one rat looked like a little bit weak and curled in the corner. After 14 days the rats were sacrificed. The eyeball, kidney and liver were removed for histology sections. All the rats treated with GTE and catechins have their kidney and liver appeared as normal. So, based on this observation, there was a question. Since the dosage of the green tea extract Theaphenon®E used was higher than EGCG and the catechins combination in this study, why the behavior of the all the five rat still appeared as normal? This might

indicated the synergistic effects of the different catechins in the green tea extract on their antioxidation and bioavailability and also the green tea extract may lower the oxidative stress level indirectly in retina (Chow et al., 2001).

In conclusion, the results obtained in the present study show that oral intake of green tea extract, EGCG, catechins combination (EGCG, GC, EGC, and EC) and Theaphenon®E can reach the retina and attenuate sodium iodate-induced retinal degeneration in rats. These studies support the notion that daily oral intake of green tea extract might benefit patients suffering from retinal diseases such as early onset of age-related macular degeneration and retinal dystrophy where oxidative stress is implicated (Suzuki et al., 2007).

5.5 Low dose of catechins has no protect effect on sodium iodate-induced retinal degeneration

Based on the histological measurement, the low dose of the Theaphenon®E, catechins combination with EGCG, cactechins combination without EGCG, EGCG, none of these regimens has significant effect against the sodium iodate-induced retinal degeneration.

In a reported study, the 50 mg/kg or 100 mg/kg EGCG with daily administered by oral gavage 30 min before forced swim session for 28 days, EGCG could ameliorate behavioral and biochemical deficits in rats with load-induced chronic fatigue syndrome (Sachdeva et al., 2011). In another study, 10 g dry tea was added to 750 ml tap water in diabetic rats for 12 weeks (Kumar et al., 2012). Compared to these reported studies. However, in our study, after these catechins combinations and green tea extract treated there were still patchy degeneration of the outer retina. Although these low dosages catechins and green tea extract has no protective effect, it help us

to further understand the pathophysiology of the toxic effect of the sodium iodate. So, the reasons of why our low dose herbal molecules has no protective effect might be: 1) 40 mg/kg sodium iodate may be a little bit higher to cause the retinal damage, so the 100 mg/kg green tea extract cannot neutralize such high oxidant effect to the retina. 2) The catechins have not distributed into the retina at sufficient quantity. 3). we fed the low dose catechins to the rat for a short period. If we fed the catechins 2 weeks to rats before the sodium iodate injection (to maintain a sustain level of catechins in the rat retina), and 2 weeks after sodium iodate injection, it might have significant protective effect.

So, in future work, we can decrease the dosage of the sodium iodate, start the dosage range from 10-25 mg/kg, and work out the reasonable lower dosage of sodium iodate-induced retinal degeneration, and also test the sodium iodate effect in kidney, liver, and central neural system, like the SOD, Caspase 3, and GSH/GSSG levels in liver and kidney, use histological preparations and immunostaining to assess any degeneration effect in brain. Low dose of sodium iodate may cause milder, and chronic toxic effect to retina, which is more relevant to the clinical situation, unlike the 40 mg/kg cause the effect more severe and dramatically. Then we can use the lower optimal dose of sodium iodate to test the daily intake of lower dose of the EGCG, different catechins combinations, and GTE, whether there would be protective effect would be detected. This could be a very excited study.

Chapter 6: Conclusion and future prospects

Based on a previous report, the central pole of the retina is more sensitive to the sodium iodate than the periphery part (Machalinska et al., 2010). These pathological changes are similar to that during early onset of age-related macular degeneration characterize initially involve the central part of the retina, and then spread gradually to the periphery region. Moreover, we show further from the dose dependent essays that 40 mg/kg is the selected dosage that generates consistently retinal lesions in the outer retinal layers but without obvious adverse effects to other organs, indicating that administration of drug intravenously at this dosage can be considered as a good model for experimental study of ocular degeneration diseases that involved the outer retina layers, for example age-related macular degeneration and retinitis pigmentosa.

In this study, the Spectralis HRA + OCT register the confocal scan laser ophthalmoscopy and spectral–domain optical coherence tomography system along with the histological measurement were used to monitor the reflectivity and structural changes over time in the different dosages of sodium iodate treated rat retinal degeneration. Our results showed 40 mg/kg sodium iodate treated rat retinal characterized by changes in the optical reflectivity, thickness, shape, integrity without generate toxicity to the kidney and liver. Results from this study largely indicated sodium iodate-induced retinal degeneration may serve as a feasible model useful for studying retinal damage and drug testing, also might could potentially to help better understand the retinal degeneration diseases, for example age-related macular degeneration and retinitis pigmentosa. And also for the clinical situation, there were few reports of accidental poisoning sodium iodate by oral administration, the people developed visual field defect. Ophthalmoscopic examination revealed severe retinal damage with degeneration of photoreceptors, and the dosage was

assessed exceeded 100 mg/kg (Singalavanija et al., 2000). The retinal changes may similar to our findings. Another report of iodate-induced people blindness has occurred in China, the dosage is around 10-20 mg/kg (Tong, 1995). We proposed that if the sodium iodate poisoning in human with sufficient dosage by an accident, we may suggest the patient to drink green tea extract for a period, it definitely benefit the eye against retinal degeneration.

The present study shows that EGCG, catechins combination with EGCG, and green tea extract orally consumption could attenuates a number of detrimental effects to the retina following sodium iodate injection. They could benefit the retina against oxidative stress damage.

Consequently, since the high dose of the EGCG, catechins combination and the green tea extract give an impressive antioxidant effect in the sodium iodate model. So, the future green tea studies in ocular tissues should use other *in vivo* models to mimic retinal degeneration in different kinds of mechanisms, like the ischemia/reperfusion model, knockout or transgenic mice model. And also some in vitro studies should be performed. However, in this project, we heavily focus on the structural consequences of retinal degeneration caused by sodium iodate. The functional consequences after green tea extract and catechins combinations should be the irreplaceable and important direction in the further study. Based on the literature review, the electroretinogram (ERG) was performed as functional evaluation. For the 40 mg/kg sodium iodate intravenous injected rats, it demonstrated that RPE degeneration is accompanied by neurosensory dysfunction. On Day 1, the b-wave amplitude decreased after white flash of low intensity, indicating impairment of the rod neurosensory retina. The b-wave amplitudes were decreased in a wider range, particularly on Day 3-28 days **(Figure 5.1) (Machalinska et al., 2010, Ohtaka et al.,**

2006).

It is clearly necessary in the future to determine the long term effects of daily oral intake of specific low dose of green tea extract should also be investigated in order to provide an understanding for the potential use of catechins or green tea extract in patients. The administration approach, different catechins combinations formulation, and the treated period should be investigated in details. At the same time, we also have to investigate the whether the treatment of sodium iodate affect the pharmacokinetic distribution profile of the catechins and green tea extract in the ocular tissues, especially in retina.
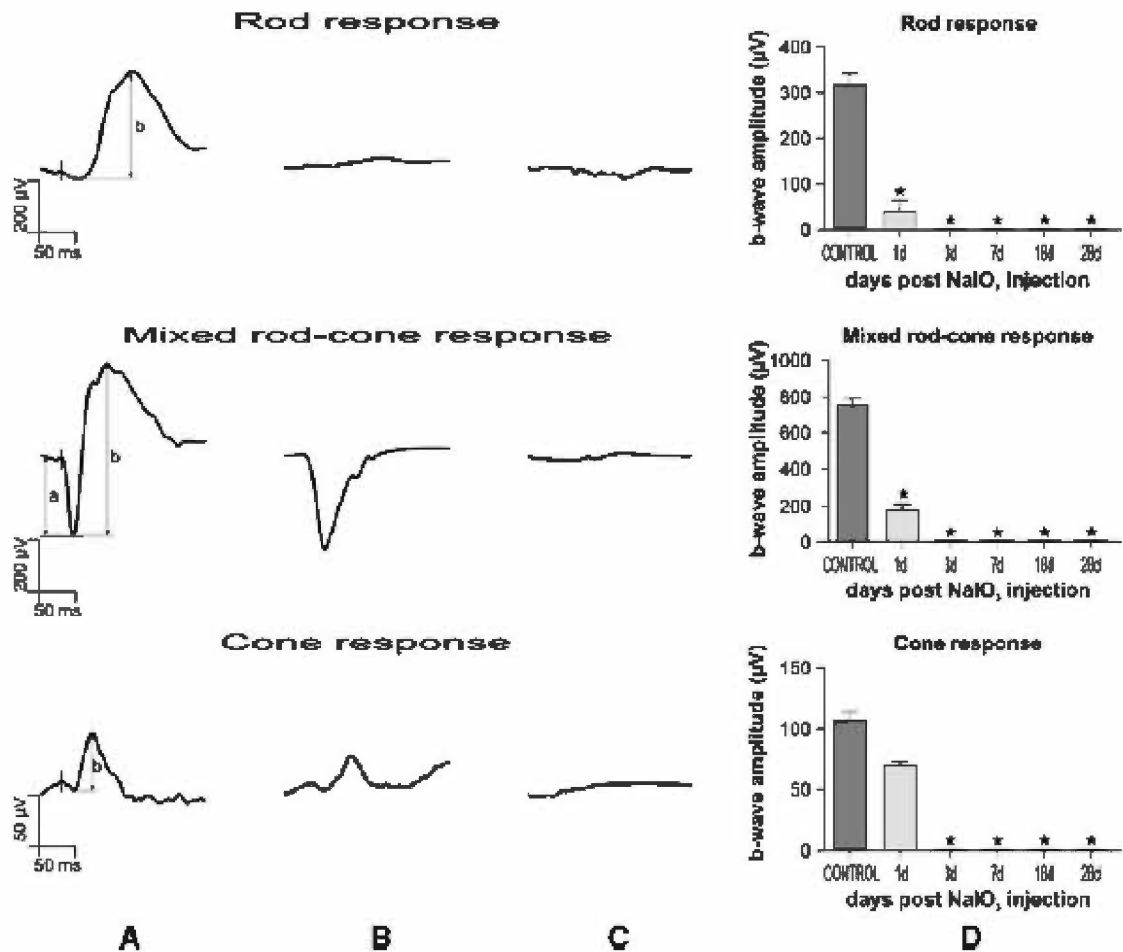
Figure 5.1 Electroretinogram (ERG) response recorded at different time points after 40 mg/kg sodium iodate administration. A. Saline-treated control. **B**. ERG recorded on Day 1 after sodium iodate injection. **C**. ERG photography on Day 3 with sodium iodate treated. **D**. The b-wave amplitude measurements on Day 1, 3, 7, 18, 28 after sodium iodate administration. * P<0.05 versus control. (Picture from Ohtaka K, Machida S, Ohzeki T, Tanaka M, Kurosaka D, Masuda T, Ishii T.. Protective effect of hepatocyte growth factor against degeneration of the retinal pigment epithelium and photoreceptor in sodium iodate-injected rats. Current Eye Research. 2006 Apr;31(4):347-55)

References

ADEMOGLU, E., OZBEY, N., ERBIL, Y., TANRIKULU, S., BARBAROS, U., YANIK, B. T., BOZBORA, A. & OZARMAGAN, S. 2006. Determination of oxidative stress in thyroid tissue and plasma of patients with Graves' disease. *Eur J Intern Med,* 17, 545-50.

AHMAD, N. & MUKHTAR, H. 1999. Green tea polyphenols and cancer: biologic mechanisms and practical implications. *Nutr Rev,* 57, 78-83.

AHMED, S., RAHMAN, A., HASNAIN, A., LALONDE, M., GOLDBERG, V. M. & HAQQI, T. M. 2002. Green tea polyphenol epigallocatechin-3-gallate inhibits the IL-1 beta-induced activity and expression of cyclooxygenase-2 and nitric oxide synthase-2 in human chondrocytes. *Free Radic Biol Med,* 33, 1097-105.

ALDER, V. A. & CRINGLE, S. J. 1985. The effect of the retinal circulation on vitreal oxygen tension. *Curr Eye Res,* 4, 121-9.

ALEX, A. F., SPITZNAS, M., TITTEL, A. P., KURTS, C. & ETER, N. 2010. Inhibitory effect of epigallocatechin gallate (EGCG), resveratrol, and curcumin on proliferation of human retinal pigment epithelial cells in vitro. *Curr Eye Res,* 35, 1021-33.

ALLEN, R. G. & TRESINI, M. 2000. Oxidative stress and gene regulation. *Free Radic Biol Med,* 28, 463-99.

ANSTADT, B., BLAIR, N. P., RUSIN, M., CUNHA-VAZ, J. G. & TSO, M. O. 1982. Alteration of the blood-retinal barrier by sodium iodate: kinetic vitreous fluorophotometry and horseradish peroxidase tracer studies. *Exp Eye Res,* 35, 653-62.

ASHBURN, F. S., JR., PILKERTON, A. R., RAO, N. A. & MARAK, G. E. 1980. The effects of iodate and iodoacetate on the retinal adhesion. *Invest Ophthalmol Vis Sci,* 19, 1427-32.

ASLAN, M., DOGAN, S. & KUCUKSAYAN, E. 2013. Oxidative stress and potential applications of free radical scavengers in glaucoma. *Redox Rep.*

BAE, J. Y., CHOI, J. S., CHOI, Y. J., SHIN, S. Y., KANG, S. W., HAN, S. J. & KANG, Y. H. 2008. (-)Epigallocatechin gallate hampers collagen destruction and collagenase activation in ultraviolet-B-irradiated human dermal fibroblasts: involvement of mitogen-activated protein kinase. *Food Chem Toxicol,* 46, 1298-307.

BAICH, A. & ZIEGLER, M. 1992. The effect of sodium iodate and melanin on the formation of glyoxylate. *Pigment Cell Res,* 5, 394-5.

BAZAN, N. G. 1989. The metabolism of omega-3 polyunsaturated fatty acids in the eye: the possible role of docosahexaenoic acid and docosanoids in retinal physiology and ocular pathology. *Prog Clin Biol Res,* 312, 95-112.

BELFORTE, N. A., MORENO, M. C., DE ZAVALIA, N., SANDE, P. H., CHIANELLI, M. S., KELLER SARMIENTO, M. I. & ROSENSTEIN, R. E. 2010. Melatonin: a novel neuroprotectant for the treatment of glaucoma. *J Pineal Res,* 48, 353-64.

BETTUZZI, S., BRAUSI, M., RIZZI, F., CASTAGNETTI, G., PERACCHIA, G. & CORTI, A. 2006. Chemoprevention of human prostate cancer by oral administration of green tea catechins in volunteers with high-grade prostate intraepithelial neoplasia: a preliminary report from a one-year proof-of-principle study. *Cancer Res,* 66, 1234-40.

BIRRER, L. 1970. [Histochemistry of sodium iodate and sodium iodoacetate retinopathy]. *Ophthalmologica,* 160, 176-94.

BLANCO, A. R., LA TERRA MULE, S., BABINI, G., GARBISA, S., ENEA, V. & RUSCIANO, D. 2003. (-)Epigallocatechin-3-gallate inhibits gelatinase activity of some bacterial isolates from ocular infection, and limits their invasion through gelatine. *Biochim Biophys Acta,* 1620, 273-81.

BLANCO, A. R., SUDANO-ROCCARO, A., SPOTO, G. C., NOSTRO, A. & RUSCIANO, D. 2005. Epigallocatechin gallate inhibits biofilm formation by ocular staphylococcal isolates. *Antimicrob Agents Chemother*, 49, 4339-43.

CAO, L., LIU, H., LAM, D. S., YAM, G. H. & PANG, C. P. 2010. In vitro screening for angiostatic potential of herbal chemicals. *Invest Ophthalmol Vis Sci*, 51, 6658-64.

CAVET, M. E., HARRINGTON, K. L., VOLLMER, T. R., WARD, K. W. & ZHANG, J. Z. 2011. Anti-inflammatory and anti-oxidative effects of the green tea polyphenol epigallocatechin gallate in human corneal epithelial cells. *Mol Vis*, 17, 533-42.

CHAN, C. M., HUANG, J. H., LIN, H. H., CHIANG, H. S., CHEN, B. H., HONG, J. Y. & HUNG, C. F. 2008. Protective effects of (-)-epigallocatechin gallate on UVA-induced damage in ARPE19 cells. *Mol Vis*, 14, 2528-34.

CHAN, M. M., FONG, D., HO, C. T. & HUANG, H. I. 1997. Inhibition of inducible nitric oxide synthase gene expression and enzyme activity by epigallocatechin gallate, a natural product from green tea. *Biochem Pharmacol*, 54, 1281-6.

CHANDRA, J., SAMALI, A. & ORRENIUS, S. 2000. Triggering and modulation of apoptosis by oxidative stress. *Free Radic Biol Med*, 29, 323-33.

CHANG, G. Q., HAO, Y. & WONG, F. 1993. Apoptosis: final common pathway of photoreceptor death in rd, rds, and rhodopsin mutant mice. *Neuron*, 11, 595-605.

CHECCHIN, D., SENNLAUB, F., SIRINYAN, M., BRAULT, S., ZHU, T., KERMORVANT-DUCHEMIN, E., HARDY, P., BALAZY, M. & CHEMTOB, S. 2006. Hypercapnia prevents neovascularization via nitrative stress. *Free Radic Biol Med*, 40, 543-53.

CHEN, L., LEE, M. J., LI, H. & YANG, C. S. 1997. Absorption, distribution, elimination of tea polyphenols in rats. *Drug Metab Dispos*, 25, 1045-50.

CHOW, H. H., CAI, Y., ALBERTS, D. S., HAKIM, I., DORR, R., SHAHI, F., CROWELL, J. A., YANG, C. S. & HARA, Y. 2001. Phase I pharmacokinetic study of tea polyphenols following single-dose administration of epigallocatechin gallate and polyphenon E. *Cancer Epidemiol Biomarkers Prev*, 10, 53-8.

CHOW, H. H., HAKIM, I. A., VINING, D. R., CROWELL, J. A., CORDOVA, C. A., CHEW, W. M., XU, M. J., HSU, C. H., RANGER-MOORE, J. & ALBERTS, D. S. 2006. Effects of repeated green tea catechin administration on human cytochrome P450 activity. *Cancer Epidemiol Biomarkers Prev*, 15, 2473-6.

CHRYSOSTOMOU, V., REZANIA, F., TROUNCE, I. A. & CROWSTON, J. G. 2013. Oxidative stress and mitochondrial dysfunction in glaucoma. *Curr Opin Pharmacol*, 13, 12-5.

CHU, K. O., CHAN, K. P., WANG, C. C., CHU, C. Y., LI, W. Y., CHOY, K. W., ROGERS, M. S. & PANG, C. P. 2010. Green tea catechins and their oxidative protection in the rat eye. *J Agric Food Chem*, 58, 1523-34.

CHU, K. O., WANG, C. C., CHU, C. Y., CHAN, K. P., ROGERS, M. S., CHOY, K. W. & PANG, C. P. 2006. Pharmacokinetic studies of green tea catechins in maternal plasma and fetuses in rats. *J Pharm Sci*, 95, 1372-81.

CHU, K. O., WANG, C. C., CHU, C. Y., CHOY, K. W., PANG, C. P. & ROGERS, M. S. 2007. Uptake and distribution of catechins in fetal organs following in utero exposure in rats. *Hum Reprod*, 22, 280-7.

CHU, K. O., WANG, C. C., CHU, C. Y., ROGERS, M. S., CHOY, K. W. & PANG, C. P. 2004. Determination of catechins and catechin gallates in tissues by liquid chromatography with coulometric array detection and selective solid phase extraction. *J Chromatogr B Analyt Technol Biomed Life Sci*, 810, 187-95.

CHUNG, J. H., HAN, J. H., HWANG, E. J., SEO, J. Y., CHO, K. H., KIM, K. H., YOUN, J. I. & EUN, H. C. 2003. Dual mechanisms of green tea extract (EGCG)-induced cell survival in human epidermal keratinocytes. *FASEB J*, 17, 1913-5.

CLIFTON, L. & MAKOUS, W. 1973. Iodate poisoning: early effect on regeneration of rhodopsin and the ERG. *Vision Res*, 13, 919-24.

COLEMAN, H. R., CHAN, C. C., FERRIS, F. L., 3RD & CHEW, E. Y. 2008. Age-related macular degeneration. *Lancet*, 372, 1835-45.

CONGDON, N., O'COLMAIN, B., KLAVER, C. C., KLEIN, R., MUNOZ, B., FRIEDMAN, D. S., KEMPEN, J., TAYLOR, H. R. & MITCHELL, P. 2004. Causes and prevalence of visual impairment among adults in the United States. *Arch Ophthalmol,* 122, 477-85.

COSTA, B. L., FAWCETT, R., LI, G. Y., SAFA, R. & OSBORNE, N. N. 2008. Orally administered epigallocatechin gallate attenuates light-induced photoreceptor damage. *Brain Res Bull,* 76, 412-23.

DASS, K., AHMAD, A., AZMI, A. S., SARKAR, S. H. & SARKAR, F. H. 2008. Evolving role of uPA/uPAR system in human cancers. *Cancer Treat Rev,* 34, 122-36.

DROGE, W. 2002. Free radicals in the physiological control of cell function. *Physiol Rev,* 82, 47-95.

DUARTE, D. A., SILVA, K. C., ROSALES, M. A., DE FARIA, J. B. & DE FARIA, J. M. 2012. The Concomitance of Hypertension and Diabetes Exacerbating Retinopathy: The Role of Inflammation and Oxidative Stress. *Curr Clin Pharmacol.*

ENNIS, S. R. & BETZ, A. L. 1986. Sucrose permeability of the blood-retinal and blood-brain barriers. Effects of diabetes, hypertonicity, and iodate. *Invest Ophthalmol Vis Sci,* 27, 1095-102.

ENZMANN, V., HOWARD, R. M., YAMAUCHI, Y., WHITTEMORE, S. R. & KAPLAN, H. J. 2003. Enhanced induction of RPE lineage markers in pluripotent neural stem cells engrafted into the adult rat subretinal space. *Invest Ophthalmol Vis Sci,* 44, 5417-22.

ENZMANN, V., ROW, B. W., YAMAUCHI, Y., KHEIRANDISH, L., GOZAL, D., KAPLAN, H. J. & MCCALL, M. A. 2006. Behavioral and anatomical abnormalities in a sodium iodate-induced model of retinal pigment epithelium degeneration. *Exp Eye Res,* 82, 441-8.

ESPINOSA-HEIDMANN, D. G., SUNER, I. J., CATANUTO, P., HERNANDEZ, E. P., MARIN-CASTANO, M. E. & COUSINS, S. W. 2006. Cigarette smoke-related oxidants and the development of sub-RPE deposits in an experimental animal model of dry AMD. *Invest Ophthalmol Vis Sci,* 47, 729-37.

FILIPE, P., LANCA, V., SILVA, J. N., MORLIERE, P., SANTUS, R. & FERNANDES, A. 2001. Flavonoids and urate antioxidant interplay in plasma oxidative stress. *Mol Cell Biochem,* 221, 79-87.

FISCHER, M. D., HUBER, G., BECK, S. C., TANIMOTO, N., MUEHLFRIEDEL, R., FAHL, E., GRIMM, C., WENZEL, A., REME, C. E., VAN DE PAVERT, S. A., WIJNHOLDS, J., PACAL, M., BREMNER, R. & SEELIGER, M. W. 2009. Noninvasive, in vivo assessment of mouse retinal structure using optical coherence tomography. *PLoS One,* 4, e7507.

FLAGE, T. 1983. Changes in the juxtapapillary retinal pigment epithelium following intravenous injection of sodium iodate. A light and electron microscopic study using horseradish peroxidase as a tracer. *Acta Ophthalmol (Copenh),* 61, 20-8.

FLIESLER, S. J. & ANDERSON, R. E. 1983. Chemistry and metabolism of lipids in the vertebrate retina. *Prog Lipid Res,* 22, 79-131.

FRANCO, L. M., ZULLIGER, R., WOLF-SCHNURRBUSCH, U. E., KATAGIRI, Y., KAPLAN, H. J., WOLF, S. & ENZMANN, V. 2009. Decreased visual function after patchy loss of retinal pigment epithelium induced by low-dose sodium iodate. *Invest Ophthalmol Vis Sci,* 50, 4004-10.

FRANKEL, E. N., KANNER, J., GERMAN, J. B., PARKS, E. & KINSELLA, J. E. 1993. Inhibition of oxidation of human low-density lipoprotein by phenolic substances in red wine. *Lancet,* 341, 454-7.

GANDHI, S. & ABRAMOV, A. Y. 2012. Mechanism of oxidative stress in neurodegeneration. *Oxid Med Cell Longev,* 2012, 428010.

GARBISA, S., SARTOR, L., BIGGIN, S., SALVATO, B., BENELLI, R. & ALBINI, A. 2001. Tumor gelatinases and invasion inhibited by the green tea flavanol epigallocatechin-3-gallate. *Cancer,* 91, 822-32.

GOKULAKRISNAN, A., VINAYAGAM, M. M., RAHMAN, L. A. & THIRUNAVUKKARASU, C. 2010. Attenuation of cardiac oxidative stress by (-)-epigallocatechin-gallate (EGCG) in CS exposed rats. *Biomed Pharmacother*.

GOMES, E. C., SILVA, A. N. & DE OLIVEIRA, M. R. 2012. Oxidants, antioxidants, and the beneficial roles of exercise-induced production of reactive species. *Oxid Med Cell Longev*, 2012, 756132.

GONG, L., WU, Q., SONG, B., LU, B. & ZHANG, Y. 2008. Differentiation of rat mesenchymal stem cells transplanted into the subretinal space of sodium iodate-injected rats. *Clin Experiment Ophthalmol*, 36, 666-71.

GRIGNOLO, A., ORZALESI, N. & CALABRIA, G. A. 1966. Studies on the fine structure and the rhodopsin cycle of the rabbit retina in experimental degeneration induced by sodium iodate. *Exp Eye Res*, 5, 86-97.

GUPTA, S., HASTAK, K., AFAQ, F., AHMAD, N. & MUKHTAR, H. 2004. Essential role of caspases in epigallocatechin-3-gallate-mediated inhibition of nuclear factor kappa B and induction of apoptosis. *Oncogene*, 23, 2507-22.

HANDELMAN, G. J., MACHLIN, L. J., FITCH, K., WEITER, J. J. & DRATZ, E. A. 1985. Oral alpha-tocopherol supplements decrease plasma gamma-tocopherol levels in humans. *J Nutr*, 115, 807-13.

HARIRI, S., MOAYED, A. A., CHOH, V. & BIZHEVA, K. 2012. In vivo assessment of thickness and reflectivity in a rat outer retinal degeneration model with ultrahigh resolution optical coherence tomography. *Invest Ophthalmol Vis Sci*, 53, 1982-9.

HARIRI, S., TAM, M. C., LEE, D., HILEETO, D., MOAYED, A. A. & BIZHEVA, K. 2013. Noninvasive imaging of the early effect of sodium iodate toxicity in a rat model of outer retina degeneration with spectral domain optical coherence tomography. *J Biomed Opt*, 18, 26017.

HEE, M. R., IZATT, J. A., SWANSON, E. A., HUANG, D., SCHUMAN, J. S., LIN, C. P., PULIAFITO, C. A. & FUJIMOTO, J. G. 1995. Optical coherence tomography of the human retina. *Arch Ophthalmol*, 113, 325-32.

HERNANDEZ, C. & SIMO, R. 2012. Neuroprotection in diabetic retinopathy. *Curr Diab Rep*, 12, 329-37.

HIGDON, J. V. & FREI, B. 2003. Tea catechins and polyphenols: health effects, metabolism, and antioxidant functions. *Crit Rev Food Sci Nutr*, 43, 89-143.

HO, Y. C., YANG, S. F., PENG, C. Y., CHOU, M. Y. & CHANG, Y. C. 2007. Epigallocatechin-3-gallate inhibits the invasion of human oral cancer cells and decreases the productions of matrix metalloproteinases and urokinase-plasminogen activator. *J Oral Pathol Med*, 36, 588-93.

HONG, M. H., KIM, M. H., CHANG, H. J., KIM, N. H., SHIN, B. A., AHN, B. W. & JUNG, Y. D. 2007. (-)-Epigallocatechin-3-gallate inhibits monocyte chemotactic protein-1 expression in endothelial cells via blocking NF-kappaB signaling. *Life Sci*, 80, 1957-65.

HOSODA, L., ADACHI-USAMI, E., MIZOTA, A., HANAWA, T. & KIMURA, T. 1993. Early effects of sodium iodate injection on ERG in mice. *Acta Ophthalmol (Copenh)*, 71, 616-22.

HOU, Z., SANG, S., YOU, H., LEE, M. J., HONG, J., CHIN, K. V. & YANG, C. S. 2005. Mechanism of action of (-)-epigallocatechin-3-gallate: auto-oxidation-dependent inactivation of epidermal growth factor receptor and direct effects on growth inhibition in human esophageal cancer KYSE 150 cells. *Cancer Res*, 65, 8049-56.

HUANG, D., SWANSON, E. A., LIN, C. P., SCHUMAN, J. S., STINSON, W. G., CHANG, W., HEE, M. R., FLOTTE, T., GREGORY, K., PULIAFITO, C. A. & ET AL. 1991. Optical coherence tomography. *Science*, 254, 1178-81.

INOUE, M., SATO, E. F., NISHIKAWA, M., PARK, A. M., KIRA, Y., IMADA, I. & UTSUMI, K. 2003. Mitochondrial generation of reactive oxygen species and its role in aerobic life. *Curr Med Chem*, 10, 2495-505.

ISBRUCKER, R. A., EDWARDS, J. A., WOLZ, E., DAVIDOVICH, A. & BAUSCH, J. 2006. Safety studies on epigallocatechin gallate (EGCG) preparations. Part 2: dermal, acute and short-term toxicity studies. *Food Chem Toxicol*, 44, 636-50.

JAGER, R. D., MIELER, W. F. & MILLER, J. W. 2008. Age-related macular degeneration. *N Engl J Med*, 358, 2606-17.

JARRETT, S. G., LIN, H., GODLEY, B. F. & BOULTON, M. E. 2008. Mitochondrial DNA damage and its potential role in retinal degeneration. *Prog Retin Eye Res*, 27, 596-607.

KATIYAR, S. K., AFAQ, F., AZIZUDDIN, K. & MUKHTAR, H. 2001. Inhibition of UVB-induced oxidative stress-mediated phosphorylation of mitogen-activated protein kinase signaling pathways in cultured human epidermal keratinocytes by green tea polyphenol (-)-epigallocatechin-3-gallate. *Toxicol Appl Pharmacol*, 176, 110-7.

KHAN, N., AFAQ, F., SALEEM, M., AHMAD, N. & MUKHTAR, H. 2006. Targeting multiple signaling pathways by green tea polyphenol (-)-epigallocatechin-3-gallate. *Cancer Res*, 66, 2500-5.

KIM, C. H. & MOON, S. K. 2005. Epigallocatechin-3-gallate causes the p21/WAF1-mediated G(1)-phase arrest of cell cycle and inhibits matrix metalloproteinase-9 expression in TNF-alpha-induced vascular smooth muscle cells. *Arch Biochem Biophys*, 435, 264-72.

KIM, H. S., KIM, M. H., JEONG, M., HWANG, Y. S., LIM, S. H., SHIN, B. A., AHN, B. W. & JUNG, Y. D. 2004. EGCG blocks tumor promoter-induced MMP-9 expression via suppression of MAPK and AP-1 activation in human gastric AGS cells. *Anticancer Res*, 24, 747-53.

KIM, J. W., KANG, K. H., BURROLA, P., MAK, T. W. & LEMKE, G. 2008. Retinal degeneration triggered by inactivation of PTEN in the retinal pigment epithelium. *Genes Dev*, 22, 3147-57.

KIRYU, J., YAMAMOTO, F. & HONDA, Y. 1992. Effects of sodium iodate on the electroretinogram c-wave in the cat. *Vision Res*, 32, 2221-7.

KIUCHI, K., YOSHIZAWA, K., SHIKATA, N., MORIGUCHI, K. & TSUBURA, A. 2002. Morphologic characteristics of retinal degeneration induced by sodium iodate in mice. *Curr Eye Res*, 25, 373-9.

KLEIN, R., PETO, T., BIRD, A. & VANNEWKIRK, M. R. 2004. The epidemiology of age-related macular degeneration. *Am J Ophthalmol*, 137, 486-95.

KONDA, B. R., PARARAJASEGARAM, G., WU, G. S., STANFORTH, D. & RAO, N. A. 1994. Role of retinal pigment epithelium in the development of experimental autoimmune uveitis. *Invest Ophthalmol Vis Sci*, 35, 40-7.

KORTE, G. E., REPPUCCI, V. & HENKIND, P. 1984. RPE destruction causes choriocapillary atrophy. *Invest Ophthalmol Vis Sci*, 25, 1135-45.

KUMAR, B., GUPTA, S. K., NAG, T. C., SRIVASTAVA, S. & SAXENA, R. 2012. Green tea prevents hyperglycemia-induced retinal oxidative stress and inflammation in streptozotocin-induced diabetic rats. *Ophthalmic Res*, 47, 103-8.

KUO, S. M., LEAVITT, P. S. & LIN, C. P. 1998. Dietary flavonoids interact with trace metals and affect metallothionein level in human intestinal cells. *Biol Trace Elem Res*, 62, 135-53.

KURIYAMA, S., SHIMAZU, T., OHMORI, K., KIKUCHI, N., NAKAYA, N., NISHINO, Y., TSUBONO, Y. & TSUJI, I. 2006. Green tea consumption and mortality due to cardiovascular disease, cancer, and all causes in Japan: the Ohsaki study. *JAMA*, 296, 1255-65.

LEE, M. J., MALIAKAL, P., CHEN, L., MENG, X., BONDOC, F. Y., PRABHU, S., LAMBERT, G., MOHR, S. & YANG, C. S. 2002. Pharmacokinetics of tea catechins after ingestion of green tea and (-)-epigallocatechin-3-gallate by humans: formation of different metabolites and individual variability. *Cancer Epidemiol Biomarkers Prev*, 11, 1025-32.

LEUNG, C. K., CHEUNG, C. Y., LIN, D., PANG, C. P., LAM, D. S. & WEINREB, R. N. 2008a. Longitudinal variability of optic disc and retinal nerve fiber layer measurements. *Invest Ophthalmol Vis Sci*, 49, 4886-92.

LEUNG, C. K., CHEUNG, C. Y., WEINREB, R. N., LEE, G., LIN, D., PANG, C. P. & LAM, D. S. 2008b. Comparison of macular thickness measurements between time domain and spectral domain optical coherence tomography. *Invest Ophthalmol Vis Sci*, 49, 4893-7.

LEVINE, M., WANG, Y., KATZ, A., ECK, P., KWON, O., CHEN, S., LEE, J. H. & PADAYATTY, S. J. 2001. Ideal vitamin C intake. *Biofactors*, 15, 71-4.

LI, Z. W., LIU, S., WEINREB, R. N., LINDSEY, J. D., YU, M., LIU, L., YE, C., CUI, Q., YUNG, W. H., PANG, C. P., LAM, D. S. & LEUNG, C. K. 2011. Tracking dendritic shrinkage of retinal ganglion cells after acute elevation of intraocular pressure. *Invest Ophthalmol Vis Sci*, 52, 7205-12.

LIANG, F. Q., ALEMAN, T. S., ZAIXINYANG, CIDECIYAN, A. V., JACOBSON, S. G. & BENNETT, J. 2001. Melatonin delays photoreceptor degeneration in the rds/rds mouse. *Neuroreport*, 12, 1011-4.

LIANG, F. Q. & GODLEY, B. F. 2003. Oxidative stress-induced mitochondrial DNA damage in human retinal pigment epithelial cells: a possible mechanism for RPE aging and age-related macular degeneration. *Exp Eye Res*, 76, 397-403.

LIANG, F. Q., GREEN, L., WANG, C., ALSSADI, R. & GODLEY, B. F. 2004. Melatonin protects human retinal pigment epithelial (RPE) cells against oxidative stress. *Exp Eye Res*, 78, 1069-75.

LIANG, Y. C., LIN-SHIAU, S. Y., CHEN, C. F. & LIN, J. K. 1999. Inhibition of cyclin-dependent kinases 2 and 4 activities as well as induction of Cdk inhibitors p21 and p27 during growth arrest of human breast carcinoma cells by (-)-epigallocatechin-3-gallate. *J Cell Biochem*, 75, 1-12.

LIN, L. C., WANG, M. N., TSENG, T. Y., SUNG, J. S. & TSAI, T. H. 2007. Pharmacokinetics of (-)-epigallocatechin-3-gallate in conscious and freely moving rats and its brain regional distribution. *J Agric Food Chem*, 55, 1517-24.

LIU, C., FUKUHARA, C., WESSEL, J. H., 3RD, IUVONE, P. M. & TOSINI, G. 2004. Localization of Aa-nat mRNA in the rat retina by fluorescence in situ hybridization and laser capture microdissection. *Cell Tissue Res*, 315, 197-201.

LIU, S., LI, Z. W., WEINREB, R. N., XU, G., LINDSEY, J. D., YE, C., YUNG, W. H., PANG, C. P., LAM, D. S. & LEUNG, C. K. 2012. Tracking retinal microgliosis in models of retinal ganglion cell damage. *Invest Ophthalmol Vis Sci*, 53, 6254-62.

MACHALINSKA, A., LUBINSKI, W., KLOS, P., KAWA, M., BAUMERT, B., PENKALA, K., GRZEGRZOLKA, R., KARCZEWICZ, D., WISZNIEWSKA, B. & MACHALINSKI, B. 2010. Sodium iodate selectively injuries the posterior pole of the retina in a dose-dependent manner: morphological and electrophysiological study. *Neurochem Res*, 35, 1819-27.

MARGIS, R., DUNAND, C., TEIXEIRA, F. K. & MARGIS-PINHEIRO, M. 2008. Glutathione peroxidase family - an evolutionary overview. *FEBS J*, 275, 3959-70.

MATHEW, M. C., ERVIN, A. M., TAO, J. & DAVIS, R. M. 2012. Antioxidant vitamin supplementation for preventing and slowing the progression of age-related cataract. *Cochrane Database Syst Rev*, 6, CD004567.

MECKLENBURG, L. & SCHRAERMEYER, U. 2007. An overview on the toxic morphological changes in the retinal pigment epithelium after systemic compound administration. *Toxicol Pathol*, 35, 252-67.

METODIEWA, D., JAISWAL, A. K., CENAS, N., DICKANCAITE, E. & SEGURA-AGUILAR, J. 1999. Quercetin may act as a cytotoxic prooxidant after its metabolic activation to semiquinone and quinoidal product. *Free Radic Biol Med*, 26, 107-16.

MIAO, L. & ST CLAIR, D. K. 2009. Regulation of superoxide dismutase genes: implications in disease. *Free Radic Biol Med*, 47, 344-56.

MICELI, M. V., LILES, M. R. & NEWSOME, D. A. 1994. Evaluation of oxidative processes in human pigment epithelial cells associated with retinal outer segment phagocytosis. *Exp Cell Res,* 214, 242-9.

MORROW, J. D. & ROBERTS, L. J., 2ND 1999. Mass spectrometric quantification of F2-isoprostanes in biological fluids and tissues as measure of oxidant stress. *Methods Enzymol,* 300, 3-12.

MORROW, J. D., ZACKERT, W. E., YANG, J. P., KURHTS, E. H., CALLEWAERT, D., DWORSKI, R., KANAI, K., TABER, D., MOORE, K., OATES, J. A. & ROBERTS, L. J. 1999. Quantification of the major urinary metabolite of 15-F2t-isoprostane (8-iso-PGF2alpha) by a stable isotope dilution mass spectrometric assay. *Anal Biochem,* 269, 326-31.

MURAOKA, Y., IKEDA, H. O., NAKANO, N., HANGAI, M., TODA, Y., OKAMOTO-FURUTA, K., KOHDA, H., KONDO, M., TERASAKI, H., KAKIZUKA, A. & YOSHIMURA, N. 2012. Real-time imaging of rabbit retina with retinal degeneration by using spectral-domain optical coherence tomography. *PLoS One,* 7, e36135.

NAGLE, D. G., FERREIRA, D. & ZHOU, Y. D. 2006. Epigallocatechin-3-gallate (EGCG): chemical and biomedical perspectives. *Phytochemistry,* 67, 1849-55.

NAKAGAWA, K. & MIYAZAWA, T. 1997. Absorption and distribution of tea catechin, (-)-epigallocatechin-3-gallate, in the rat. *J Nutr Sci Vitaminol (Tokyo),* 43, 679-84.

NAKANO, M., OTSUKA, F. & VIRMANI, R. 2011. Letter by Nakano et Al regarding article, "optical coherence tomographic analysis of in-stent neoatherosclerosis after drug-eluting stent implantation". *Circulation,* 124, e954; author reply e955.

NAM, S., SMITH, D. M. & DOU, Q. P. 2001. Ester bond-containing tea polyphenols potently inhibit proteasome activity in vitro and in vivo. *J Biol Chem,* 276, 13322-30.

NIJVELDT, R. J., VAN NOOD, E., VAN HOORN, D. E., BOELENS, P. G., VAN NORREN, K. & VAN LEEUWEN, P. A. 2001. Flavonoids: a review of probable mechanisms of action and potential applications. *Am J Clin Nutr,* 74, 418-25.

NILSSON, S. E., KNAVE, B. & PERSSON, H. E. 1977a. Changes in ultrastructure and function of the sheep pigment epithelium and retina induced by sodium iodate. I. The ultrastructure of the normal pigment epithelium of the sheep. *Acta Ophthalmol (Copenh),* 55, 994-1006.

NILSSON, S. E., KNAVE, B. & PERSSON, H. E. 1977b. Changes in ultrastructure and function of the sheep pigment epithelium and retina induced by sodium iodate. III. Delayed effects. *Acta Ophthalmol (Copenh),* 55, 1027-43.

OGASAWARA, M. A. & ZHANG, H. 2009. Redox regulation and its emerging roles in stem cells and stem-like cancer cells. *Antioxid Redox Signal,* 11, 1107-22.

OHTAKA, K., MACHIDA, S., OHZEKI, T., TANAKA, M., KUROSAKA, D., MASUDA, T. & ISHII, T. 2006. Protective effect of hepatocyte growth factor against degeneration of the retinal pigment epithelium and photoreceptor in sodium iodate-injected rats. *Curr Eye Res,* 31, 347-55.

OSBORNE, N. N., NASH, M. S. & WOOD, J. P. 1998. Melatonin counteracts ischemia-induced apoptosis in human retinal pigment epithelial cells. *Invest Ophthalmol Vis Sci,* 39, 2374-83.

PARKE, D. V. & SAPOTA, A. 1996. Chemical toxicity and reactive oxygen species. *Int J Occup Med Environ Health,* 9, 331-40.

PARKER, R. S. 1989. Carotenoids in human blood and tissues. *J Nutr,* 119, 101-4.

PENG, P. H., CHIOU, L. F., CHAO, H. M., LIN, S., CHEN, C. F., LIU, J. H. & KO, M. L. 2010. Effects of epigallocatechin-3-gallate on rat retinal ganglion cells after optic nerve axotomy. *Exp Eye Res,* 90, 528-34.

PERSSON, I. A., JOSEFSSON, M., PERSSON, K. & ANDERSSON, R. G. 2006. Tea flavanols inhibit angiotensin-converting enzyme activity and increase nitric oxide production in human endothelial cells. *J Pharm Pharmacol,* 58, 1139-44.

PFAFFL, M. W. 2001. A new mathematical model for relative quantification in real-time RT-PCR. *Nucleic Acids Res,* 29, e45.

PIETTA, P. G. 2000. Flavonoids as antioxidants. *J Nat Prod,* 63, 1035-42.

POLI, G., LEONARDUZZI, G., BIASI, F. & CHIARPOTTO, E. 2004. Oxidative stress and cell signalling. *Curr Med Chem,* 11, 1163-82.

QIN, J., XIE, L. P., ZHENG, X. Y., WANG, Y. B., BAI, Y., SHEN, H. F., LI, L. C. & DAHIYA, R. 2007. A component of green tea, (-)-epigallocatechin-3-gallate, promotes apoptosis in T24 human bladder cancer cells via modulation of the PI3K/Akt pathway and Bcl-2 family proteins. *Biochem Biophys Res Commun,* 354, 852-7.

RANGAN, U. & BULKLEY, G. B. 1993. Prospects for treatment of free radical-mediated tissue injury. *Br Med Bull,* 49, 700-18.

RICE-EVANS, C. 1995. Plant polyphenols: free radical scavengers or chain-breaking antioxidants? *Biochem Soc Symp,* 61, 103-16.

RICE-EVANS, C. A. & DIPLOCK, A. T. 1993. Current status of antioxidant therapy. *Free Radic Biol Med,* 15, 77-96.

RIVERA, J. C., SAPIEHA, P., JOYAL, J. S., DUHAMEL, F., SHAO, Z., SITARAS, N., PICARD, E., ZHOU, E., LACHAPELLE, P. & CHEMTOB, S. 2011. Understanding retinopathy of prematurity: update on pathogenesis. *Neonatology,* 100, 343-53.

ROBERTS, L. J., 2ND & MORROW, J. D. 1997. The generation and actions of isoprostanes. *Biochim Biophys Acta,* 1345, 121-35.

ROSEN, R., HU, D. N., PEREZ, V., TAI, K., YU, G. P., CHEN, M., TONE, P., MCCORMICK, S. A. & WALSH, J. 2009. Urinary 6-sulfatoxymelatonin level in age-related macular degeneration patients. *Mol Vis,* 15, 1673-9.

ROSENKRANZ, S., KNIREL, D., DIETRICH, H., FLESCH, M., ERDMANN, E. & BOHM, M. 2002. Inhibition of the PDGF receptor by red wine flavonoids provides a molecular explanation for the "French paradox". *FASEB J,* 16, 1958-60.

ROY, A. M., BALIGA, M. S. & KATIYAR, S. K. 2005. Epigallocatechin-3-gallate induces apoptosis in estrogen receptor-negative human breast carcinoma cells via modulation in protein expression of p53 and Bax and caspase-3 activation. *Mol Cancer Ther,* 4, 81-90.

RUGGERI, M., WEHBE, H., JIAO, S., GREGORI, G., JOCKOVICH, M. E., HACKAM, A., DUAN, Y. & PULIAFITO, C. A. 2007. In vivo three-dimensional high-resolution imaging of rodent retina with spectral-domain optical coherence tomography. *Invest Ophthalmol Vis Sci,* 48, 1808-14.

SACHDEVA, A. K., KUHAD, A. & CHOPRA, K. 2011. Epigallocatechin gallate ameliorates behavioral and biochemical deficits in rat model of load-induced chronic fatigue syndrome. *Brain Res Bull,* 86, 165-72.

SCHRAERMEYER, U. & HEIMANN, K. 1999. Current understanding on the role of retinal pigment epithelium and its pigmentation. *Pigment Cell Res,* 12, 219-36.

SHAHINFAR, S., EDWARD, D. P. & TSO, M. O. 1991. A pathologic study of photoreceptor cell death in retinal photic injury. *Curr Eye Res,* 10, 47-59.

SHIMIZU, M., DEGUCHI, A., HARA, Y., MORIWAKI, H. & WEINSTEIN, I. B. 2005. EGCG inhibits activation of the insulin-like growth factor-1 receptor in human colon cancer cells. *Biochem Biophys Res Commun,* 334, 947-53.

SHIN, H. Y., KIM, S. H., JEONG, H. J., KIM, S. Y., SHIN, T. Y., UM, J. Y., HONG, S. H. & KIM, H. M. 2007. Epigallocatechin-3-gallate inhibits secretion of TNF-alpha, IL-6 and IL-8 through the attenuation of ERK and NF-kappaB in HMC-1 cells. *Int Arch Allergy Immunol,* 142, 335-44.

SINGALAVANIJA, A., RUANGVARAVATE, N. & DULAYAJINDA, D. 2000. Potassium iodate toxic retinopathy: a report of five cases. *Retina,* 20, 378-83.

SOHAL, R. S. & WEINDRUCH, R. 1996. Oxidative stress, caloric restriction, and aging. *Science,* 273, 59-63.

SORSBY, A. & READING, H. W. 1964. Experimental degeneration of the retina. XI. The effect of sodium iodate on retinal -SH levels. *Vision Res,* 4, 511-4.

STOYANOVSKY, D. A., GOLDMAN, R., DARROW, R. M., ORGANISCIAK, D. T. & KAGAN, V. E. 1995. Endogenous ascorbate regenerates vitamin E in the retina directly and in combination with exogenous dihydrolipoic acid. *Curr Eye Res,* 14, 181-9.

SUTHERLAND, B. A., RAHMAN, R. M. & APPLETON, I. 2006. Mechanisms of action of green tea catechins, with a focus on ischemia-induced neurodegeneration. *J Nutr Biochem,* 17, 291-306.

SUYAMA, T. 1967. Electron microscopic study on experimental retinal degeneration induced by sodium iodate injection. *Yonago Acta Med,* 11, 222-31.

SUZUKI, M., KAMEI, M., ITABE, H., YONEDA, K., BANDO, H., KUME, N. & TANO, Y. 2007. Oxidized phospholipids in the macula increase with age and in eyes with age-related macular degeneration. *Mol Vis,* 13, 772-8.

TAARNHOJ, J. & ALM, A. 1992. The effect of sodium iodate on the blood-retinal and blood-brain barriers. *Graefes Arch Clin Exp Ophthalmol,* 230, 589-91.

THIAGARAJAN, G., CHANDANI, S., SUNDARI, C. S., RAO, S. H., KULKARNI, A. V. & BALASUBRAMANIAN, D. 2001. Antioxidant properties of green and black tea, and their potential ability to retard the progression of eye lens cataract. *Exp Eye Res,* 73, 393-401.

TONG, Y. 1995. A case of blindness caused by acute iodine poisoning. *Chin Med J (Engl),* 108, 555-6.

TSAI, C. C., WU, S. B., CHENG, C. Y., KAO, S. C., KAU, H. C., CHIOU, S. H., HSU, W. M. & WEI, Y. H. 2010. Increased oxidative DNA damage, lipid peroxidation, and reactive oxygen species in cultured orbital fibroblasts from patients with Graves' ophthalmopathy: evidence that oxidative stress has a role in this disorder. *Eye (Lond),* 24, 1520-5.

TSAI, C. C., WU, S. B., CHENG, C. Y., KAO, S. C., KAU, H. C., LEE, S. M. & WEI, Y. H. 2011. Increased response to oxidative stress challenge in Graves' ophthalmopathy orbital fibroblasts. *Mol Vis,* 17, 2782-8.

TSO, M. O., ZHANG, C., ABLER, A. S., CHANG, C. J., WONG, F., CHANG, G. Q. & LAM, T. T. 1994. Apoptosis leads to photoreceptor degeneration in inherited retinal dystrophy of RCS rats. *Invest Ophthalmol Vis Sci,* 35, 2693-9.

VALENCIA, E., MARIN, A. & HARDY, G. 2001. Glutathione--nutritional and pharmacological viewpoints: Part III. *Nutrition,* 17, 696-7.

VALKO, M., RHODES, C. J., MONCOL, J., IZAKOVIC, M. & MAZUR, M. 2006. Free radicals, metals and antioxidants in oxidative stress-induced cancer. *Chem Biol Interact,* 160, 1-40.

WANG, H. M., HULL, B. E. & ORGANISCIAK, D. T. 1994. Long term effects of diaminophenoxypentane in the rat retina: protection against light damage. *Curr Eye Res,* 13, 655-60.

WU, G., FANG, Y. Z., YANG, S., LUPTON, J. R. & TURNER, N. D. 2004. Glutathione metabolism and its implications for health. *J Nutr,* 134, 489-92.

YANG, C. S., CHEN, L., LEE, M. J., BALENTINE, D., KUO, M. C. & SCHANTZ, S. P. 1998. Blood and urine levels of tea catechins after ingestion of different amounts of green tea by human volunteers. *Cancer Epidemiol Biomarkers Prev,* 7, 351-4.

YAO, K., YE, P., ZHANG, L., TAN, J., TANG, X. & ZHANG, Y. 2008. Epigallocatechin gallate protects against oxidative stress-induced mitochondria-dependent apoptosis in human lens epithelial cells. *Mol Vis,* 14, 217-23.

YOON, Y. H. & MARMOR, M. F. 1993. Retinal pigment epithelium adhesion to Bruch's membrane is weakened by hemicholinium-3 and sodium iodate. *Ophthalmic Res,* 25, 386-92.

YOSHINO, M. & MURAKAMI, K. 1998. Interaction of iron with polyphenolic compounds: application to antioxidant characterization. *Anal Biochem,* 257, 40-4.

ZARBIN, M. A. 2004. Current concepts in the pathogenesis of age-related macular degeneration. *Arch Ophthalmol,* 122, 598-614.

ZARKOVIC, M. 2012. The role of oxidative stress on the pathogenesis of graves' disease. *J Thyroid Res,* 2012, 302537.

ZHANG, B. & OSBORNE, N. N. 2006. Oxidative-induced retinal degeneration is attenuated by epigallocatechin gallate. *Brain Res,* 1124, 176-87.

ZHANG, B., SAFA, R., RUSCIANO, D. & OSBORNE, N. N. 2007. Epigallocatechin gallate, an active ingredient from green tea, attenuates damaging influences to the retina caused by ischemia/reperfusion. *Brain Res,* 1159, 40-53.

ZHAO, C., YASUMURA, D., LI, X., MATTHES, M., LLOYD, M., NIELSEN, G., AHERN, K., SNYDER, M., BOK, D., DUNAIEF, J. L., LAVAIL, M. M. & VOLLRATH, D. 2011. mTOR-mediated dedifferentiation of the retinal pigment epithelium initiates photoreceptor degeneration in mice. *J Clin Invest,* 121, 369-83.